Slutrapport projekt TRV 2016/92229

SAFT

Simulering av Atmosfär och Flygtrafik för en Tystare omvärld

(Final report SAFT - Simulation of Atmosphere and air traFfic for a more silenT environment)

Stockholm, 30 Augusti 2019

Projektdeltagare:

KTH:
Huvudsökande
Professor
Mats Åbom
- projektledare
Centrum för Hållbar Luftfart
100 44 Stockholm

Ulf Tengzelius
- huvudansvarig för
kodutveckling SAFT

Ilkka Karasalo
- expert ljudutbredning

Chalmers:
Professor
Tomas Grönstedt
-ansvarig källmodeller

Fatemeh Bahmani
-kodutveckling

Sammanfattning (summary in Swedish)

SAFT - Simulering av Atmosfär och Flygtrafik för en Tystare omvärld - är namnet både på det projekt som redovisas i denna rapport och på det datorprogram som utvecklats inom projektet. Simuleringsplattformen SAFT inkluderar flera metoder för bullerkartering från flygtrafik, från en så kallade "integrerad metod", i form av en ECAC Doc.29 implementering, över mer avancerade och potentiellt mer exakta simuleringsmetoder, inkluderande effekter för ljudutbredning i en "verklig" atmosfär från rörliga, frekvensberoende och direktiva ljudkällor.

Chalmers metoder för flygplansmodellering, framdrivnings prestanda och konceptuell design är kopplade till SAFT och medger forskningsstudier på hur ny teknologi och design val för flygplan och motorer påverkar ljudgenerering, och i förlängningen också mark-ljudkonturer för ny teknologi. Chalmers verktyg tillåter också fysikaliskt baserade simuleringar av flyplanstrajektorier som kan kopplas till SAFT för att användas olika inflygningsprocedurer och hur dessa påverkar CO_2 och buller.

Rapporten har två huvudsakliga syften: 1. Redovisning av resultat från arbetet inom SAFT-projektet och 2. Erbjuda en introduktion och överblick för användare och utvecklare av SAFT-beräkningsprogram.

Den sista punkten, introduktion för användare/utvecklare har varit styrande i organisationen av texten, med resultatet att den röda tråden i dokumentet följer möjliga beräkningsvägar vid användning av SAFT.

Efter en kort bakgrund och introduktion, ges läsaren en orientering av den indata som krävs vid efter val av alternativ beräkningsväg , sen följer lite fylligare information om vad dessa beräkningsalternativ innehåller och därefter resultat från några beräkningsexempel och avslutningsvis slutsatser och en blick framåt.

I sin nuvarande version är SAFT-programmet ämnad för bullerkartering för individuella flyghändelser och körs via interaktiv inmatning av indata för varje fall. Möjliga beräkningar omfattar: nya ankomstrutter för existerande flygplanstyper och standard- procedurer, nya procedurer och (vertikala) flyg-profiler, bullerkonturer för dagens eller framtida flygplanstyper.

Eftersom SAFT-programmet kommer att fortsätta utvecklas i kommande projekt, har begränsningar och möjliga eller nödvändiga framtida uppdateringar och implementeringar noterats i rött (t.ex. som i: [NOTE: ...]) för att underlätta överblicken av dessa framtida insatser.

SAFT programmets arkitektur och design är utvecklad med avsikten att etablera en forskningsplattform som kombinerar följande egenskaper:

1. "State of the art" vetenskaplig och teknisk nivå
2. Enkelt att förstå och använda
3. Användbarhet – d.v.s. fylla luckor/brister hos dagens s.k. integrerade metoder såsom att erbjuda flygbullerkartering/kontutkurvor som bättre överensstämmer med verklig flygtrafik, rådande väder och dess variation – för såväl existerande trafiksituation, bananvändarmönster, flygplan, procedurer och flygvägar som för framtida d:o.

1. Summary

SAFT is the acronym of the project outlined in this report as well as the computer code for aircraft environmental noise simulation developed within the project. The SAFT simulation platform covers several methods for aircraft noise mapping, from a so called integrated method, a standard ECAC Doc.29 implementation, over more advanced, and potentially more accurate simulation methods accounting for "real" atmosphere/sound propagation conditions as well as for directive and frequency dependent noise sources.

Chalmers methods for aircraft modelling, propulsion performance and propulsion conceptual design are interfaced with SAFT allowing for research studying how new technology and design choices of aircraft and engines influence noise sources, and in its extension also predict noise contours for new technology. Chalmers tools also allows physics-based simulations of aircraft trajectories to be linked to SAFT and be used to study different inflight procedures and how these influence CO2 emissions and noise.

This document has two main purposes, namely: 1. Present the outcome of work performed within the project SAFT and 2. Offer an introduction and overview for users and developers of the computer program SAFT.

This last point, i.e. giving an overview for coming SAFT users and -developers, has been ruling in the organisation of the text, with the result of a main thread corresponding to the possible computational paths when running the SAFT-program. After a short background and intro, the reader gets a picture of the input needed by the different computational alternatives, some information about the methods themselves and then samples of output from different simulations or runs.

In its current phase of development SAFT is aimed for noise mapping of single aircraft pass-by events and is run by interactive input for each case. Possible runs and studies cover: new approach routes for existing aircraft and standard procedures, new procedures and profiles, noise footprints from todays or not yet existing aircraft.

Since the SAFT-program is intended to be further developed in upcoming projects, current limitations and possible or needed future updates and implementations are noted in the text. Typically these notes, in the first place aimed for SAFT developers and users, are given in in red text like: [NOTE: ...].

The SAFT architecture and design is made with the intentions to establish a research tool that combines the features of:

1. State of the art scientific and technical level
2. Easy to understand and use
3. Usefulness – i.e. filling the gaps/shortcomings of today's standard integrated methods such as offering the capabilities of producing ground noise patterns that better reflects a real air traffic and prevailing weather and its variation - could be for an existing traffic situation, runway use or for new runways, aircraft, procedures or flight route design
4. Flexibility in terms of integrating future updates such as new methods, algorithms as well as functionality

Content

2. Background

This research was financed by The Swedish Transport Administration through the Centre for Sustainable Aviation (CSA) in order to strengthen the Swedish research on the environmental impact of aviation, in particular noise. The overall aim with the SAFT project, and other CSA-projects is to generate societal benefits in both the short and long-term and both in a local and an international perspective. Such benefits could be reduced noise impact on citizens living around airports, e.g. reached by optimised aircraft operational behaviour, flight routes design or distribution of air traffic over time or else. To be able to perform studies aiming for the identification and validation of such optimised patterns and measures one need an aircraft simulation tool capable of involving the complete chain from aircraft noise generation, over propagation to the resulting noise on the ground and its impact on people. Moreover, this computational chain has to be capable of integrating future, not yet existing, aircraft with regard to noise emissions, representative weather and air traffic scenarios.

The need for the above outlined studies is in turn motivated, on one hand, by the increasing knowledge on the adverse health effects from environmental noise and the related trend of stronger noise restrictions [1] - and on the other - to the expected growth of the Swedish [2] as well as the worlds air traffic. Despite the forecasted more dense air traffic and the rather slow replacement of the aircraft fleet into a less noisy one, at least one study [3], applying simulation tools in line with SAFT, indicate no increase in future noise exposure around typical airports. Though, much more studies plus efforts to optimise the operational behaviour + TMA routing has to be carried out the coming years in order to assure a future balance between existing and coming environmental requirements and the expected increase in air traffic volumes. In all, it is clear that we need a better understanding of the complete picture of aircraft noise, and its impact on the society as a whole. In the process aiming for solutions to such matters, integrated methods like ECAC Doc.29 and AEDT can give some input but we regard that more accurate and versatile simulation tools like SAFT, well applied, would constitute a much morepowerful support and are needed for the quantification of more realistic (= complex) noise reduction measures.

3. Overview of SAFT

3.1 Introduction to SAFT computations

The SAFT aircraft noise mapping simulation platform offers the possibilities to compute ground noise contours and noise time histories in selected points on ground for aircraft pass-by events. The noise events could typically be represented by the approach trajectory for a medium sized commercial aircraft such as an Airbus 320. The trajectory section selected by the user could be the last, say 20 nautical miles before touch down + the deceleration distance on the runway (RW). The studied 4D trajectories are defined by their groundtrack (lat, long) and their profile (altitude as a function of time). The groundtrack may be selected among a set of existing flight routes or new ones may be defined around Arlanda airport, the main airport of Stockholm, having 6 runways (i.e. 3 paved paths), and 4 TMA[1] [4] main entry points [5]. Knowing the main properties along the trajectory, aircraft speed, thrust setting etc. – the dataset content is depending on the selected computational method - SAFT computes the resulting noise from the aircraft in a ground grid. From these noise histories in the ground grid points, noise contours in dB are computed. The noise metric for these contours (and local position data) could be either A-weighted max levels or sound exposure levels (SEL or L_E), i.e. the sound pressure level integrated over time ("energy-wise" - "pressure squared") during an aircraft pass-by and presented as occurring during a fixed time interval of one second.

Both the representation of the aircraft as a sound source and the propagation of sound, including the atmospheric impact, may be covered by different levels of complexity – and related accuracy. The different computational methods for: sound propagation, aircraft sound sources and atmosphere representations, plus the needed input data for the different computational approaches in SAFT are outlined in chapter 3.3 below.

3.2 Simulation methods vs integrated methods

The most fundamental difference between the noise contour prediction methods implemented in SAFT is found between the integrated[2] method, ECAC Doc.29 [6], and the other simulation methods. While simulation methods allow for: 1. a time stepping along the aircraft trajectory, as well as in receiving points on ground, 2. a possibility to account for a separation of the noise source and the sound propagation and 3. a frequency dependent and directive moving sound source, the integrated methods do not. The integrated methods rely on the so called NPD-data (Noise-Power-Distance) [7]. In the NPD-data both the sound source and propagation effects are condensed into a 2D interpolation matrix which links the total (ground) noise level with: A. distances (accounting for a "standard case" atmospheric and ground impact on propagation) and B. aircraft thrust setting . In the case of approach the NPD-data represents level flight for a constant velocity of 160 knots for "full" landing configuration, i.e. full flap/slat deployment and landing gear down. I.e. according to this model only

[1] Terminal Manoeuvring Area – controlled airspace around an airport, for Stockholm-Arlanda (ESSA) ca 90-100 nautical miles(160-190 km) wide polygon centered close to Stockholm

[2] integrated in the sense that noise source strength and noise propagation are integrated into one combined variable.

one independent variable determines the predicted noise level on ground[3]. With this follows that, with the integrated methods - in contrary to simulation methods - there is no possibility to examine the receiving noise signal time or frequency wise[4], neither accounting for a refractive atmosphere or different flight conditions or varying aircraft configurations. The only purpose of including also an integrated method in SAFT was to enable possibilities for comparisons with such methods, which still is the common practice around most airports. More information about the integrated methods can be found in the AEDT documentation, the North American correspondence to ECAC Doc.29, [8]. The weakest point of ECAC Doc.29 and AEDT, is, as we see it, the mentioned strongly reduced set of the central input data, i.e. the individual aircraft type noise data given in the NPD-database. But, this NPD-data could at same time be seen as the most significant strength of the integrated methods. This is, though the information content in the NPD data is strongly reduced, there is no open correspondence of aircraft noise data to find when it comes to the number of aircraft types included. The more detailed data that do exist, at least for some aircraft types, is mostly industry propriety and not open for research or to the public. As an alternative, in line with the aim for better noise mapping, we see a tendency of "local" more detailed aircraft noise databases built up from noise measurement on real air traffic by individual research organisations or stakeholders involved in the matter of noise around airports. Some examples of such initiatives to go towards aircraft noise computations supported with higher quality aircraft noise source data are mentioned in references [9], [10] and [11].

The trend towards more accurate and informative aircraft noise computation methods is actually expressed also in ECAC Doc.29 (at least in edition 3 of year 2005 but probably discussed a long time before that):

a) "integrated models represent current best practice" [referring to long time noise level estimates]
b) "This situation [i.e., that simulation methods are to be used also for long-term noise mapping] may change at some point in the future: 'simulation' models have greater potential and it is only a shortage of the comprehensive data they require, and their higher demands on computing capacity, that presently restrict them to special applications (including research)."

I.e. even within ECAC Doc.29 it is anticipated that 'simulation models' in the future may be used not only as research tools, but also as replacements for 'integrated methods'. We believe that today, all needed components for a fast and effective aircraft noise simulation are available, and that technical reasons to stick to integrated methods do no longer exist – the matter of agreement on detail methods would be more of a pedagogical and political matter among stakeholders. This conclusion is based on the judgement that neither complexity, lack of computational methods, time for computations or costs for more detailed noise measurements or else not any longer constitute an obstacle.

[3] more precisely also the flight velocity is included in ECAC Doc 29 calculations, but not by increasing airframe noise levels or similar, which could be expected, but reducing time integrated noise levels like SEL due to reduced exposure times linked with higher flight velocities.

[4] Though, some aircraft noise frequency information is available in the ANP-data, namely spectra which should be representative for groups of aircraft types. This strongly condensed dataset contains one spectra for take-off and one for approach for each group of aircraft. These spectra relates to one speed and as for NPD-data to only one configuration/max noise level. No directivity is given. The spectral data is rather old (1986 and 1999 aircraft data, [58] and [27] resp.) and it is unclear to which extent it represents todays aircraft/engines.

3.3 Outline of SAFT and computational path alternatives

3.3.1 General

SAFT is programmed in Matlab and offers in its current version 1 a set of 4 main computational paths stretching from "aircraft trajectory" over "noise propagation" to "noise on ground". (the 5th under implementation, June 2019). "Noise on ground" could either be a noise contour map, for a selected noise metric, or a the noise event in a limited set of ground points. A noise event could be presented as the total A-weighted sound pressure level or the 1/3-octave spectrum level as a function of time.

These different computational paths are distinguished by: the applied *computational method*, the type of *input data required* and the kind of *output* created. Among these 4(5) computational paths the first 2 is based on the ECAC Doc.29 method. Here, it might seem superfluous to bring in an ECAC Doc..29 implementation, with its limitations compared with the time-stepping simulation paths in SAFT, but, the idea is to make direct comparisons[5] possible – i.e. ,"delta-dB" between results based on the Doc.29-method, the current standard integrated method, and results from the more sophisticated simulation methods implemented in SAFT. All the SAFT noise mapping computational paths could be represented by the block scheme in Figure 1 below:

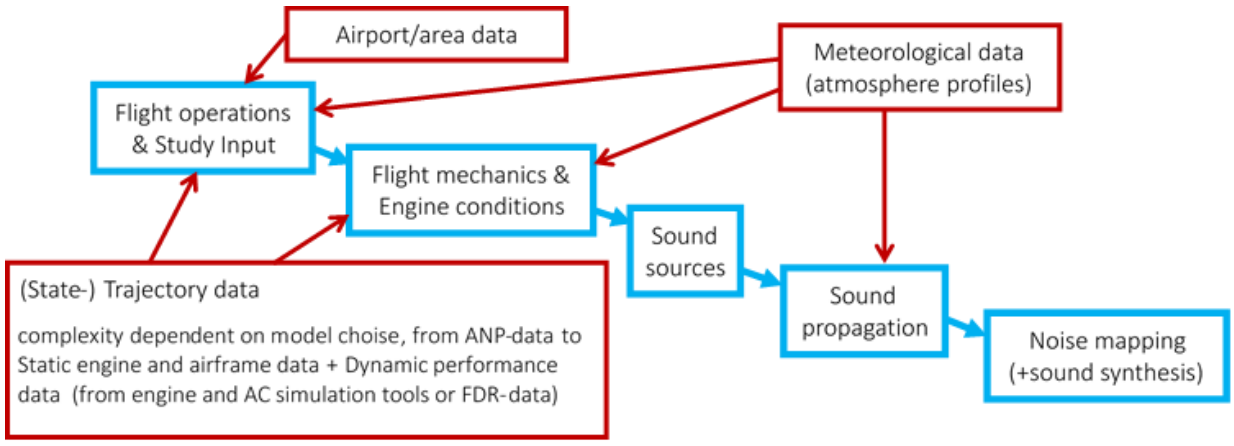

Figure 1. Noise mapping computational blocks in SAFT
blue *= original work packages which also corresponds to the main blocks in the SAFT computer code*
red *= user input data*

Beside the selection of any of these 4(5) SAFT-paths, resulting in ground noise contours based on a noise field defined on a 2D ground grid, the SAFT–user also has the alternative to choose the above mentioned "delta-dB" computation starting out from any two previously created SAFT-results generated on the same ground grid. This "delta-dB" choice is made already as the first input in a SAFT run, called "General SAFT action", as choice no 3, where the alternatives are: 1. Standard interactive

[5] such "delta-dB" noise contour comparisons is not only possible between simulation- and ECAC Doc 29 results but between any SAFT computation applying the same ground grid, could be between different atmospheric models or data (with a fix sound propagation model) or between different simulation models – with a fix "atmosphere" or else.

input run for Aircraft pass-by noise mapping or - 2. NOTE: under implementation: as 1. but Input from file, i.e. on-interactive run and 3. Compute difference between previous runs – "delta-dB".

Moreover, in the second input step, the user may, instead of the current 4 (coming 5) direct "aircraft noise source – propagation – noise map" computation alternatives, also select a "Transmission Loss (TL) – computation"[6]. In this type of computation a TL-interpolant matrix (TL_{ip_mat}) is created. These TL_{ip_mat} :s are established with ray-tracing and aimed for later use in any of the simulation methods, i.e. in the "noise source to noise map" paths. This new TL-interpolation matrix concept[7], which reduces CPU-times significantly, is outlined in chapter 4.9. It shall be noted that the user do not need to do this pre-computation of a TL_{ip_mat}, but may equally well choose to establish the TL_{ip_mat} within the run of a noise contour computation.

The last two computational paths, both related to aircraft noise measurements within CSA project ULLA [12], are under development and are planned to be established within the run of the upcoming CSA-project CIDER (to be presented on the CSA-website, [13]). With the implementation of these two path's SAFT will have in all 7 main computational choices, 5 for direct noise mapping and 2 "extra", compared with the current 5 (where of one "extra). The two to be added will regard:

a. (path no 4, noise mapping) "Simulation, total AC-sound sources established from measurements of pass-by noise events"
   and
b. (path no 7, "extra") "AC sound source estimate outgoing from sound measurements on ground and related trajectory data"

The SAFT-run alternatives might become clearer in the below user's screen view of the start of a SAFT-run.

3.3.2 Screen view of a SAFT-run start

After executing the command: 'SAFT_[version name]' in a Matlab command window the user will have to respond to the following with interactive inputs:

```
----    General SAFT action    ----

1. Please choose your wanted kind of SAFT action:
  1. Define and run a new noise event case with input given interactively (Default)
                  or
  [2. Read in, modify and run previously prepared input files - NOT YET IMPLEMENTED!]
                  or
  3. Difference between grid field results from two previous runs ("Delta-dB contours")

Please give a number, 1 or 3 (REM:  2 - NOT YET IMPLEMENTED!]):
```

---

[6] TL, Transmission Loss – is a common way to describe the loss a propagating sound wave experience in noise pressure level, or noise intensity level, measured in dB re $20\mu Pa$, or re $1pWatt$ respectively, between two points along a propagation path.

[7] this method, i.e. applying an TL interpolant matrix linking any source point in the air with any ground point is as far as we know not found previously in the literature.

1 selected

---- Interactive user input from screen ----

2. Decide the type of noise computation you want to run among the following SAFT run-modes:

-- **ECAC Doc.29 integrated-/sound immission model, AC's within the ANP-database** [14], Output: Noise Contours in Google Earth (saved in .kml-files) --

1. Original NPD-data sound immission - fix atm./absorp.model SAE-ARP-1845 (Default)

2. Atmosphere and absorption adjusted NPD-data sound immission - choice of atm./absorp.model follows - no refraction

-- **Simulation-/sound emission models** Output: Noise Contours in Google Earth (saved in .kml-files) and/or Noise Event Time Histories in matlab plots + .png-files --

3. Reversed engineering combined sound source from NPD-SEL and given spectral and directivity data (i.e. merged individual, fan+jet+...) - choice of atm./absorp. model follows - Option: full refractive atmosphere.

[4. Simulation, total AC-sound sources established from measurements of pass-by noise events. Option: full refractive atmosphere. NOT YET IMPLEMENTED !]

5. Full Simulation, semi-empirically modelled individual sound sources. Option: full refractive atmosphere. AC: A321-V2533

-- **TL only (no AC involved) for later use** Output: TL interpolant matrix saved in file --

6. Creation of a Transmission Loss (TL) matrix for a selected atmosphere dataset (to be applied in later SAFT-runs)

-- **Establish an AC sound source sample for later use** Output: frequency, directivity, speed- and AC configuration dependent sound source saved in file --

7. AC sound source estimate outgoing from sound measurements on ground and related trajectory data (to be applied in later SAFT-runs) [UNDER DEVELOPMENT!]

Please give a number between 1 and 7:

After this choice of run-path the interactive inputs follows in a similar manner for the user input of trajectory, grid etc. It is very easy to get a fast first view of the code capabilities and input needs since it is possible to go for the "Default" alternative in all input cases. After running SAFT this "all Default-way" the first time, and thereby getting noise contour-plots for an Airbus A321-232 landing on RW26 at Arlanda coming in along on a specific approach rout from the north along a standard ANP-profile, the user can start to change a few input to test other routes, aircraft or computational methods and atmospheric data.

3.4 The alternative computational paths

The alternative computational paths are repeated and summarised in Table 1 below and further described in paragraph 4 and 5. It could be noted that for an noise event (General SAFT action = A in Table 1) around 10-30 more inputs follows, dependent on the second input, before the SAFT run starts. In the "delta-dB"(C-type) case the run starts directly after the previous two output noise data grid results has been given.

No	TYPE / description	Comment
	General SAFT action	
A	Define and run a new noise event case with input given interactively (Default)	
B	[Read in, modify and run previously prepared input files]	*NOT YET IMPLEMENTED!*
C	Difference between grid field results from two previous runs ("Delta-dB contours")	
A/B*	*Alternatives available if A or B* of "General SAFT action" above is selected (NOTE: alt. B of "General SAFT action" not yet implemented)* ***Type of noise computation run wanted***	
	ECAC Doc.29 integrated-/sound immission model, AC's within the ANP-database	*Only the approach case is implemented!*
1	Original NPD-data sound immission – fix atm./absorp.model SAE-ARP-1845 (Default)	
2	Atmosphere and absorption adjusted NPD-data sound immission	
	Simulation-/sound emission models	
3	Reversed engineering combined sound source from NPD-SEL and given spectral and directivity data	
4	[Simulation, total AC sound sources established from measurements of pass-by noise events]	*NOT YET IMPLEMENTED!*
5	Full Simulation, semi-empirically modelled individual sound sources. Option: full refractive atmosphere. Aircraft: A321-V2533	
	TL only (no AC involved) for later use	
6	Creation of a Transmission Loss (TL) interpolation matrix for a selected atmosphere dataset	
	Establish an AC sound source sample for later use	
7	[AC sound source estimate outgoing from sound measurements on ground and related trajectory data]	*NOT YET IMPLEMENTED!*
	- further input follows... –	
	- SAFT run starts -	
C	*Alternative available if C of "General SAFT action" above is selected* ***Computation of Difference (Delta-dB) between results from two previous runs on the same ground-grid***	
1	Choose the 1st of the two 'NoiseGr.mat' files from previous runs	
2	Choose the 2nd of the two 'NoiseGr.mat' files from previous runs in the same way as for the 1st file	
	(no more input)	
	- SAFT run starts –	

Table 1. SAFT Alternative computational paths (planned not yet implemented paths in grey)

As seen in the command window example, on page 10 - 12, The input questions are written in thick-blue text, alternative inputs and other informative text in black and default alternatives in green. For all inputs the user have a default alternative, this is written in green text. By this input design its very simple to start running SAFT and learning by smoothly go to more advanced input and run-types. In the simplest run type ECAC Doc29. SAE ARP1845 atmosphere, SAFT run path type 1, ca 20 inputs are needed while the simulation based SAFT run paths need more than the double and in some cases supporting data established within previous SAFT-runs or externally.

3.5 Output examples

The output from a SAFT noise computation run, i.e. any of the runs of type 1 to 5 in Table 1 above, is a set of noise contours and/or a noise history in one or more selected points. The noise contours may either be given as A-weighted max levels, L_{Amax}, or as A-weighted Sound Exposure Level, often written L_E or SEL. The SEL-value represents an integrated value of the rms sound pressure squared, $\tilde{p}^2$, over the duration of the noise event where the noise event duration is defined as the time when the sound pressure stays > $p_{\max}$ of the pass-by event. The noise contour data are saved in .kml-files, a format for geographic information readable into Google Earth and other GIS-programs. The noise event A-weighted sound pressure levels in specific points are, if this alternative is selected by the user, plotted in Matlab plots on the screen and saved to disk. A specific output directory is automatically designated, or named by the user, to each SAFT run. Example outputs are shown in Figure 2 to Figure 4 below.

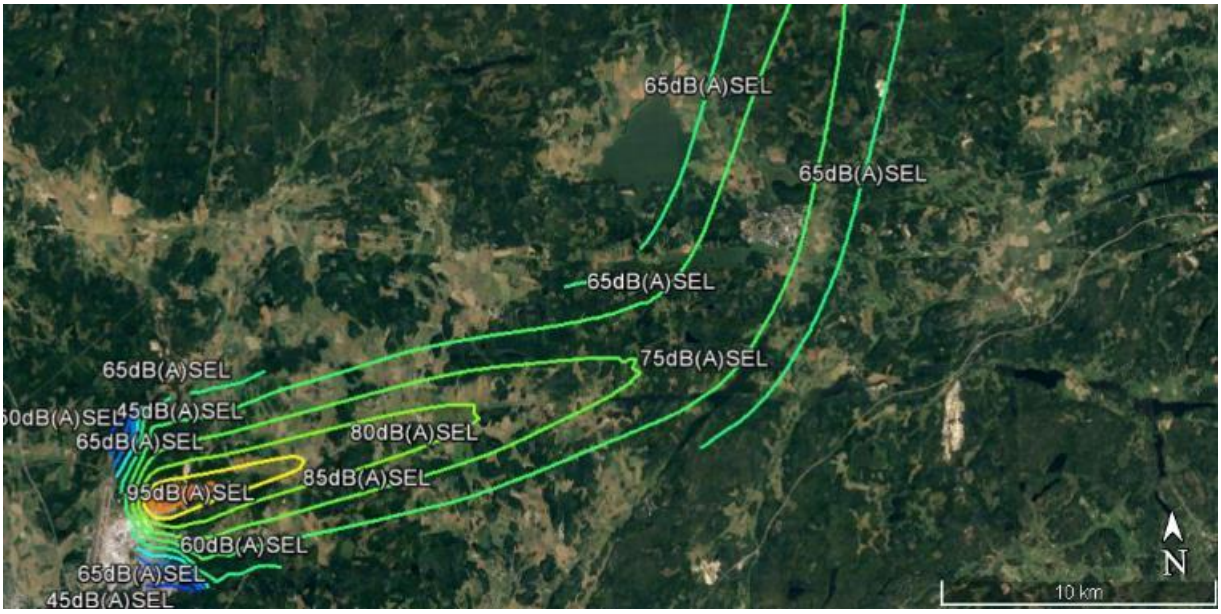

Figure 2. Example of noise contour plot – as produced by SAFT run type 1-5
(A321-232 approach+landing SAFT run 3, reversed engineering computation)

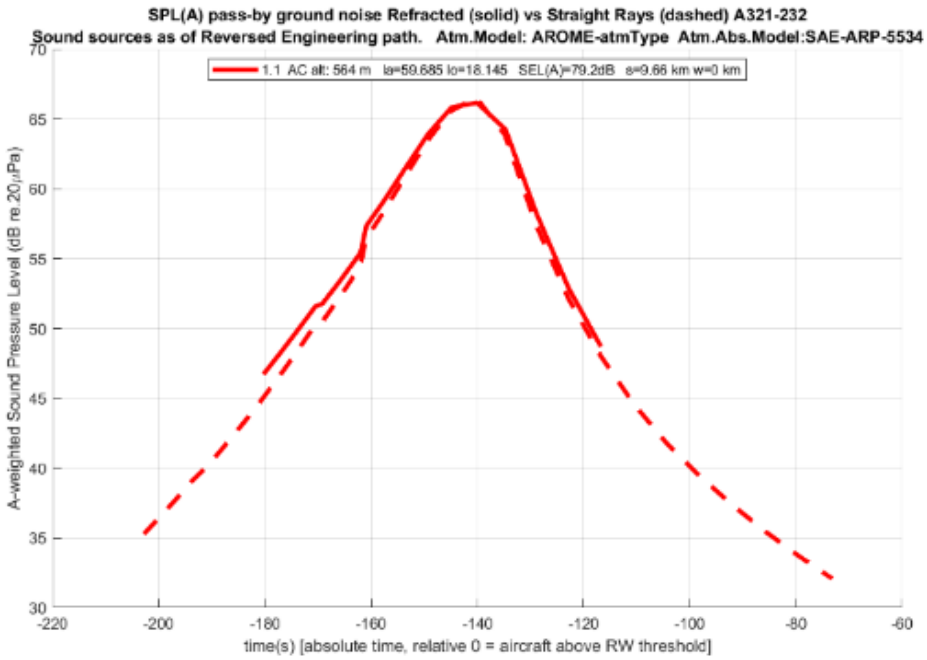

Figure 3. Example of aircraft pass-by noise total sound pressure level L_A *(t)*
Receiving point on groundtrack , i.e. straight below the aircraft
(solid line = refracted rays, dashed = straight rays)

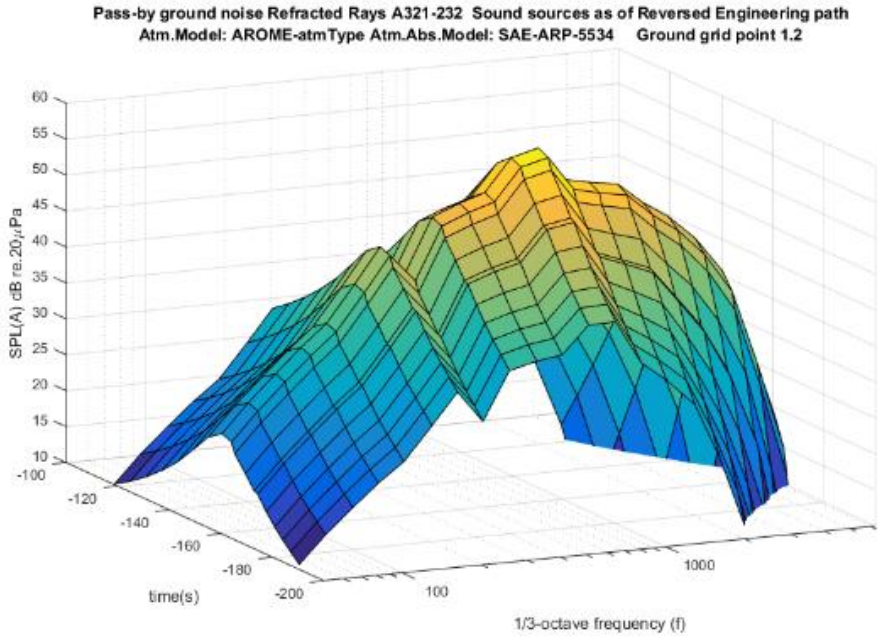

Figure 4. Example of aircraft pass-by noise 1/3-octave spectrum, L_A *(t,*$f_{1/3\ oct}$*)*

4. SAFT computational models and their input

In this chapter we go through the central SAFT computational models and their input. The disposition follows basically the order in which the user meets the different models and corresponding input when running SAFT. First an outline of the central input: the aircraft state-trajectories and input to these and the representation of sound sources in general (4.1). Then follows, in chapter 4.2 to 4.5 presentation of the needed state-trajectory input and models behind the different computational paths for single pass-by noise contours computation. These involves: the "integrated method"/ECAC Doc.29 (4.2), NPD-data based reversed engineering (4.3), measurement based noise sources (4.4) and full semi-empirical sound source modelling (4.5). After this review of the individual computational paths an outline of specific SAFT features and sub-models within those main computational paths are outlined in chapter 4.6 to 4.9. Comprising: current ground grid technique (4.6), selection of specific receiving points for noise time histories (4.7), atmosphere model and data (4.8) and the Transmission Loss, TL (4.9).

4.1 Overview state trajectories and noise sources

The concept "state trajectory" in SAFT regards not only the aircraft position as a function of time, but also some additional data about the "state" of the aircraft needed to define the aircraft as a moving noise source. The type and amount of data needed for defining the state and the related noise source depends on the type of noise source and the method for determination of the resulting noise on ground.

Typically a state trajectory is established in three steps: step 1 - the profile (distance flown + altitude), step 2 - groundtrack (lat, long) and in step 3 - the complementary data enough to get either a time and frequency dependent directive noise source for simulation methods or simply an engine power setting as a function of time for integrated methods.

In the noise computation run-types 1-3 as of Table 1 , i.e. either an integrated/ECAC Doc.29 based one (1,2) or the simplest simulation based one, a so called "Reversed engineering NPD-based" SAFT-run (3), the route is selected by a choice of a runway[8] and TMA entry point[9] -pair, see Figure 5 and Figure 6. From these start- and end positions either a standard route is selected [5] or the user may define a new arbitrary route with the support of SAFT. On top of this route/groundtrack the flight profile is positioned and resulting in a 4D-trajectory[10] fitted to a 50 feet altitude at the runway threshold. Currently in SAFT, the only pre-programmed flight profile alternative is the default approach ANP-data profile for the selected aircraft type. Though, if the user want to model a profile differing from the default case approach ANP-profile, which usually would be the case, e.g. compared with default one, none, or a longer, level flight might be wanted, and other configurations/speeds and trust settings as well, the following work-around has to be applied: The file containing the default ANP-profile data is originally named Default_approach_procedural_steps.csv [7]. This file has to be

[8] More specifically: a runway (RW) threshold position is selected, then if nothing else is done the touchdown is made such as that the RW-threshold is passed by the aircraft at a height of 50 feet.

[9] Runway and TMA regards in the current version Arlanda airport outside Stockholm, more airports could rather straight forward be added if asked for.

[10] 4D here relates to the position+time

renamed and then replaced with a file with the same name but the new wanted profile data given by the user. [NOTE: This is a functionality which is planned to be refined in coming SAFT-versions].

In the [NOTE:] not yet implemented computation run-type 4 as of Table 1, i.e. the "noise measurement based noise source" case, the 4D trajectory data could come from either a flight simulation (outside SAFT), real flight ADS-B [15] data, radar track data or even a standard ANP profile + groundtrack. The noise source for a specific aircraft type will in this case be established from a number of pass-by noise measurements on ground + "back propagation", i.e. a removal of noise propagation effects on the measured noise to reach the approximate noise at the source.[11]

A full noise source simulation, as from a Table 1 run-type 4, is preceded by a state-trajectory preparation with the Chalmers computer programs GESTPAN [16] for engine-performance and CHOICE [17] for the establishment of individual semi-empirical[12] noise sources.

The four main groups of noise source models are outlined in the following paragraphs, Integrated method and its state trajectory input (ECAC Doc.29) in paragraph 4.2 – not a noise source model in the real sense, but a direct resulting noise level on ground correlated to the thrust setting - and sound source models for the different simulation methods in paragraph 4.3 to 4.5. These last, "real", sound source models all represent the sound intensity level at 1 m as a function of time and frequency. Currently "frequency" within SAFT relates to 1/3-octaves broad band noise from 50Hz to 5kHz. NOTE: Tonal ("narrow band") noise, such as from fan blade pass frequencies, is not yet handled but is planned to be introduced in future versions of SAFT.

It should be emphasised again that the NPD-data, which SAFT run-path 1 to 3 rely on, constitute a strong simplification, this is since the original noise data (gathered and established in conjunction with noise certification measurements of aircraft [18]) represent only one speed (160 knots) and "full" configuration. Consequently the NPD data lacks possibilities to reflect general procedures and approach scenarios in any detail. Moreover, for some aircraft, e.g. A321-232, the NPD data, an interpolant matrix setting up the noise levels at a set of distances as a function of the CNT, is given only for 2 CNT-values, thus making a questionable extrapolation outside the CNT-span needed in many cases.

At this stage only one airport is integrated in SAFT, Arlanda (ESSA) airport, the main Stockholm airport ca 35 km north of the city. This means that today's standard route within the TMA are predefined and ready to read in with regard to TMA-entry-point, groundtrack and runway. See Figure 5 and Figure 6. NOTE: at least for all the simulation based computational methods a free choice of trajectory groundtrack and positioning of this in lat, long is recommended to be implemented in future – i.e. no need to incorporate a RW threshold or other fixed 2-or 3D point.

---

[11] Here a standard procedure for defining sound sources is applied, i.e. specifying its sound intensity at a distance at 1m as a fcn of direction, time and frequency

[12] "Semi-empirical" is, with regard to noise sources, relating to models based on correlations established through noise measurements on running turbo-fan engines, typically reduced to a few independent flow and thermodynamic variables

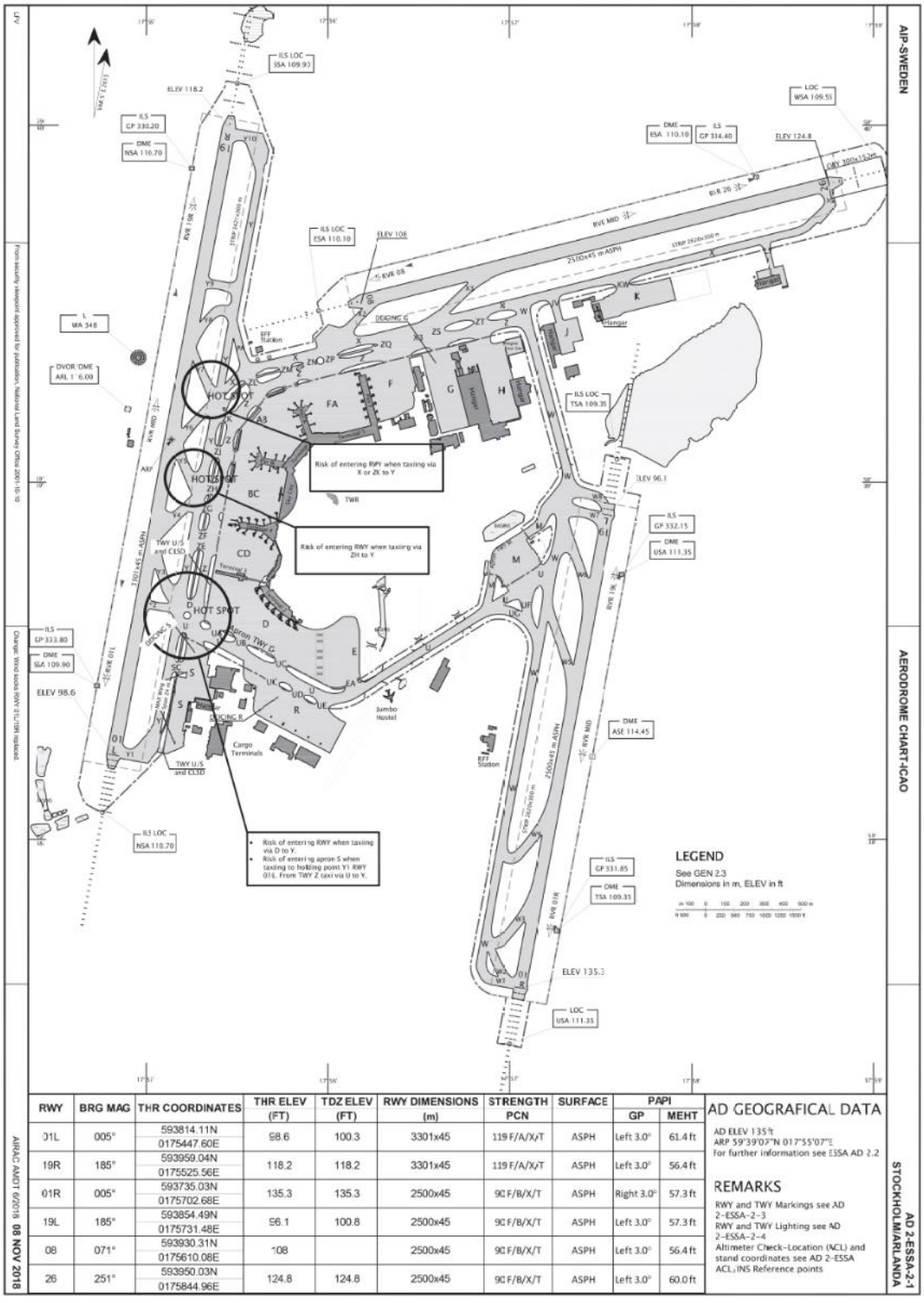

RWY	BRG MAG	THR COORDINATES	THR ELEV (FT)	TDZ ELEV (FT)	RWY DIMENSIONS (m)	STRENGTH PCN	SURFACE	PAPI GP	PAPI MEHT
01L	005°	593814.11N 0175447.60E	98.6	100.3	3301x45	119 F/A/X/T	ASPH	Left 3.0°	61.4 ft
19R	185°	593959.04N 0175525.56E	118.2	118.2	3301x45	119 F/A/X/T	ASPH	Left 3.0°	56.4 ft
01R	005°	593735.03N 0175702.68E	135.3	135.3	2500x45	90 F/B/X/T	ASPH	Right 3.0°	57.3 ft
19L	185°	593854.49N 0175731.48E	96.1	100.8	2500x45	90 F/B/X/T	ASPH	Left 3.0°	57.3 ft
08	071°	593930.31N 0175610.08E	108		2500x45	90 F/B/X/T	ASPH	Left 3.0°	56.4 ft
26	251°	593950.03N 0175844.96E	124.8	124.8	2500x45	90 F/B/X/T	ASPH	Left 3.0°	60.0 ft

AD GEOGRAFICAL DATA

AD ELEV 135 ft
ARP 59°39'07"N 017°55'07"E
For further information see ESSA AD 2.2

REMARKS

RWY and TWY Markings see AD 2-ESSA-2-3
RWY and TWY Lighting see AD 2-ESSA-2-4
Altimeter Check-Location (NCL) and stand coordinates see AD 2-ESSA ACL, INS Reference points

Figure 5. Arlanda airport, ESSA runways (01L, 19R, 01R, 19L, 08, 26) [4]

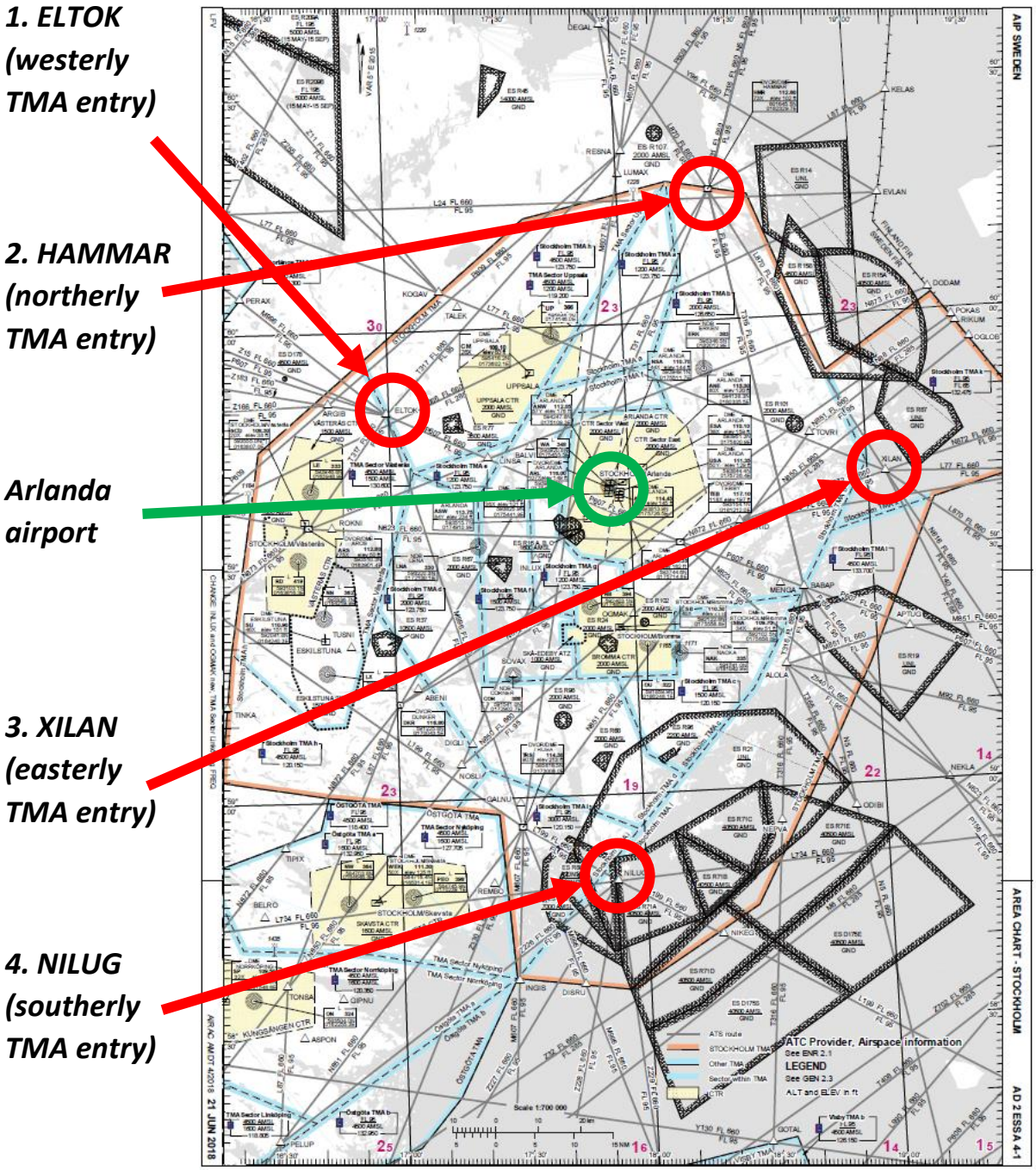

Figure 6. Stockholm TMA with its entry points and Arlanda Airport [5]

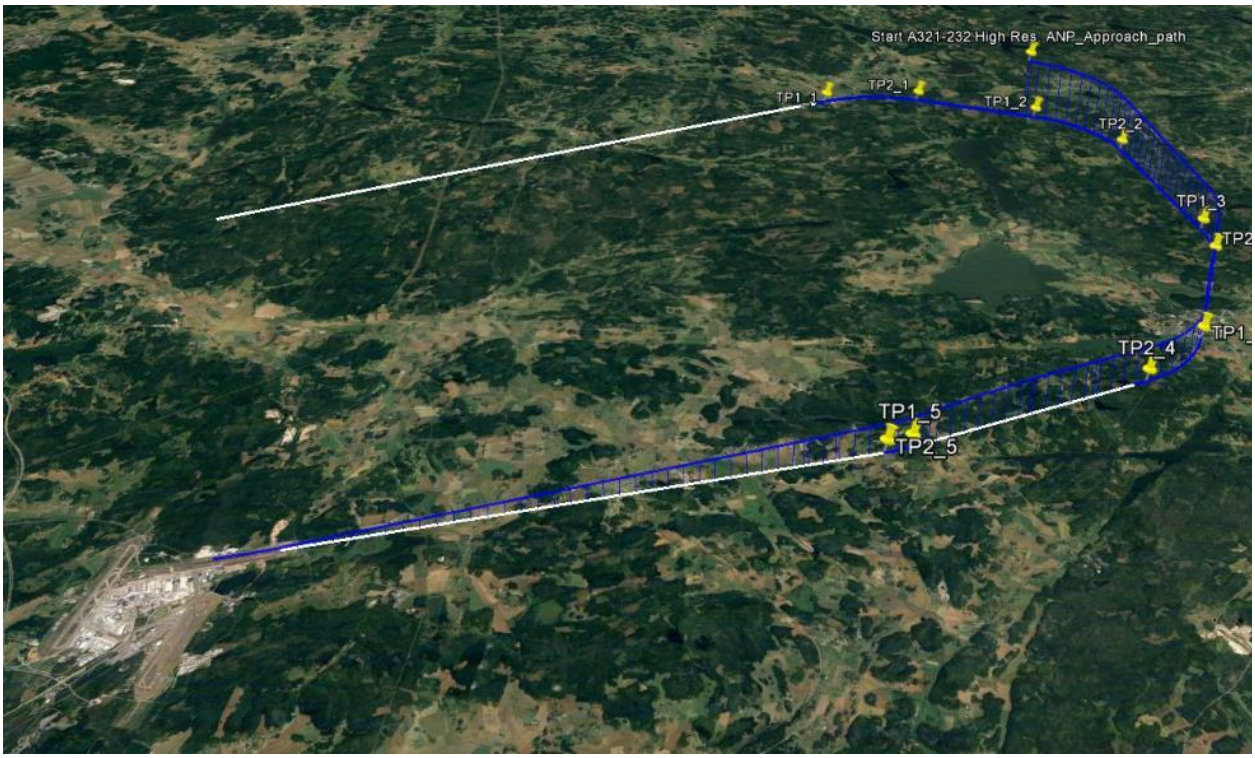

Figure 7. Example of user defined groundtrack approach to RW 26 from west (TMA entry ELTOK) ANP standard profile for A321-232 added

Comment with regard to aircraft profile and procedures:

During the SAFT project a performance database for a A321-232 based on PEP [19] runs has been established. This dataset spans basically the complete parameter-space for possible A321-232 approach state-trajectories with regard to descent angle, speed, engine power, fuel consumption, configuration and mass. These building block data are aimed for modelling general approach procedures but is not yet structured in a manner that allows for a direct algoritmised application.

NOTE: if found needed these data could be structured into simpler read-in building blocks and supported by semi-graphical routines or similar in order to exploit the full potential of them.

The noise sources are defined in an aircraft body coordinate system with a longitudinal directivity, θ, and a circumferential d:o, φ. as shown in below.

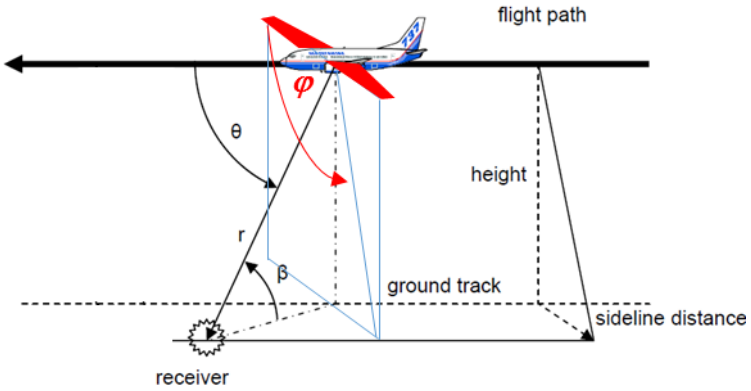

Figure 8. Definition of aircraft noise source directivity angles and incident angle, β

4.2 Integrated method and its state trajectory input (ECAC Doc.29)

In the case of the ECAC Doc.29 method the needed input state trajectory data is limited to position (lat, long, altitude) as a function of time and related to this a knowledge of the corresponding mass and thrust setting. The 4D-trajectory might either be simulated, in tools outside SAFT, or relate to real flight, e.g. radar or ADS-B data [15]. In the situation we get this 4D-trajectory from real flight data estimates of the thrust setting is needed for each configuration[13] + the overall aerodynamic properties for each configuration along the trajectory. The aerodynamic properties are, for a large part of the current aircraft fleet, given in the ANP-data [14] – integrated in SAFT and in data related to the BADA-tool [20] (to be run beside SAFT). It could be noted here that for some aircraft types no aerodynamic data is given and thrust estimates modelling is not possible outgoing from the ANP-data set. For these other aircraft types only so called fixed point sets of profile positions, thrust and speed are given, i.e. no freedom for state-trajectory modelling given these last kind of ANP-data.

As mentioned above, in the current SAFT-version, a change of the content in the (fixed) input file Default_approach_procedural_steps.csv has to be made in order to input a state-trajectory/procedural sequence that differs from the standard ANP-input case. The current internal SAFT way to get a thrust setting when knowing the aircraft configuration and the 4D-trajectory, is based on equation *B-20*, *B-21* and *B-22* in [6], where *B-20* is repeated here as eq.(1)1

$$\frac{F_n}{\delta} = W\frac{R\,cos\,\gamma + \sin\gamma + a/g}{N\delta} \qquad (1)$$

where: F_n = net thrust per engine (lbf)
δ = ratio of ambient air pressure vs standard air pressure at sea level
F_n/δ = corrected net thrust per engine , CNT, (lbf)
N = number of engines
R = ratio of the aircrafts drag and lift coefficients (=D/L) for the current configuration
D = Drag coefficient, L = Lift coefficient
γ = descent angle
a = acceleration (ft/s^2)
g = acceleration due to gravity (ft/s^2)
W = aircraft weight (lbf)

The unknowns in eq. (1), assuming a known 4D-trajectory, are the aircraft weight, W, and configuration - only the airline has access to these data, e.g. from FDR-data [21] and accordingly assumptions about the amount of fuel left and payload has to be made in most cases. Supporting estimation approaches for aircraft mass, configuration and other performance parameters may be found in BADA resources (trajectory simulation) and in [22], [23], [24] and references therein. Typically aircraft mass estimation methods applied on real flight data are based on a Bayesian approach and need a rather long stretch of the flightpath to reach an good estimate.

NOTE: The current SAFT-version do not cover ECAC Doc.29 based departure data, only approach procedures and related data are implemented yet – (Further: Since the ECAC Doc.29 based integrated method

[13] configuration = aircraft high lift devises positions + landing gear in/out

in SAFT is primarily thought of as a complementary tool aimed to enable comparisons with the more detailed simulation methods, the main effort in future work is directed towards these latter methods, which may suggest that an implementation of an ECAC Doc.29 computational path for take-off/departures is not stressed at the moment.)

NOTE: Only a few aircraft types – with related ANP data - has been run and tested within SAFT run-path 1 to 3 yet. Among them: A320-211, A320-232, A321-232, 737-700, 777-3ER (and 737-800[14])

Figure 9 and Figure 10 below show examples of standard ANP-approach state trajectory data for an Airbus 320-211 and a Boeing 737-700 as read in and plotted by SAFT. Note the two different curves in both figures, one showing the CNT (per engine) and the other the altitude as a function of distance from the runway threshold. For some unknown reason the ANP profile data for the A320 aircraft contain a level segment while the Boeing 737-700 does not. Moreover the Boeing data, for this plane, goes over 3 different steps of slat/flap configurations between "zero/clean" and landing while the Airbus data, rather unrealistic, goes directly from "zero/clean" to "full" configuration. When running SAFT the user have to select a time resolution for the trajectory data, typically one or a few seconds, on which an interpolation of position and thrust is based, starting out from data such as in Figure 9 and Figure 10. For a more comprehensive description of the ECAC Doc.29 method see [6].

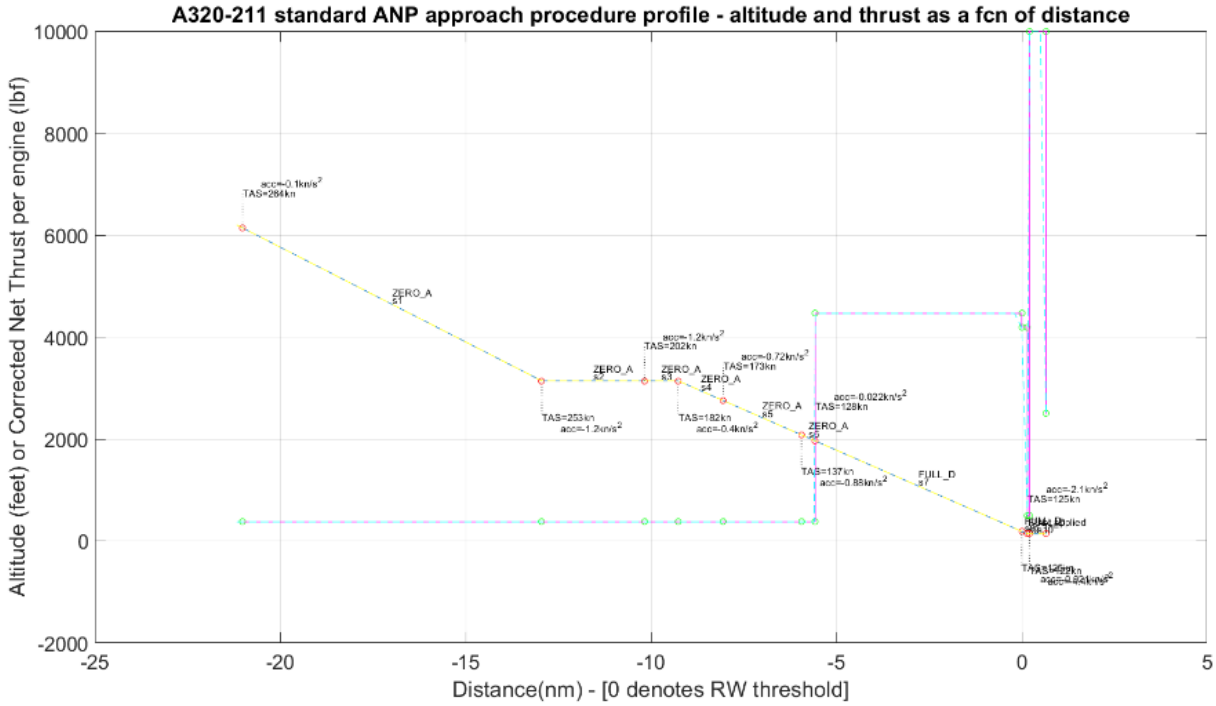

Figure 9. Example standard ANP-data altitude and CNT for an Airbus 320-211 as a fcn of distance
Text: TAS =True Air Speed, acc = acceleration, ZERO_A, FULL_D = configurations denoting "clean" and full slat+flap + LG[15] down respectively

[14] The 737-800 ANP state-trajectory data is given as a so-called "fixed point set" which means that not enough parameters (such as *D/L* data) are given to make it possible to modify/model other trajectories within SAFT based on these, other resources outside SAFT and the ANP-database are needed to handle this and other "fixed point data – aircraft"

[15] LG = Landing Gear

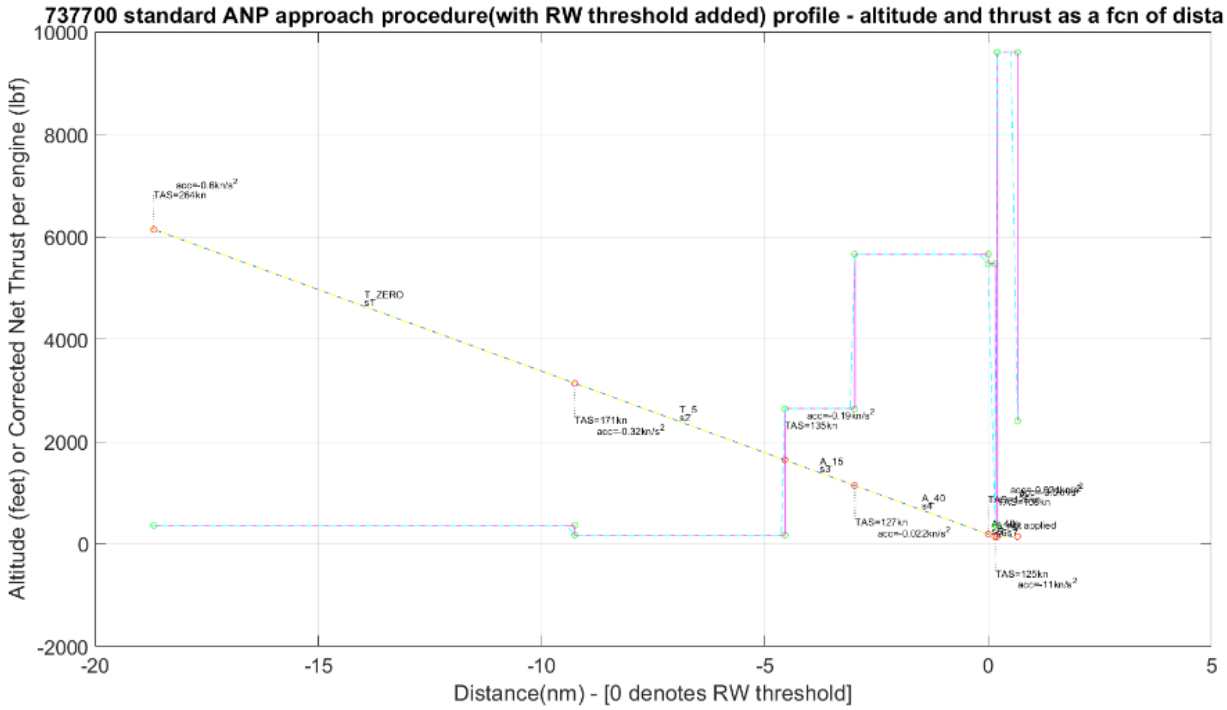

Figure 10. Example standard ANP-data altitude and CNT for an Boeing 737-700 as a fcn of distance Text: TAS =True Air Speed, acc = acceleration, T_ZERO, T_S, A_15 and A_40 = configurations denoting different stages of flaps/slats deployment (in degrees)

4.3 Reversed engineering NPD-based model and input

The name "Reversed engineering" refers here to a backward computation of sound intensity level at the noise source given a known sound intensity level at a receiver, sometimes called "backpropagation". In our SAFT case, "NPD-based reversed engineering", the starting point ground noise is taken from the ANP/NPD-data, and more precisely the SAFT algorithm starts out from the NPD-data given as SEL (Sound Exposure Levels) of the selected input aircraft type.

In short the procedure to reach a directive sound source need:

1. ground noise estimates, in our case the NPD SEL-levels.
2. the flight and trajectory circumstances these data represents, namely an aircraft passage at a constant distance with the speed of 160 knots passage in configuration "Full" [18], i.e. full flap/slat deployment + LG down
3. *an assumed 1/3 octave spectrum* for the aircraft type to study
4. *an assumed directivity of the source* (NOTE: should better be a frequency dependent directivity, but currently in SAFT only a simplified "total" directivity input is applied)
5. the absorption damping inherent in the NPD-data, i.e. as given in the SAE AIR-1845 standard [25]

As seen above, the needed state-trajectory input[16] here differs from a ECAC Doc.29-based run by the added point 3, 4 and 5 data.

By running the same situation as represented by the NPD-SEL data in a time-stepping code like SAFT, i.e. an aircraft of the wanted kind flying in a straight line over a receiving position (at 1.2 m height above ground as specified) at the same altitudes as in the NPD-data with a *fixed arbitrary spectral sound intensity level (=candidate source)* we can get a SEL estimate for the different sound propagation distances given in NPD-data (in meter: 61 122 192 305 610 1219 1920 3048 4877 and 7620 m). This biased estimates are then trimmed by adding a constant to the candidate source which gives the best fit to the NPD-data SEL-levels. The approach follows with some exceptions the method proposed in the EU-project IMAGINE [26]. These differences in SAFT are believed to be mainly:

- the user need to select a default or previously saved longitudinal directivity, theta=0:10:180 degrees, or generate a new arbitrary directivity, from nose to aft (NOTE: in current SAFT version the circumferential directivity is determined by the analytical function given in ECAC Doc.29 3rd.Ed. Vol.2 eq.4.12 for all frequencies. Also this directivity could be changed and made frequency dependent in future SAFT-versions)

- sound intensity (instead of sound power) is created for the given atmospheric condition, rho, c accounted for

- Doppler effects is by default included in the source generation, but the user may disregard these when creating the sound source

It should be emphasised that the user may apply any spectral shape, while the ANP spectral class alternative is default [27]. It could be noted that these spectra typically show a large spectral dip which might suggest that ground effects are not properly removed therein, see Figure 11. Here we also see the rather unrealistic invariant spectral shape though the speed and configuration changes along the flight (the configuration changes only once, from "clean" to "full" in the last segment, the final approach – a very unconventional approach but anyhow the default ANP approach trajectory for A321-232 and A320-211/232).

NOTE: Currently – due to limitations of NPD-data with regard to configurations (only "full" configuration reflected in NPD-data) – there is no straight forward way to account for spectral changes with regard to either thrust setting, configuration or speed. - Future ways to fill these gaps are expected from supporting SAFT with ULLA-project noise measurements.

NOTE: in the current version a new sound source estimate is generated each time a new "NPD-based reversed engineering case" is run. - Instead a re-use of previously saved source estimates could considered to be implemented. New runs could then be based on these previous source estimates by introducing interpolation with regard to thrust setting and speed, assuming previous estimates are spanning the needed parameter space.

[16] It may be noted here that beside the state-trajectory input another significant difference between a SAFT ECAC Doc.29-run (integrated method) and a "NPD-based Reversed engineering"-run (simulation method) is that the last one has a possibility to include a refractive atmosphere and a need for reading in or creating + applying a TL-representation of the atmosphere (see chapter 4.8 Atmosphere model and data)

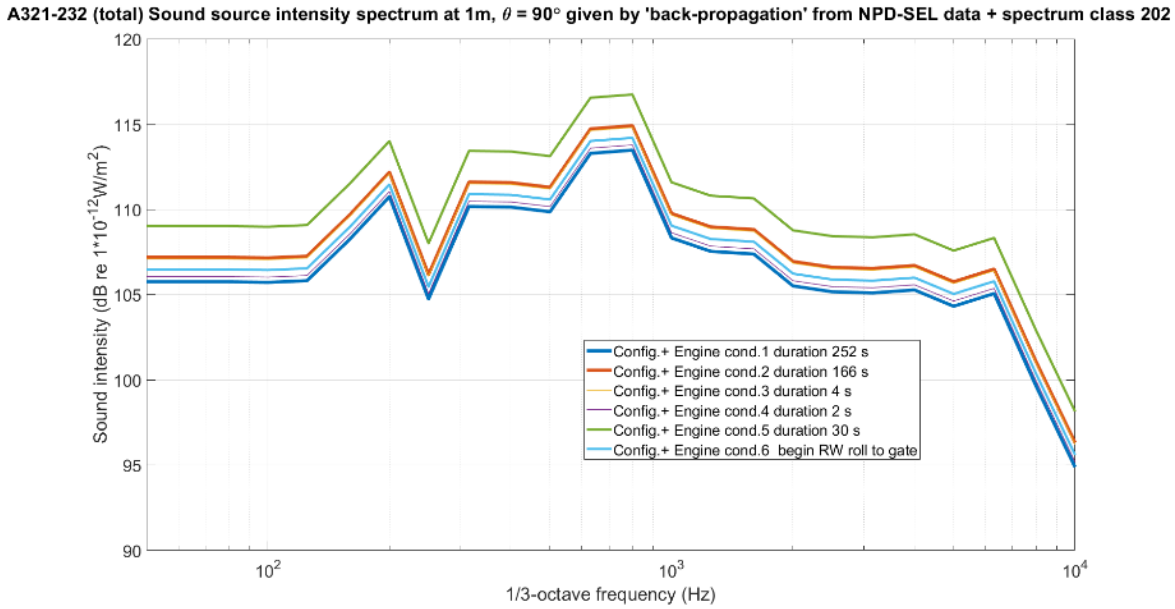

Figure 11. Example sound source spectrum given for A321-232 if default ANP-state trajectory and directivity as of Figure 12 and default ANP-spectra 202 for approach is selected.

The default total (over all frequencies) longitudinal directivity in the NPD-based reversed engineering source establishment is taken as a slightly trimmed 777-300ER with GE90 engines during approach. The reason for this choice is simply that it is one of the few cases found in the literature of directivity for a modern high by-pass turbo fan engine in approach, expected to show rather weak jet noise compared with the fan noise, and stronger in the forward direction than backwards. The trimming in this SAFT default directivity, compared with measurement result shown in ref. [28], is related to a limitation of the directivity of ±10 dB (relative 90°) at any frequency and in any direction. See Figure 12 and Figure 13 below.

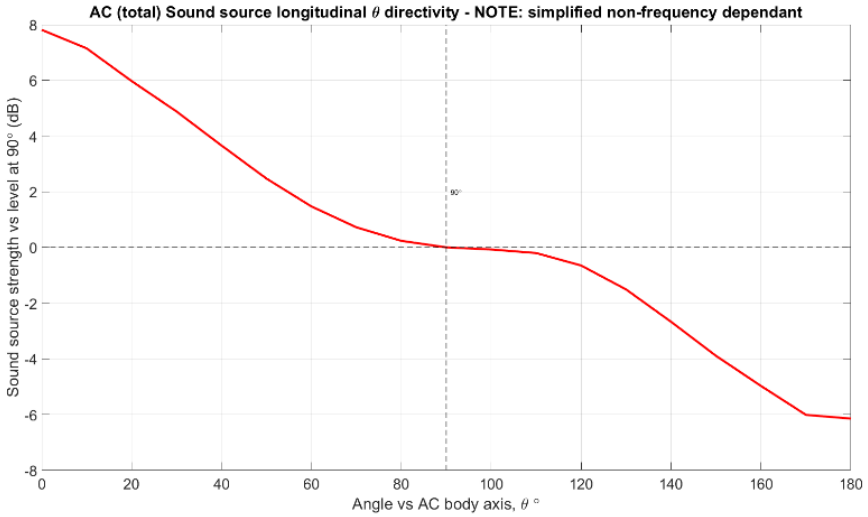

Figure 12. Default longitudinal directivity for total sound intensity (used for all frequencies) in SAFT NPD-based reversed engineering noise source related to source strength levels in Figure 11.

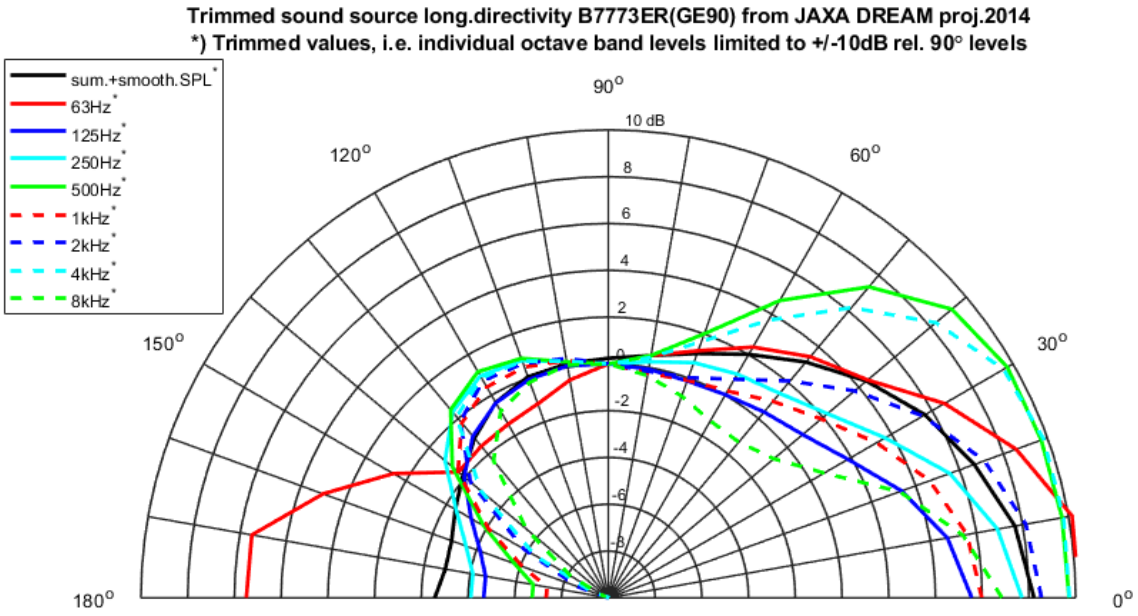

Figure 13. Individual 1/3-octave band longitudinal directivities behind artificial total level trimmed *[28]* directivity shown in Figure 12.

Note that these default spectra and directivities should be seen just as a starting point before better data are at hand, could be from CSA aircraft noise measurement project ULLA [12] or else. In the long run even the original NPD-data might be extended to cover more flight conditions.

4.4 ADS-B trajectory and "back-propagation" noise source (ULLA-project)

This part is still in its planning stage and will be carried out as a part of the coming CSA-financed project CIDER, starting during the fall of 2019 [13]. The work will be carried out in tight cooperation with the CSA project ULLA [12]. The ULLA project will contribute with high quality aircraft pass-by noise measurements. Some of the CIDER pre-studies and ULLA result from this cooperation is outlined below.

The coming work is dedicated to a measurement based aircraft sound source, a method we given the preliminary name MRS as in Measurement and Reversed engineering based noise Source. The idea is to apply high quality aircraft noise measurements which are time correlated with the real aircraft flight trajectory. The link between these two resources is a time-stepping program that accurately (time-, frequency- and amplitude wise) catches the same physical events, i.e. a physical model of the complete sound propagation chain, in our case SAFT. With such a simulation source code at hand an implementation of a "back-propagation" is not far away, at least in principle, given the rather simple eq.(5) below. Starting with the sample *i* source sound intensity given as:

$$L_{I,source,i}(t, f, \varphi, \theta, \text{config}, \text{"thrust"}, Mach\ no, \text{"}AC-type\text{"}, p(z), T(z), \dots) \tag{2}$$

and then looking at what it may produce in terms of noise on ground, eq.(3) :

$$L_p = L_{I,source,i} + TL_{tot} \tag{3}$$

where TL_{tot} represents all physical factors contributing to the losses and/or amplification of noise intensity level along the propagation path + the factor between sound intensity level to sound pressure level. Assuming we can estimate all the parts of TL_{tot} (see chapter 4.9 below) we may establish eq.(3) both from measurements and numerically, but with different unknowns (green = known variable, red = unknowns), eq.(4):

$$L_{p,mic,i}^{meas} = L_{I,source,i} + TL_{tot} \ \ and \ \ L_{p,mic,i}^{SAFT} = L_{I,source,i}^{SAFT} + TL_{tot}^{SAFT} \tag{4 a,b}$$

where *"SAFT"* denotes numeric simulation and *"meas"* noise measurements. With the knowledge of the position (and orientation) of the aircraft + atmospheric conditions we get the "back-propagation", the central equation of the MRS-approach:

$$\hat{L}_{I,source,i} = L_{p,mic,i}^{meas} - TL_{tot}^{SAFT} \tag{5}$$

where $\hat{L}_{I,source,i}$ is an estimate of the total sound source intensity of the aircraft at a certain time, over all geometry of source-receiver system, speed, configuration, engine and surrounding air conditions, source directivity, ground properties as a function of frequency. After gathering source estimates of this kind, eq. (5), from several SAFT runs (path 7), error estimates, statistical- and system recognition methods are planned to be applied in order to determine total combined sound sources for a selected set of common aircraft types over an parameter space found sufficient.

For the bulk of data sets aircraft positioning, speed and to find acceleration- (and thereby) thrust-patterns, ADS-B data as given by OpenSky [15] is planned be applied. For specific aircraft individuals, of the type A321neo, also FDR-data is planned to be applied.

For the environmental variables, atmosphere and ground, AROME data, when possible checked and trimmed with local measured weather data, and ground altitude + surface type at microphone positions will be used in the source estimate procedure.

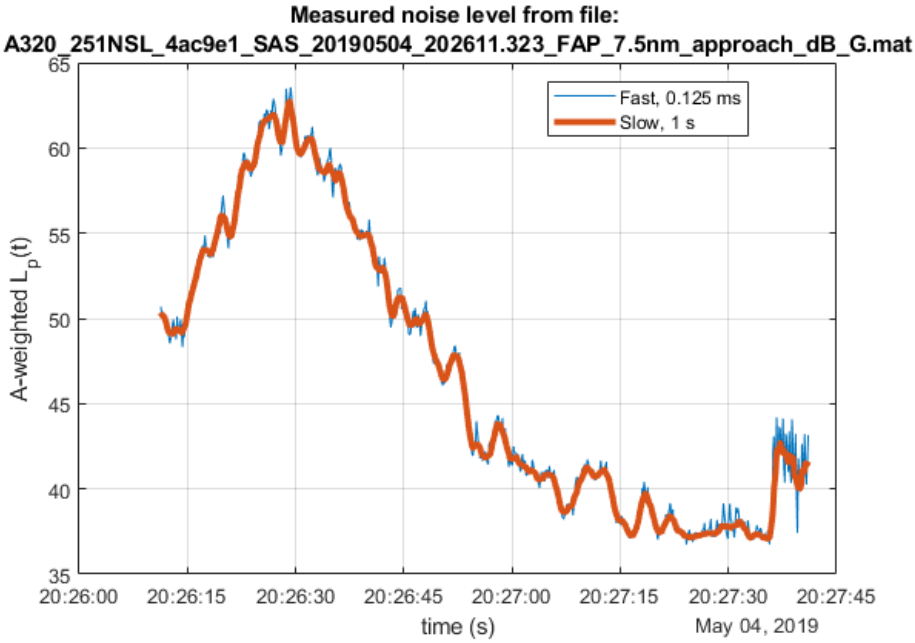

Figure 14. Example ULLA A320 pass-by noise measurement, SPL as a fcn of time

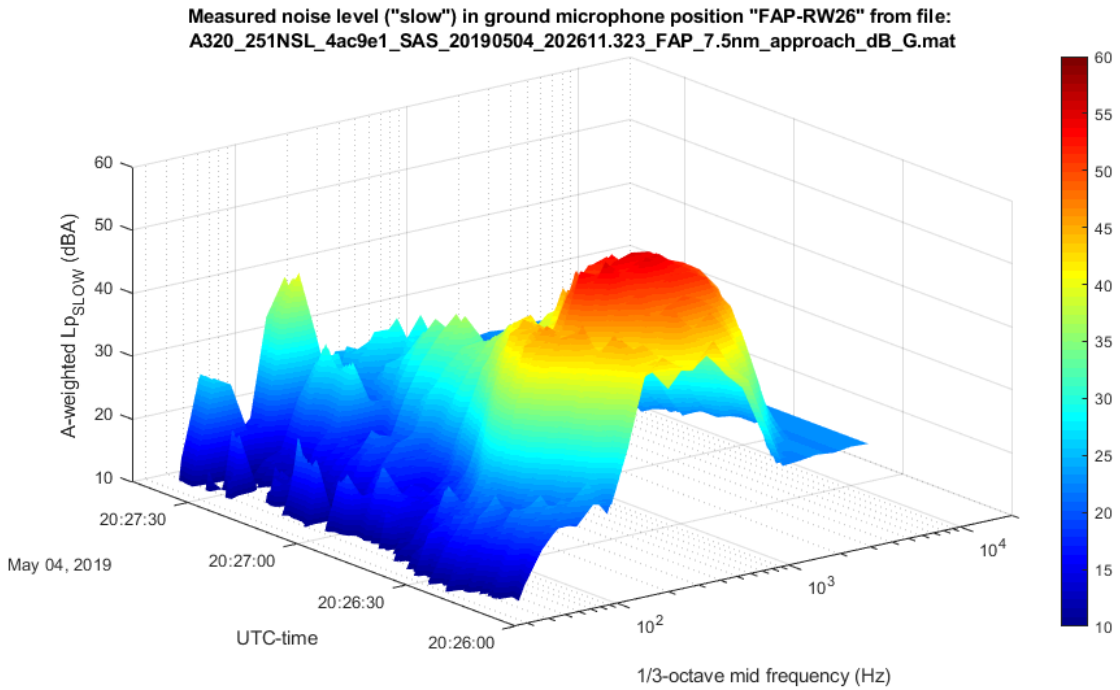

Figure 15. Example ULLA A320 pass-by noise measurement, spectrum as a fcn of time

In Figure 14 and Figure 15 above an example aircraft pass-by noise measurement is shown, and in the following, Figure 16 to Figure 21, ADS-B trajectory data related to these noise measurements are presented.

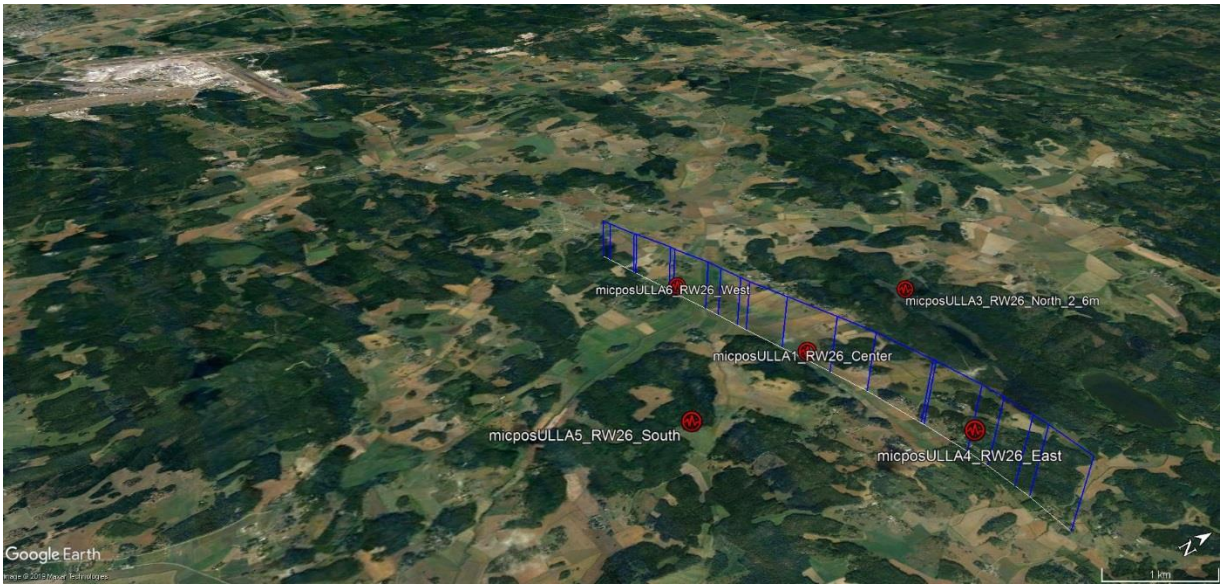

Figure 16. Example ADS-B trajectory related to noise measurement shown in Figure 14

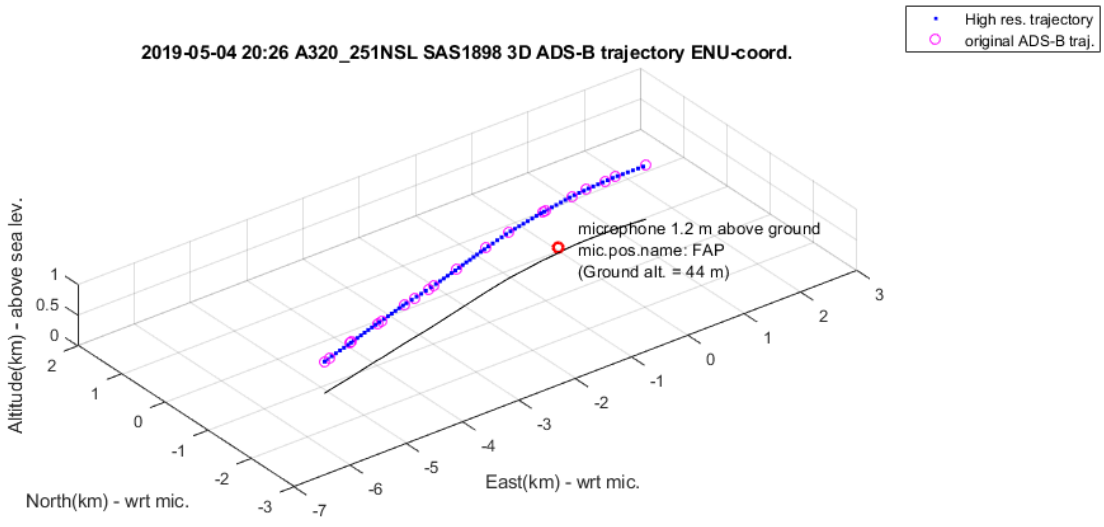

Figure 17. Example ADS-B trajectory same data as in Figure 16 but re-sampled

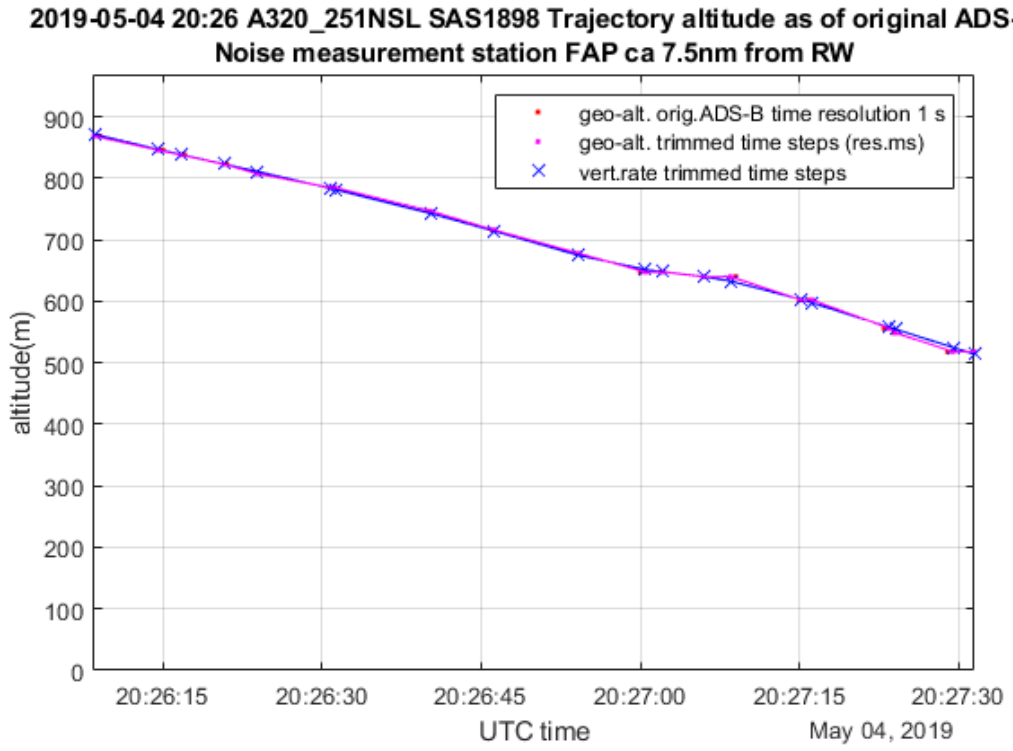

Figure 18. Example ADS-B trajectory altitude related to noise meas. shown in Figure 14

In ULLA independent weather resilient measurement stations are positioned around Arlanda airport. These stations consist of :

microphone, computer (Raspberry Pi), internet connection and solar power/battery support

Noise measurement as well as related trajectory (ADS-B) data can thereby be reached by project members from their office over internet. The noise measurements are triggered, supported by OpenSky ADS-B, when an aircraft movement take place within a certain area.

Some open matters with regard to these data are:

- variation, uncertainties along the complete computational chain
- identification of independent variables, thrust, configuration/LG, speed, static pressure and temperature at aircraft altitude, ... ?
- optimal positioning of microphones wrt aircraft axial directivity and other searched properties?

Figure 19. ULLA measurement station

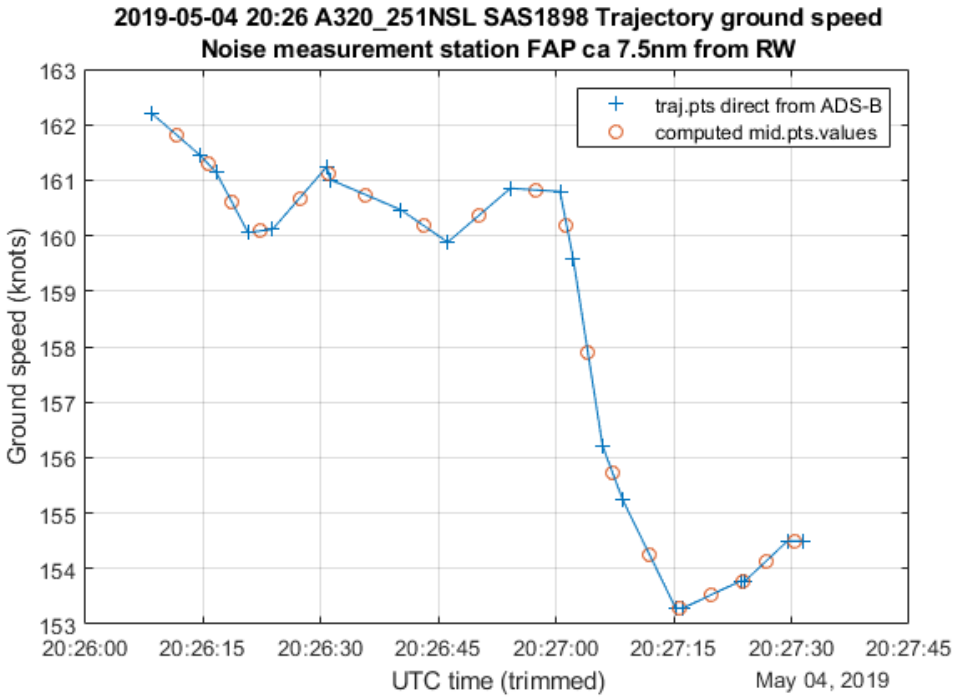

Figure 20. Example ADS-B trajectory ground speed related to noise meas. shown in Figure 14

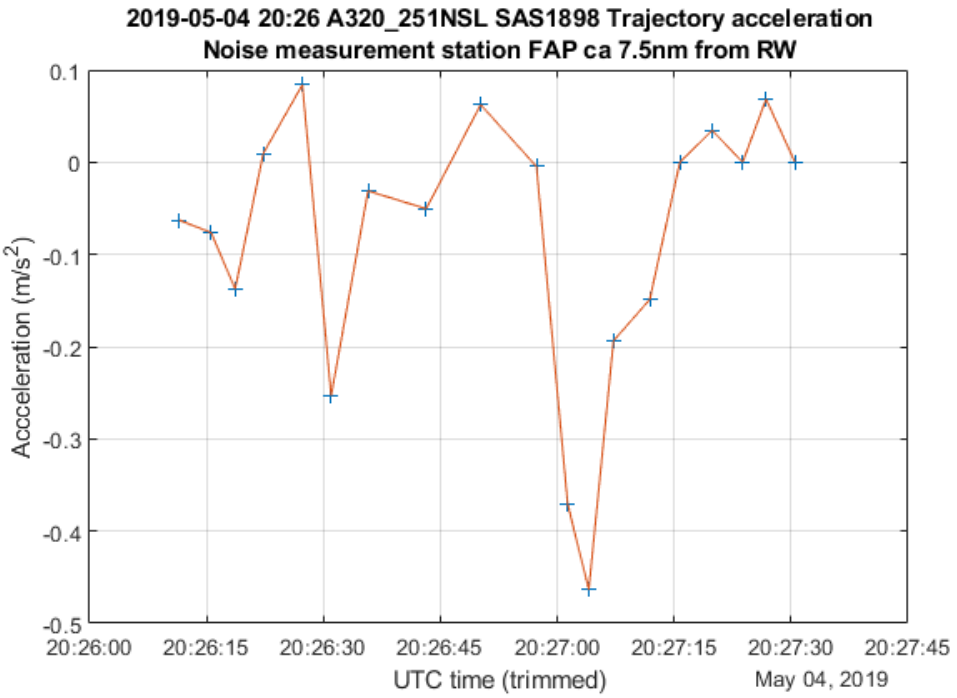

Figure 21. Example ADS-B trajectory acceleration computed from ground speed with given time resolution related to noise measurement shown in Figure 14

An open matter in the coming noise source estimations is whether the ADS-B time resolution will be enough for estimates of the aircraft thrust via accelerations such as shown in Figure 21. Matters and patterns like: a) deceleration found in combination with source noise level reduction = possible reduced engine power reduction(?) and b) deceleration found in combination with source noise level increase = possible configuration change to higher flap or/and LG deployment (?) to be studied in detail, together with related (estimated) source spectrum changes.

4.5 Full semi-empirical noise source modelling and input

4.5.1 Flight mechanics & engine conditions

Flight mechanics is most straightforwardly solved as a system of nonlinear equations coupled to the dynamic equations of the aircraft. Although the propulsion system is also dynamic system with multivariable controls being active, it is usually more then sufficient to assume that the propulsion system can be approximated as stationary. This gives rise to a set of non-linear equations, typically 10-15 degrees of freedom. The non-linearity is usually modest, but the solution process is complicated by limited ranges of component definitions and singularities that may arise if formulated in unsuitable parameters. An example is when sections in the engine reaches supersonic speed upon which further increase in a rotational speed does not generate an increase in mass flow. Whereas it is usually sufficiently accurate to treat the propulsion system equations as steady state, the aircraft equations of motion have to be treated as dynamic and at least solved in 2D. This normally implies using the angle of attack α which determines aircraft aerodynamic performance and the motion of the centre of gravity, denoted γ, to describe the state of the aircraft.

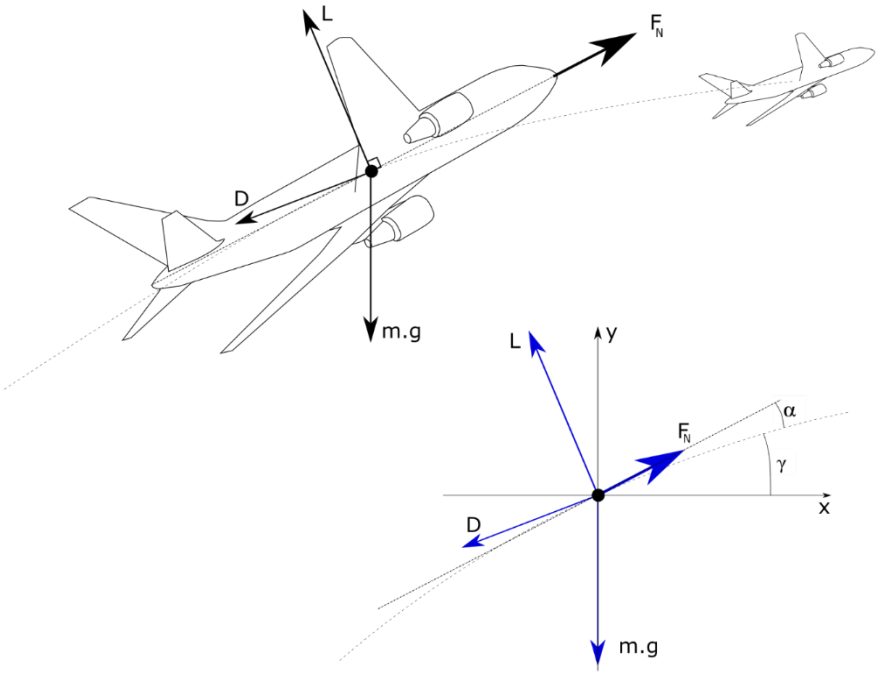

Figure 22. Schematic force balance – generic aircraft

Normally the flight performance is established from the fundamental aerodynamic forces such as Drag (D) and Lift (L). Semi-empiric methods to establish these forces with quite good accuracy exist both for existing aircraft designs and for predicting the performance of future aircraft.

A physics-based representation of the propulsion system and the aircraft allows a number of different data and computation paths to be used for a certain simulation problem. Firstly, an aircraft and propulsion system model can be set up and using assumptions on engine rating, climb out procedures and ambient weather conditions, a flight path can be computed and conditions in the engine can be derived. These, then form input to the semi-empiric sound source modelling as schematically illustrated in Figure 1. This computational is also the approach that is taken if future aircraft noise performance is to be predicted. For the SAFT project particular project this way to

establish the computational path was demonstrated by modelling the Airbus321-231 having the V2533-A5 propulsion system.

The physics based formulation gives a substantial degree of freedom to completely, or partially use additional data to the modelling. For instance, the flight path may be known, allowing acceleration and thrust to be computed. Then, this degree of freedom and large parts of its associated uncertainty can be eliminated. The engine performance is then matched to the computed thrusts rather than that the thrust is predicted. It is also often the case that engine data is recorded and is available for more accurate modelling. These data are then usually applied by updating the assumptions underlying the thermodynamic engine model.

Another interesting case is the case of approach flight. Normally, approach is undertaken using a constant γ, see Figure 22, and a constant indicated speed. These additional path constraints actually means that sufficient data (assuming that aircraft settings such as flaps, landing gear position etc is known) actually decouples the engine and aircraft modelling. With known aircraft aerodynamics and initial conditions (aircraft mass) thrust requirements are readily computed. This fact gives some hope that simplified source based models for propulsion can be an effective way to establish inflight noise around airports without exceptional knowledge and data requirements.

4.5.2 Sound sources

Work on a semi-empiric noise code was actually launched at Chalmers almost 10 years ago. At that time it was a master thesis work that laid the first foundations for this modelling environment. Within the SAFT project the MATLAB code was generalized. The original model was cumbersome to update. Changing to a new aircraft or engine required a number of parameters to be hardcoded into the model. This resulted in that every new model was a new MATLAB code. Also, no really useful interface existed so that the model could be used for different purposes. Within the SAFT project the MATLAB model was transferred to Chalmers performance code GESTPAN which allows the source models to be used, not only within the SAFT project but also within future EU-projects predicting performance of future aircraft and engines.

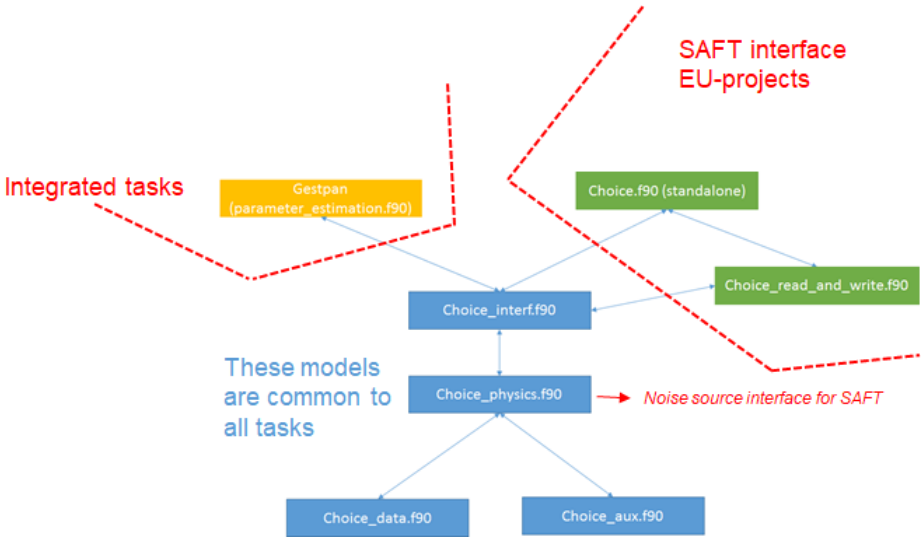

Figure 23. Multi-use of CHOICE (CHalmers nOise CodE)

Choice can be executed stand-alone, be asked to generate noise source matrices to SAFT or be hard-linked to GESTPAN. This software solution does not require any extra overhead, but is automatically achieved by a once and for all structuring of the simulation codes.

In the legacy variant of CHOICE there is still the possibility to go on and evaluate EPNdB at the receiver. This is used to estimate certification noise levels for new propulsion cycles. However, this part of the code will not be developed further, since the ambition with SAFT and the activities in CSA are to develop much more refined and high fidelity models for propagation and simulations. The two simulation scenarios are exemplified in below.

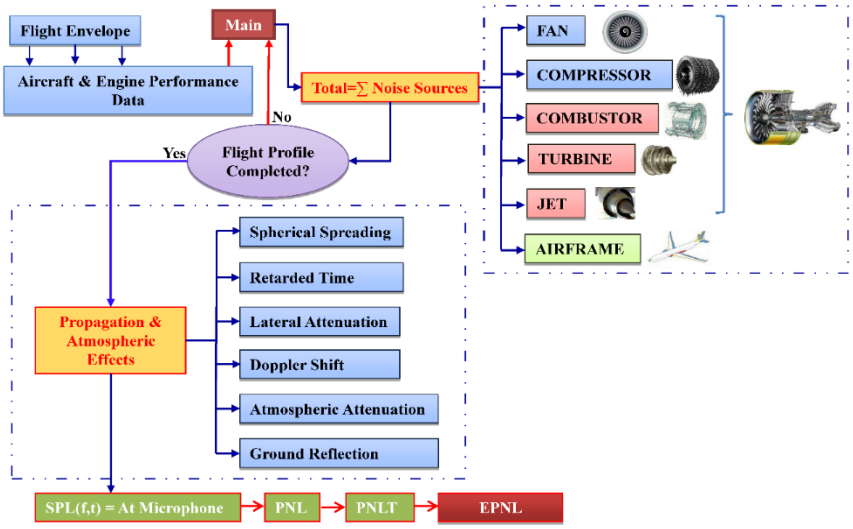

Figure 24. Full noise prediction scheme. Legacy model still used outside CSA and SAFT (from trajectory to microphone)

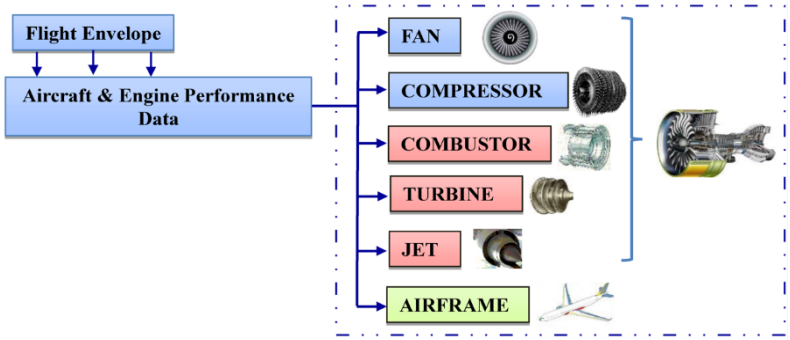

Figure 25. Choice transplant used within SAFT (from trajectory to noise source)

4.5.3 Fan and compressor noise

The methodology used for predicting the noise from fan and compressor inlet duct and fan discharge duct is based on NASA Technical Memorandum X71763 ”Interim Prediction Method for Fan and Compressor Source Noise” [29]. The method employed here is for noise prediction of one stage of fan and compressor. The compressor noise prediction method involves only noise emitted from the inlet duct for the first compression stage. For computing the noise for a two-stage fan, the noise energy of the two stages should be summed to compute the total noise. The correlations are introduced to obtain the broadband, discrete tone and combination tone components for compressor and fan inlet noise and broadband and discrete tone components for fan discharge noise. The total

noise for each noise source will be the summation of all noise energy components. The sound pressure level is calculated in one-third octave band frequencies at free field one meter radius. In our noise prediction case, there is no fan inlet guide vane, duct inlet flow distortions are taken into account and the fan is assumed to be single stage.

4.5.4 Core noise

The combustor noise prediction method is based on ”Aeroacoustic Prediction Codes, NASA/R-2000-210244” [30] and is used for low emission combustor design using acoustic measurements of modern engines. Empirical correlations are developed for two types of single annular combustor (SAC) and double annular combustor (DAC). The correlation for SPL takes into account the combustor geometry, engine cycle conditions, directivity and spectral frequency content. Recent core noise prediction model developed by NASA has taken into account the combustor geometry and the multiple stage fuel injection which will lead to multiple-lobe spectral shape [31]. The discrimination of core noise from other noise sources shows that the spectral noise peaks for single-annular combustors are at 63, 160 and 630 Hz while for double-annular combustors the peaks are found to be at 160 and 500 Hz at the corresponding peak angles. Thus the corrections are developed for the peak SPL at these frequencies for SAC and DAC combustor types separately.

4.5.5 Turbine noise

Turbine noise is estimated based on the method described in ”Aircraft Noise Source And Contour Estimation, NASA CR-114649” [32]. The turbine noise is composed of broadband and discrete tone noise components. Both of these components are related to the turbine’s last stage relative tip velocity, the primary mass flow and local speed of sound at the turbine exit. Furthermore, the discrete tone noise component is also related to the stator/rotor spacing. The broadband and discrete tone noise levels are computed at a radius of 45.7 m from the source. Corrections are applied to obtain the noise level at a free-field, index (R=1 m). Also, both components are normalized with respect to f_0, the fundamental blade passage frequency of the last stage of the turbine. The turbine broadband noise is related to the turbine’s last stage relative tip velocity, the primary mass flow and local speed of sound at the turbine exit. The turbine discrete tone noise is related to turbine’s last stage relative tip velocity, primary mass flow, local sound speed at the turbine exit and also stator/rotor spacing.

4.5.6 Jet noise

Jet noise is estimated based on NASA CR-3786, Russel, J. W., ” [33]. The method is based on the extensive test data to predict the jet mixing noise from circular and coaxial subsonic jet flows. The unique feature of this method is that it can be used both for circular and coaxial jets. Circular jets can be considered as a special case of coaxial jets. The sound pressure levels from the test data are curve fitted as bicubic splines using the least square method as a function of frequency parameter and directivity parameter. A third order Taylor series is employed to do the curve fitting. The equivalent parameters for a coaxial jet are computed by equating the mass, momentum and enthalpy equations of the coaxial jet with a circular jet. The coaxial jet noise is evaluated as a function of the equivalent parameters which are the equivalent flow velocity $Ve/c\infty$, equivalent jet total temperature $Te/T\infty$,

the velocity ratio of the outer stream to the inner stream V2/V1, temperature ratio T2/T1 and area ratio A2/A1. The jet sound pressure level is expressed as the summation of normalized overall power level, directivity index, power spectrum level, the relative spectrum level and three constants which account for the size of the jet, the microphone distance, ambient conditions and the ratio of reference power level and reference mean square pressure level. NOTE: The shock noise due to the supersonic jet flow stream is not included in this method.

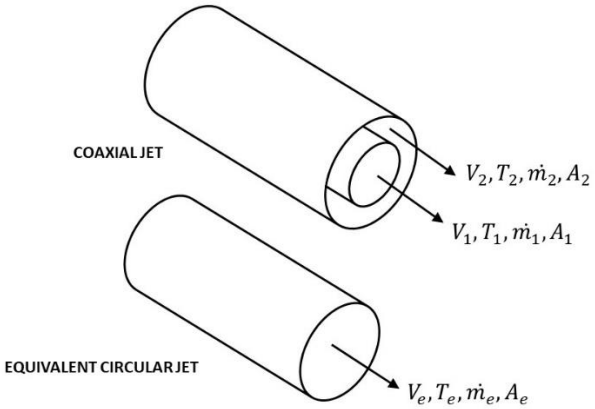

Figure 26. Jet flow state parameters

4.5.7 Airframe noise

The airframe noise estimation is based on the empirical method described in NASA/CR-2004-213255, "Airframe Noise Sub-Component Definition and Model" [34]. The acoustic measurement data is used to generate the noise source map of the wing. The major noise sources are identified, and the wing is divided into sub-components. Then the aerodynamic parameters are calculated for each sub-component and the source map is integrated to compute the far-field spectra for each sub-region. The integrated spectra is then calibrated with free microphone data. Corrections are applied to small scale data to obtain the spectra at full scale and certification conditions. The sub-regions of wing/high lift system with the major noise sources in this analysis are outboard aileron, inboard flap side edge, outboard flap side edge and slat noise. In the present approach the one third octave band spectra at $\theta = 90^\circ$ is computed using the aerodynamic and geometric parameters for each sub-component and then it is normalized in terms of the logarithmic Strouhal number. Another set of data is used to obtain the directivity factor which is defined as the difference between SPL(θ, f) at $\theta = 90^\circ$ and the desired emission angle.

4.5.8 Landing gear noise

The empirical method is used to predict the landing gear noise due to the geometry and flow complexity. This may lead to uncertainty due to limitations in the parameter range or inaccuracy due to measurement errors. The former can be improved by incorporating new database into the method and the latter by taking use of physics-based theory and scaling laws to cover a broader parameter range [35]. It is observed from the test data that the landing gear noise can be decomposed into three main spectral components. The low frequency noise is generated by wheels, the medium frequency

noise is generated by main struts and the high frequency noise is generated by small details. Sources with different length scales generate noise with different spectral and directivity characteristics. The noise spectrum is broader for broader size range of the components. It is narrowest for low frequency range which includes only the wheel size and widest for small details which is composed of parts with various sizes. The noise normalized spectra are determined as a function of Strouhal number and length scales for three groups of landing gear noise.

4.6 Ground grid

In chapter 4.1 to 4.5 above the main SAFT noise-mapping computational paths and their input have been outlined. In this chapter 4.6 and the following chapter 4 sub-chapters some specific SAFT building blocks, supporting methods and their input is outlined.

The ground grid is the positions on ground upon which the final noise contours are based. This is constituted by a discrete field at microphone height (default 1.2 m but possible to change up to 10 m above ground) where noise levels are computed. This ground grid follows the geometry of the already created groundtrack of a flight. Meaning that we apply a "grid-carpet" consisting of rectangular or circle-sector shaped patches, corresponding to the straight or curved groundtrack sections. The width and resolution of these grid-patches are defined by user input (see example of grid patches in Figure 27.). The coordinates of the grid are called w lateral to (the approximate) groundtrack, = 0 at the grid mid curve, and s along the flight, and as for the groundtrack, s and t = 0, at the runway threshold for approach. This gridding methodology is chosen in order to reduce computational efforts compared with e.g. a single rectangular grid covering the complete groundtrack, TMA or similar. In a "standard" SAFT run the width, w, of such a composed grid is limited by the previously given groundtrack radius of curvature, R_C ($w < R_C$, $R_{C,Default}$ = 2 NM). The procedure for reaching the noise contours is then the following: (significant[17]) noise levels for an aircraft pass-by is computed in each grid point, then all grid patches, including the circular ones are mapped on a rectangular grid on which contours are computed, these contours are then mapped back on the original circular (and rectangular) patches creating the final result.

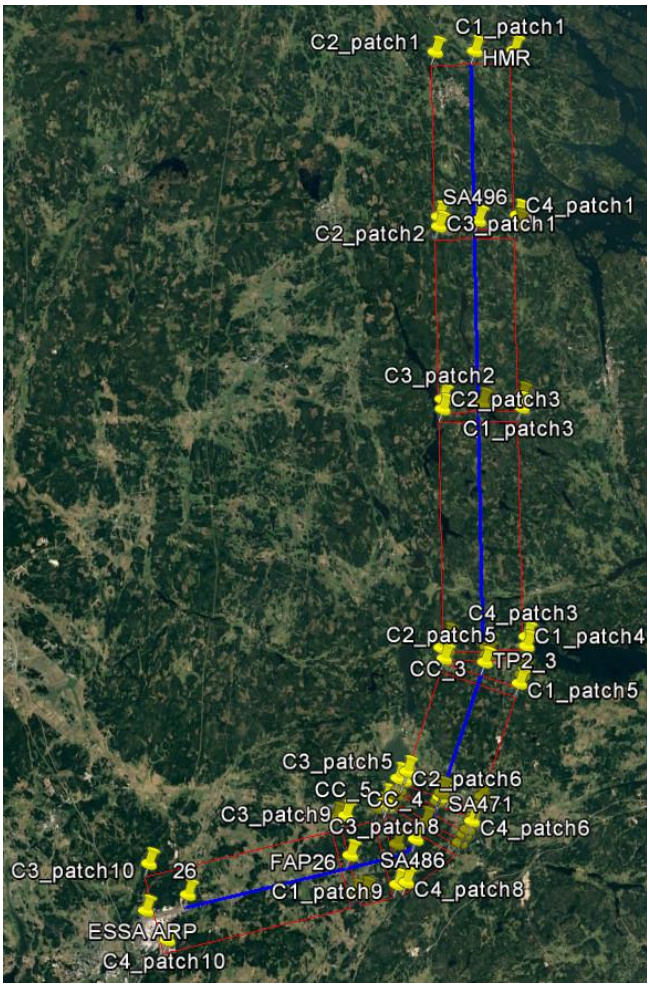

Figure 27. Grid patches and groundtrack example (Patches = red, groundtrack = blue. Default 2NM turning radii and 3.7 km wide patches. Patch corners and track turning points showed with yellow place marks)

[17] In order to reduce computational effort a check is made if the distance between the closest aircraft position to receiving grid points along the grid s-variable for ± w_{max} (i.e. along grid side borders). As for standard SEL-measurements a decay of 10 dB wrt max levels is focused on here approximated with a distance factor of 3.16, 20log(3.16) ≈ 10. (in this way grid points closer to w = 0, grid lateral mid, get a larger margin than the 10 dB decay).

The implemented standard gridding technique brings in a limitation of grid width. This is since the circular sector grid-patches cannot be wider than the groundtrack radius, which governs the default patch-width (straight sides of circle-sector grid patches crossing). In order to allow for wider patches/grids an alternative technique may be used when a wider grid than given by the groundtrack minimum radius of curvature is wanted Figure 28. NOTE: this grid-widening technique is not applicable in all situations. Though since grids are automatically plotted (Matlab + .kml/Google Earth) the result can be found and new attempts be made. If not successful even then, more straight grids may be made, saved and then read in as a work around. Modified ways to handle these kind of gridding is proposed in future versions, including an alternative of conical beside the rectangular patches.

Comment on SAFT gridding and grid-width:

When choosing a default grid-mid-width as the default ground-track curvature, typically 2 NM, the sideways extension of the noise-contour coverage might be found to small in the application of concern. In order to get an idea of what the user may get in terms of noise level span – comparing levels found straight beneath the aircraft with levels sideways at the grid border - with this grid-width around 2 NM, we take a look at an aircraft 1000 m above ground at a 3 degree descent angle, i.e. almost 20 km from the runway. Here we can expect a spherical spreading effect of: $20\log(1/3.6) \approx 11$ dB, a value which increases closer to the runway giving ca 17 dB at 500 m:s altitude (here we disregard refraction, absorption and ground effects). When including all sound propagation effects and look at an A321-232 approaching, assuming an ANP standard spectrum (202) [7] and a sample "real atmosphere" we get about the same span in noise levels for the same distance values, as seen later from SEL values around 70 down to 60 (or 55) dB. These figures may be used as an indicative benchmark at these aircraft/sound source altitudes and suggest if a wider grid is wanted or not.

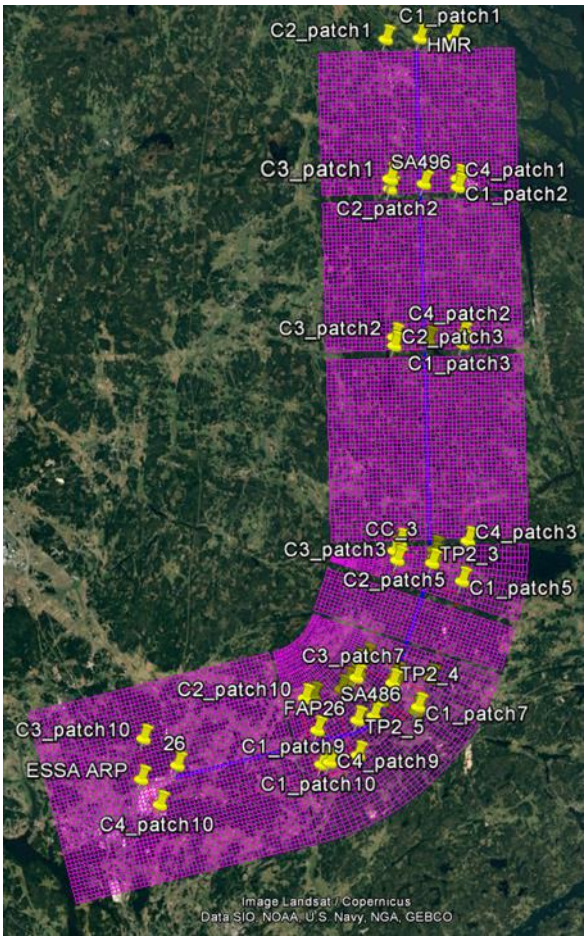

Figure 28. User modified set of grid patches widened to 9.5km shown with final grid (magenta)

Comment to approximation of ground as flat with a fixed elevation as of runway threshold altitude:

NOTE: current gridding implementation assumes a ground-grid elevation corresponding to the runway threshold altitude. This single user running choice possibility is planned to be extended with a "real" topography – though, since the SAFT run alternatives involving a realistic, refractive

atmosphere, rely on the concept of a transmission loss interpolation matrix (see chapter 4.9), do not allow for a straight forward standard implementation of a varying ground elevation this matter needs further considerations.

Around an airport as Arlanda, with a rather flat surrounding terrain, the above noted limitation related to the omitted topography do not reduce the accuracy significantly. This might be indicated by the fact that the ground surface elevation (excluding buildings) typically varies in the order of ± 25 m with regard to Arlanda runway thresholds for distances of up to 20 NM to the airport. Assuming spherical propagation effects only, the approximate noise level inaccuracies related to this elevation simplification would then be of the order of: $\Delta dB_{err} = 20 \log\left(\frac{z}{z \pm \Delta z_{err}}\right)$, where r is the nominal vertical distance, aircraft to ground, and Δz_{err} the difference relative the "real vertical distance". With Δz_{err} = 25 m and z = 100, 200, 500, 1000 and 2000 m respectively, we get: $\Delta dB_{err} \approx$ 2.5, 1.2, 0.4, 0.2 and 0.1 dB. The first values here, 2.5 dB, correspond to a distance of ca 2 km to the runway threshold, i.e. in areas where we, at least in the Arlanda case, would not find any inhabitants (and neither elevation variations as high as ± 25 m due to the terrain type). To sum up, the chosen simplification with a constant ground elevation is deemed accurate enough for airports in flat landscapes but not applicable for more mountainous regions.

NOTE: Planned future SAFT implementations involve a 2-layer gridding technique covering the complete Stockholm TMA (+ other TMAs if found needed). Here the lat, long master grid covers the complete TMA and the grid-point matching sub-grids covers individual flights. In this manner noise exposure levels for accumulated air traffic should be possible to sum up without interpolation between receiving points would be needed.

4.7 Specific receiving points on ground and their noise history

Beside the ground grid and noise contour computations the user can select points along the groundtrack where the receiving noise time histories are computed, saved and presented in plots. Presented either as total A-weighted noise levels as functions of time or as spectrograms (spectrum as a function of time). Between one and up to 15 points may be positioned laterally at a max of 5 points at 3 s-distances along the groundtrack.

Remark: by selecting ground point time histories only, i.e. excluding contours computations, significant CPU-time gains can be achieved.

4.8 Atmosphere model and data

When running SAFT-simulation methods (run path choice 3 to 5) the user make a selection about the following:

1. Atmosphere model type and data
2. Absorption model (to apply on selected atmosphere data)
3. Propagation model – straight rays or refracted rays

In the last case, ray-tracing including a refractive atmosphere (i.e. ray-bending due to variations in effective sound velocity with altitude, causing sound energy concentration, dispersion and even ”sound-shadows”) a TL-interpolation matrix as of the previously mentioned type is established, a concept which is further explained in chapter 4.9 below.

It should be noted that even for the “integrated” ECAC Doc.29 paths (path 2) all the different atmosphere and absorption models may be applied, but in this case their impact is limited to a modified absorption through a corresponding update of the NPD-data according to an atmosphere changed from the SAE AIR-1845 (i.e. refraction effects not possible to include in an ECAC Doc.29 computation).

4.8.1 Atmosphere model types

When computing sound propagation one need to know the composition and state of the medium, in our case atmospheric air up to the altitude of the noise source/aircraft down to the receiver. With the applied sound propagation models applied in SAFT we need to know the following atmospheric properties as a function of altitude: (static)pressure, temperature, humidity, density and wind speed and direction. We also can make use of the turbulent kinetic energy (TKE) in models for impact on propagation due to turbulence.

The user may choose between 3 different atmosphere model types in SAFT, these are as follows:

1. ISA - International/ICAO Standard Atmosphere [30]

2. Class of meteo-profile - from a set of (sound propagation governed) atmosphere wind and stability classes as defined in the IMAGINE project, see chapter 3 in ref. [36]

3. Atmospheric profile from AROME-MetCoOp-model based “real” weather forecasts and history [37], [38] and [39]

These three models represent an increasing versatility, complexity and realism when going from no 1 to no 3. The idea of including the first two, when having access to “real” atmospheric profiles in 3, is primarily to make comparisons with results from external studies possible but has also the possibility to support understanding and learning in the field of aircraft noise propagation.

The user input depending of the atmosphere model is outlined below:

ISA - International/ICAO Standard Atmosphere

a. Quiescent (zero wind), constant 70% RH (relative humidity) and 15ºC sea level temperature, or:

b. Added constant wind speed, RH and offset ground temperature given as user input. Wind direction opposite to RW direction (i.e. landing in headwind), or:

c. Added wind speed profile given by the power law, constant RH and an offset ground temperature. 10 m wind, constant wind direction and constant RH given as user input.

Class of meteo-profile

After user input of ground temperature and wind direction a ground (10m) wind speed class is selected among:

Class	Wind speed
W1	0 - 1 m/s
W2	1 - 3 m/s
W3	3 - 6 m/s
W4	6 - 10 m/s
W5	> 10 m/s

... this is followed by a choice of atmospheric stability category (depending on time of day and cloud cover):

Stability category	Time of day	Cloud cover
S1	day	0/8 - 2/8
S2	day	3/8 - 5/8
S3	day	6/8 - 8/8
S4	night	5/8 - 8/8
S5	night	0/8 - 4/8

NOTE: a default fixed surface roughness length of 0.025,"open flat terrain; grass, few isolated obstacles" is applied in SAFT , but could in the future be linked to ground properties

For roughness length see e.g. [40]

REMARK: The limitations of the above classification is expressed in [36] as : "*The section concludes, however, that such classification and profile generation requires a more local approach and that such localisation adjustments and validation should be carried out in several regions of Europe. Further investigation of elevated inversions, low-level jets and humidity is also recommended, including the introduction of seasonal classes.*"

Atmospheric profile from AROME-MetCoOp-model based forecast

Prognosis profiles established in cooperation by The Norwegian Meteorological Institute and SMHI (Swedish Meteorological and Hydrological Institute). Data including the forecasted weather/atmosphere profiles, for up to 72 hours ahead, are produced every 6 hour (UTC[18] 0, 6, 12

[18] UTC, Coordinated Universal Time, a reference time successor to a Greenwich Mean Time (GMT), one hour behind Central European Time used in Sweden and 2 hours behind during Central European Summer Time (CEST) from last Sunday of March to last Sunday of October.

and 18) in a grid with lat, long discretization 2.5 km covering Scandinavia. The 0-hour prognosis is stored at met.no in netCDF-format and may be read directly into SAFT.

Worth to note here: a) after downloading selected data one lat, long-position profile (for the selected time) is saved for future (fast) reuse. b) The simplification to apply only one lat, long-profile for noise mapping of a single event trajectory is deemed to generate an acceptable accuracy – this since profile data tend to show a rather weak variation laterally over flat land such as around Arlanda airport. c) Data for previous years is possible to reach when a study requires statistical, seasonal weather category or "typical" noise patterns. d) One of the altitude dependent variables in the CFD-based profile forecasts, is the turbulent kinetic energy (TKE) which usually is the most important input variable in models of sound energy leakage into so-called sound shadow-zones (where sound intensity becomes zero with standard ray-tracing approaches or typically underestimated by orders of magnitude with field-based sound propagation models that do not account for turbulence).

For a compiled MetCoOp data sample see Figure 46 and Figure 47 below.

NOTE: Other atmosphere data resources that might come to use regards atmospheric sounding. Either direct (balloon, aircraft) or indirect (SODAR-SOnic Detection And Ranging, and maybe other).

4.8.2 Absorption models

Sound absorption or attenuation is the name of a physical mechanism that reduces energy from a travelling sound wave and transfers the energy into heat through different molecular relaxation processes. Five alternative atmospheric absorption models are implemented in SAFT.

1. The original ECAC Doc.29/NPD-data related SAE-AIR-1845 [25]. This is not a real absorption model but contains fixed frequency dependent absorption data in dB/m for an artificial "mean-atmosphere" – this is outdated and not really used in any aircraft noise model today – but since it is inherent in the NPD-data its implemented in SAFT for comparison purposes.

2. The SAE ARP-866A:1975 [41] a temperature and humidity dependent model which has been the alternative to SAE-AIR-1845 fixed data in ECAC Doc 29 and AEDT.

3. SAE ARP-5534:2013 [42] proposed as an improved alternative to SAE ARP-866A in AEDT and claimed to be the best choice in the ECAC Doc.29 edition 4 (from 2016). This method is based on the ANSI S1.26-1995[19] [43] standard but with an approach that accounts for the non-linear effect of (originally "flat") 1/3-octave bands propagation (instead of narrow band) by assuming a certain representative spectra and the effect on those as a function of distance. This and the following absorption models allows also for pressure dependencies (beside the temperature and humidity)

4. Pure tones sound attenuation as of ANSI S1.26-1995/ISO9613-1:1993 [44], algebraically identical to each other. Pressure also taken into account. Considered more accurate than the older, to be outdated SAE ARP-866A.

5. Pure tones sound attenuation model as of Bass-Sutherland [45] , the newest model, including more relaxation mechanisms than the others. Remark: show no difference compared with ANSI S1.26-1995/ISO9613-1:1993 for typical standard commercial flight altitudes.

[19] ANSI S1.26-1995 is in principle equivalent to ISO9613-1:1993

4.8.3 Atmosphere data examples

In the following sequence of figures, from Figure 29 a) and b) to **Fel! Hittar inte referenskälla.**and b), example atmospheric profile data influencing the sound propagation is shown. Two different original data sets are compared side by side in the a) and b) columns respectively. Both data sets are of the MetCoOp-AROME type and represent two different atmospheric conditions taken at the same position (Arlanda airport) at two different times of the year, in the a) –column of figures: 2018 December the 5th, UTC 12 and in the b)-column: 2019 August the 15th, UTC 18. Very roughly they can be seen as representing a rather warm winter/fall midday with moderate wind and a late summer afternoon with weak wind close to ground. Neither of the two cases show any sign of temperature inversions or low level jets. The atmosphere data examples presentation starts with a figure sequence of 2 forecasted wind profiles at the respective UTC-hours, presented in 3 different ways.

The figures are further commented and clarified in text sections following directly after the figure of concern.

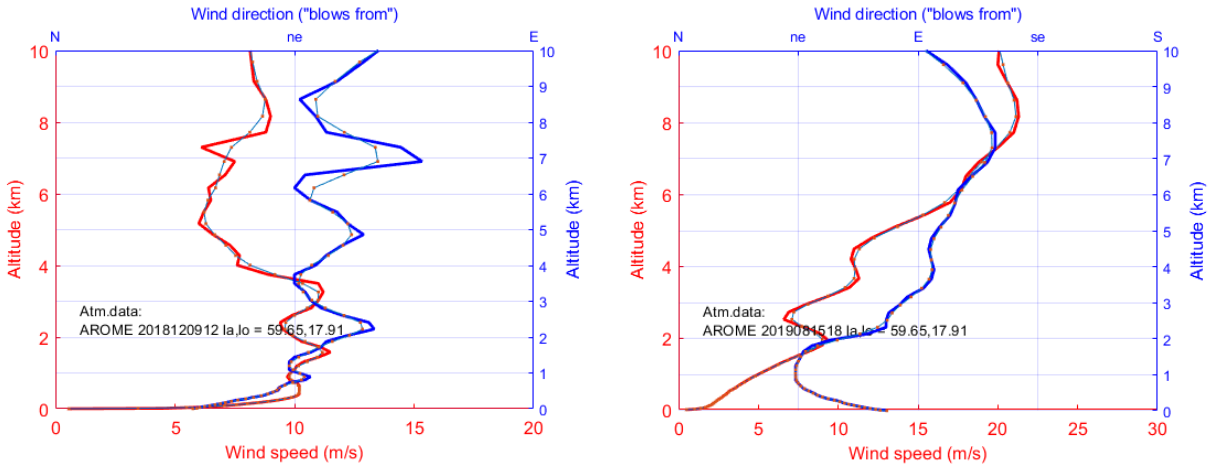

Figure 29 a and b. Wind direction and speed. a) 2018-12-05 UTC12 b) 2019-08-15 UTC18

Above, original AROME wind data shown together with splines representations of the same data.

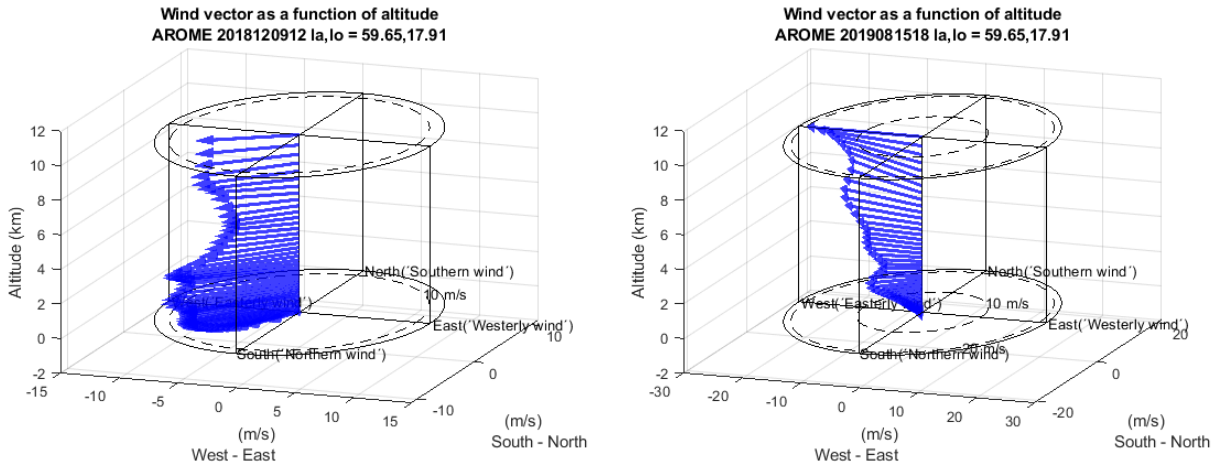

Figure 30 a and b. Wind vectors in 3D, alt. 0 - 10 km. a) 2018-12-05 UTC12 b) 2019-08-15 UTC18

Figure 30 show the same data as in Figure 29 but as 3D vectors as a fcn of altitude (no attempt to cover vertical velocities is made)

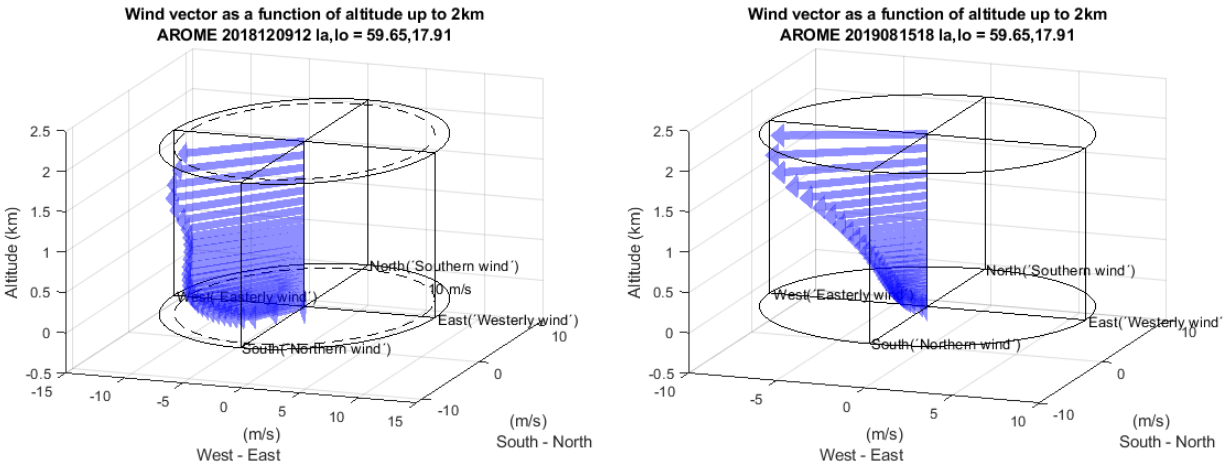

Figure 31 a and b. Wind vectors in 3D, alt. 0 - 3 km. a) 2018-12-05 UTC12 b) 2019-08-15 UTC18

Figure 31 a and b show the same data as in Figure 30 but limited to 0 -2.5 km.

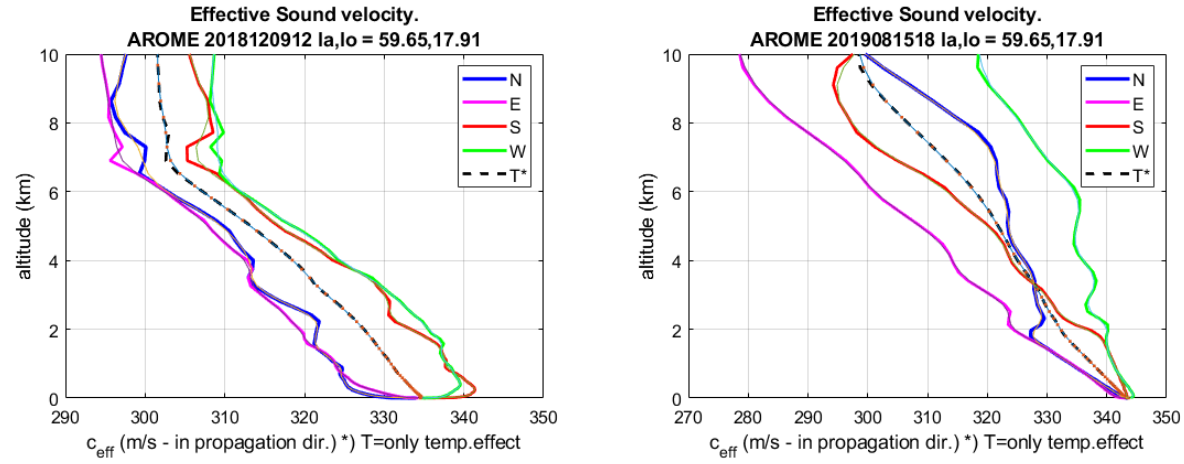

Figure 32. a and b. Effective sound speed, 0-10km. a) 2018-12-05 UTC12 b) 2019-08-15 UTC18

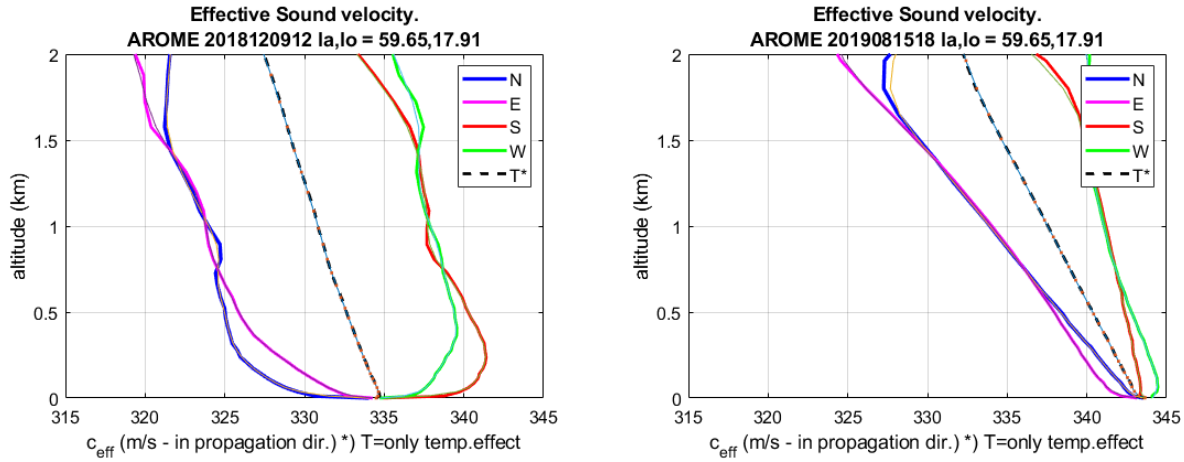

Figure 33 a and b. Effective sound speed, 0-2km. a) 2018-12-05 UTC12 b) 2019-08-15 UTC18

Figure 33 show the zoomed in 0 - 2 km of the in Figure 32 presented 0 – 10 km effective sound velocity data.

The effective wind speed is a common approximation used in ray-tracing, here the wind speed vector is added to the sound speed in a corresponding media without winds, as for the sound velocity at altitude z in the φ-direction, eq.(6):

$$c_{eff}(z,\varphi) = c(z) + v_{\varphi}(z) \tag{6}$$

where: $v_{\varphi}(z)$ = the wind component in the φ-direction

Note in Figure 32 and Figure 33 the difference of the effective sound velocity in the principal directions, N(orth), E(ast), S(outh) and W(est), between a) and b): Case a) shows a clear positive gradient in S- and W-directions (and negative d:o in E- and N-dir.) which corresponds to the change of wind speed the first ca 300 m together with the northeast wind direction[20] shown in Figure 29 a). Both cases show dominating wind directions from NE to E with the case b) tending to go to towards SE directions at higher altitudes. We also see that the temperature impact on the sound velocity, both the absolute and the effective, is negative, i.e. a negative temperature and sound velocity gradient found at all altitudes. This means that we have no temperature inversions, neither elevated or at ground in the studied data. The effective sound velocity in case b) is seen to have much weaker gradients close to ground then in the a) case, which indicate comparably less impact of refraction ("sound ray-bending").

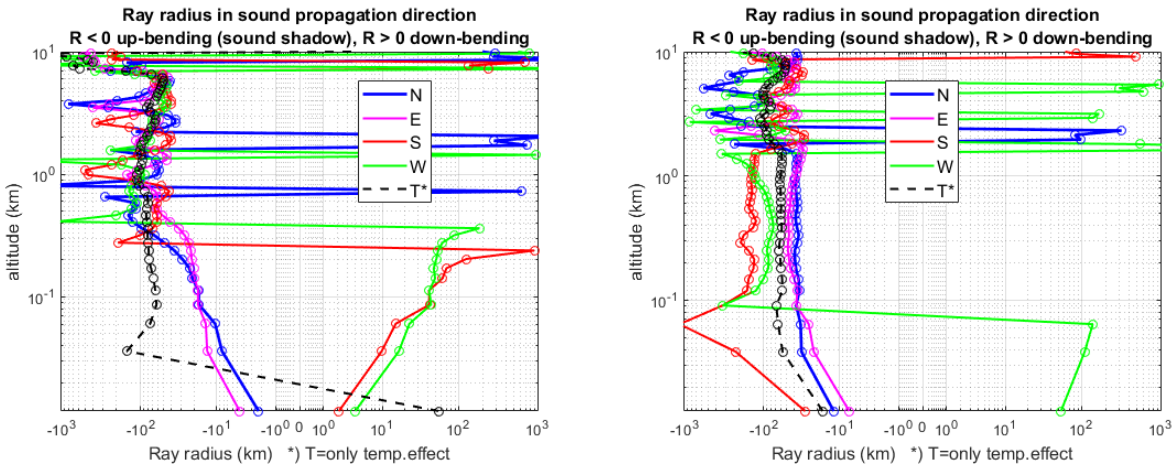

Figure 34 a and b. Ray radius as a function of alt. a) 2018-12-05 UTC12 b) 2019-08-15 UTC18

The approximation of an effective sound velocity as in eq.(6) leads to a simple expression for the local ray-bending radius, R and the effective sound speed gradient, dc_{eff}/dz, as a function of altitude, z [46], eq.(7):

$$R(z) = \frac{c_{eff(z)}}{\frac{dc_{eff}}{dz}(z)} \tag{7}$$

A positive R, i.e. given by a c_{eff} increasing with z, tend to bend sound rays towards ground while $\Delta c_{eff} < 0$ with increasing z gives a $R < 0$, or upward bending rays. The most general effects of such

[20] wind direction = (in common language and here) the direction from which the wind blows, i.e. in contrary to the wind-vector, sound propagation direction or for the effective sound velocity vector, N = "towards north", etc.

refractive patterns are that a situation with up-bending rays, up-wind propagation, may cause sound shadow zones if the source is positioned close enough to ground within or close to a "R < 0 zone". Concentrations of rays, compared with a spherical propagation in a homogenous atmosphere without winds, is linked with increased sound intensity and vice versa. In order to get an direct indication of the character of the atmospheric profiles with regard to refraction and possible sound shadow zones SAFT computes and plots the R value as shown in Figure 34 as a default action when reading in AROME atmosphere data. The impact of refraction, "sound ray bending", will be further outlined in section 4.9.2 *The TL refraction term,* TL_{Refr}.

Figure 35 below show a detail in R-range of what is already shown in Figure 34.

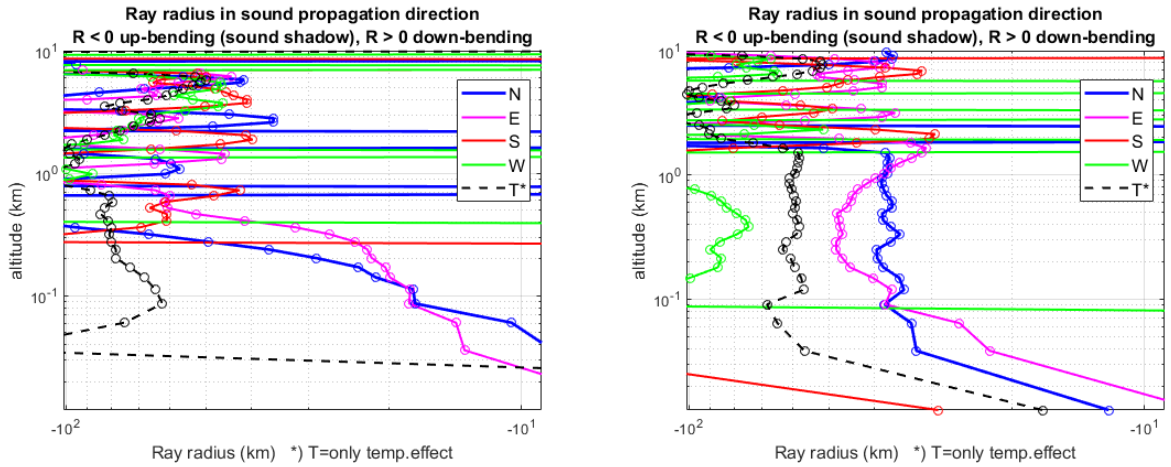

Figure 35 a and b. Ray radius – Detail as a func. of alt. a) 2018-12-05 UTC12 b) 2019-08-15 UTC18

In a thought situation with no winds at all, but a well-mixed surface layer without temperature inversions, Δc_{eff} and R are < 0 and governed by temperature only ($c_{eff} = c$). R impact from such solely temperature dependent profiles are, compared with wind effects, tend to be weaker in strength and more constant over time and altitude. The R values in Figure 35 a) and b), caused by the temperature gradient only, is seen to be around 60-100 km and 60 km respectively, as indicated by the black dashed lines. The R value impact we can expect from wind variations is more strongly linked with the properties of the boundary layer of the earth. With this follows, for a typical daytime situation, that the convective boundary layer (CBL), [47], typically ~1 km high and with a surface layer of one or a few hundred meters height, show a strong c_{eff}–gradient/small R close to ground – in Figure 35 a) $R<0$ and $|R|$ < 2 km up to z = 300 m giving 10-20 km:s ray up-bending radii for E(asterly) propagation, indicating possible sound shadow zones. While Figure 34 b) show ca 20-30 km:s ray-up-bending radii for E(asterly) and N(ortherly) propagation, indicating a comparably weaker tendency for creation of sound shadows.

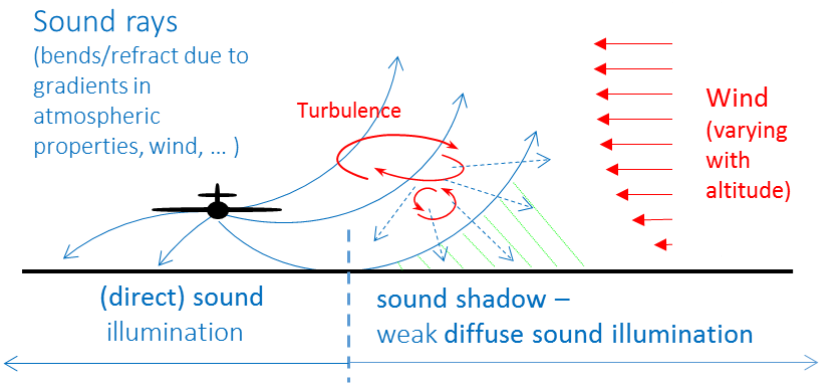

Figure 36. Principle sound shadows

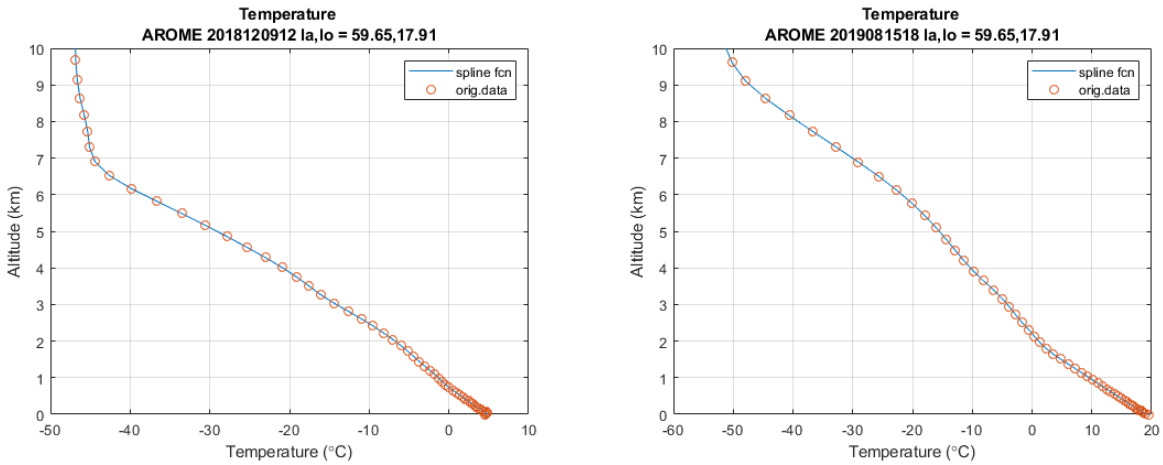

Figure 37 a and b. Temperature profiles. a) 2018-12-05 UTC12 b) 2019-08-15 UTC18

In the sample profiles no clear inversions exist. It may be noted that the temperature gradient the first to km:s above ground differs between ca 5°/km in a) and nearly 10°/km in b), compared with ca 6.5°/km for a standard atmosphere.

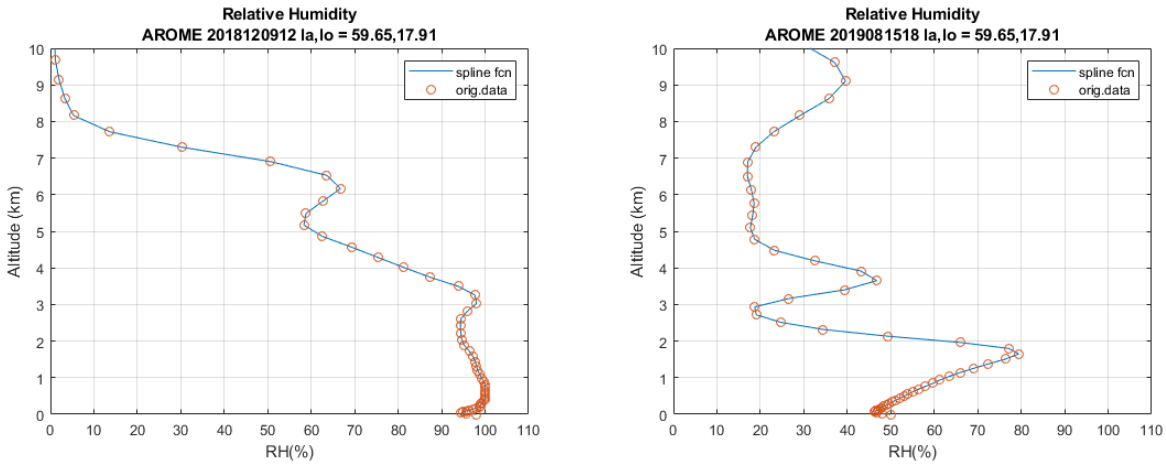

Figure 38. Relative humidity (RH) profiles. a) 2018-12-05 UTC12 b) 2019-08-15 UTC18

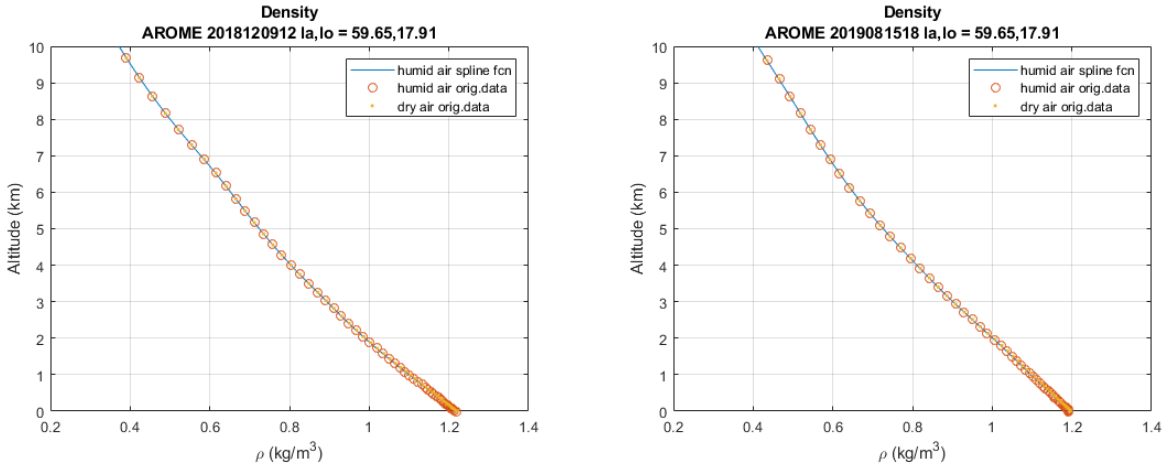

Figure 39. Air density profiles. a) 2018-12-05 UTC12 b) 2019-08-15 UTC18

The air density (and air pressure) at a specific altitude do not vary much over time in absolute terms and do neither have a significant impact on noise levels. Though, the density (and air pressure) vary quite significantly with altitude which have a significant impact on aircraft noise. First it has an effect on the source generation mechanisms, and secondly on the resulting noise on ground - depending on the difference in altitude between source and receiver. For the last effect see Figure 40 below.

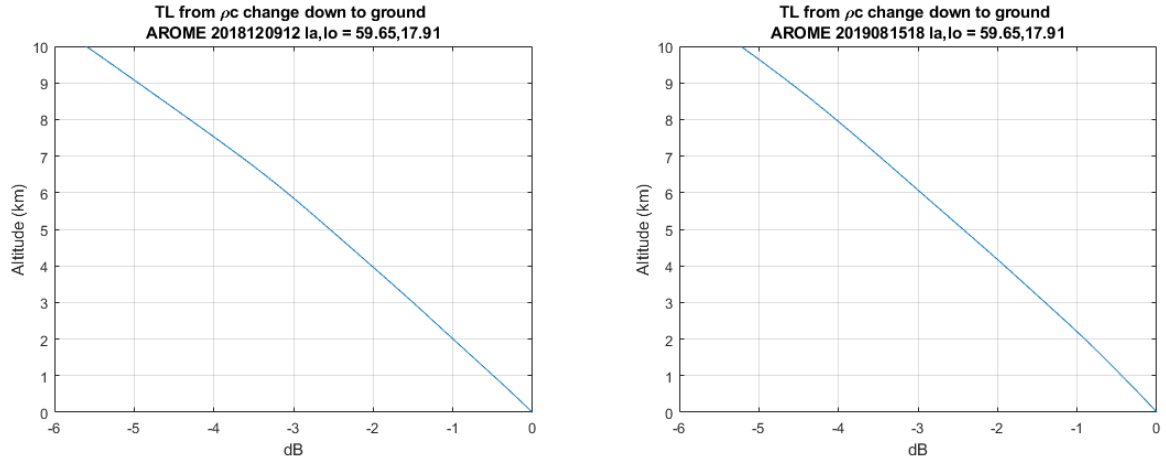

Figure 40. SPL Transmission Loss from change of ρc. a) 2018-12-05 UTC12 b) 2019-08-15 UTC18

This is an effect of loss of sound energy for a sound propagation through a media of varying specific acoustic impedance, ρc. It may be explained in the following way:

If we start out from a sound ray wave sector close to a sound source, i.e. a 2D space angle perpendicular to the propagation direction for the sound ray, and neglect any other sound energy loss mechanisms than the geometrical expansion of this sector and look at the sound intensity, I, (in W/m²), assuming a plane wave and considering the rms-value, as in eq.(8):

$$I = \frac{p^2}{\rho c} \tag{8}$$

... and then looking at the fact that the intensity would be kept constant between two altitudes when setting aside the ray-area change, we get for the sound intensity levels at altitudes z_1 and z_2:

$$I_2 = I_1, \qquad or \quad \frac{p(z_2)^2}{\rho(z_2)c(z_2)} = \frac{p(z_1)^2}{\rho(z_1)c(z_1)} \tag{9}$$

$$\Rightarrow$$

we get the difference in sound pressure and sound pressure level, $\Delta L_{p_{1to2}}$, between altitude 1 and 2 as:

$$\frac{p(z_2)^2}{p(z_1)^2} = \frac{\rho(z_2)c(z_2)}{\rho(z_1)c(z_1)}, \qquad or\ \Delta L_{p_{1to2}} = 10log\frac{\rho(z_2)c(z_2)}{\rho(z_1)c(z_1)} \tag{10}$$

which also may be named sound pressure Transmission Loss (TL) between altitude 1 and 2, which is seen in Figure 40 to have a value of about -1 dB between 1 km height and ground, i.e. an increase in sound pressure level due to the higher pressure and density at ground.

It could be mentioned that the second effect from noise level changes with altitude, namely noise sources and their noise generation mechanisms, in many cases act in the opposite way, i.e. giving a weaker source due to the source position within "thinner" air.

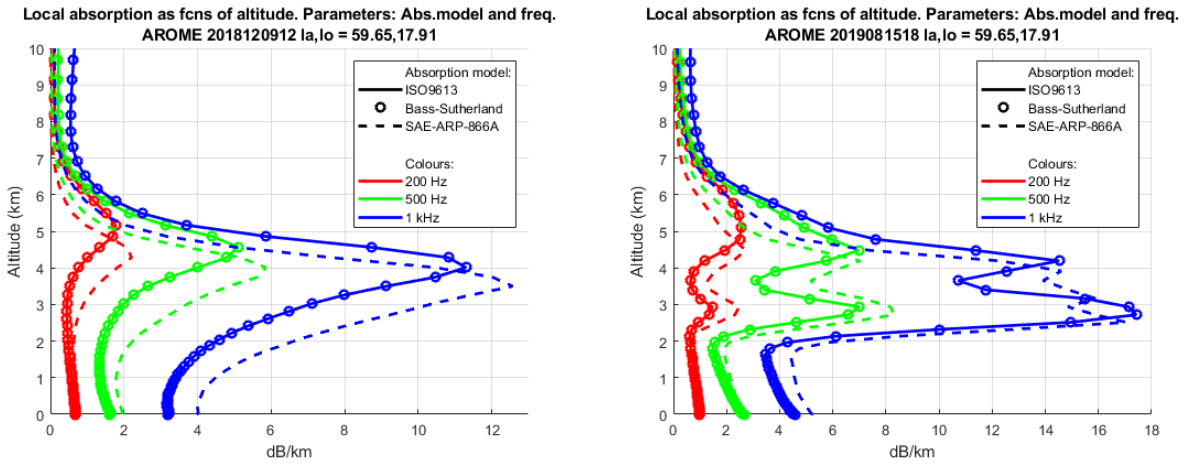

Figure 41 a and b. Sound absorption as a fcn of altitude. a) 2018-12-05 UTC12 b) 2019-08-15 UTC18

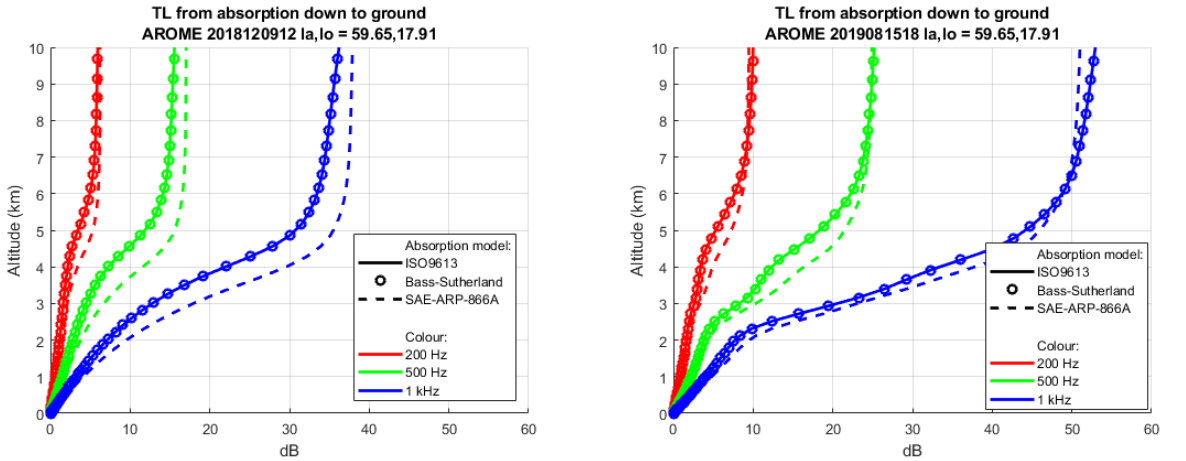

Figure 42 a and b. TL due to absorption down to ground. a) 2018-12-05 UTC12 b) 2019-08-15 UTC18

In Figure 41 and Figure 42 above the sound absorption for the two atmosphere data examples are studied. The data include 3 specific frequencies, 200, 500 and 1000 Hz, which may be seen as representative for typical aircraft noise spectra, and 3 different absorption models (outlined in chapter 4.8.2). In Figure 41 we can see a significant difference between results, in local dB/km, from the older SAE ARP-866A (dashed) and newer absorption models, Bass-Sutherland and ANSI S1.26-1995/ISO9613-1:1993 (and as expected/mentioned previously: no difference between the newer ones). These differences of several dB at higher altitudes is seen to reduce close to ground, only 1 kHz curves show a significant difference for the "winter/fall" atmosphere example (a) here with slightly less than 1 dB/km. For the "summer" example (b) the difference in local absorption between the models tend to be slightly smaller.

In Figure 42 a) and b) the total absorption from a downwards vertical sound propagation is examined. Again we see a stronger discrepancy between SAE ARP-866A and the other absorption models for the "winter/fall" atmosphere example (a), e.g. ca 3 dB weaker.

In the last plots in this chapter we look in more detail on the differences in TL a change from SAE ARP-866A to the newer absorption models may introduce. The plotting approach contains quite some information and requires thus a thorough introduction:

For the same "fall/winter" and "summer" example profiles already presented above we have chosen to look at the absorption/TL for a sample aircraft type spectrum, this spectrum is chosen to be the ANP spectrum 202 for approach, representing 2-Engine Low to High by-pass turbo-fans (among them the Airbus A321-232). Moreover, we look at the TL due to absorption, assuming straight rays, at a set of distances corresponding to the NPD distances (200, 400, 630, 1k, 2k, 4k, 6.3k, 10k, 16k and 25k feet, e.g. 100 distances between 60m and 7.6 km). For each of these distances we look at the difference in TL, with regard to ARP-866A, for vertical propagation and all angles down to horizontal propagation, though, a limitation of aircraft altitude was made to 1.8 km. Each such NPD-distance, $d_{NPD,i}$, represent a specific colour and curve set in the ΔTL plots. For each of the coming ΔTL plots, in Figure 44 and Figure 45, an individually coloured set of curves represent propagation as shown in Figure 43 below (example given for $d_{NPD,7}$= 1.9km = 6300ft). I.e. each $d_{NPD,i}$-curve is a parametric curve given by the aircraft-receiver angle towards the horizon, 90 to 0 degrees, i.e. starting at a max altitude equal to its length (though not shown above y=1800m in the ΔTL plots) which corresponds to a vertical propagation down to ground and then, for a constant NPD-distance, the source/aircraft goes continuously towards lower altitude, ending at ground, 0m, with a horizontal propagation.

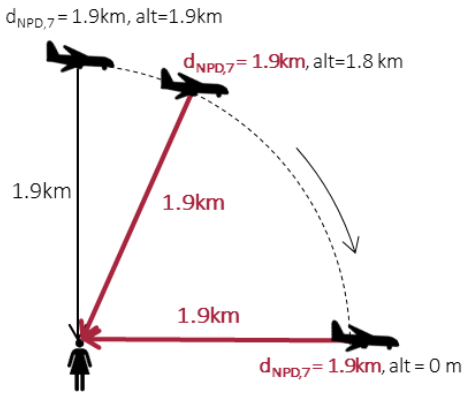

Figure 43. Principle for fixed distance TL curves, example $d_{NPD,7}$= 1.9km

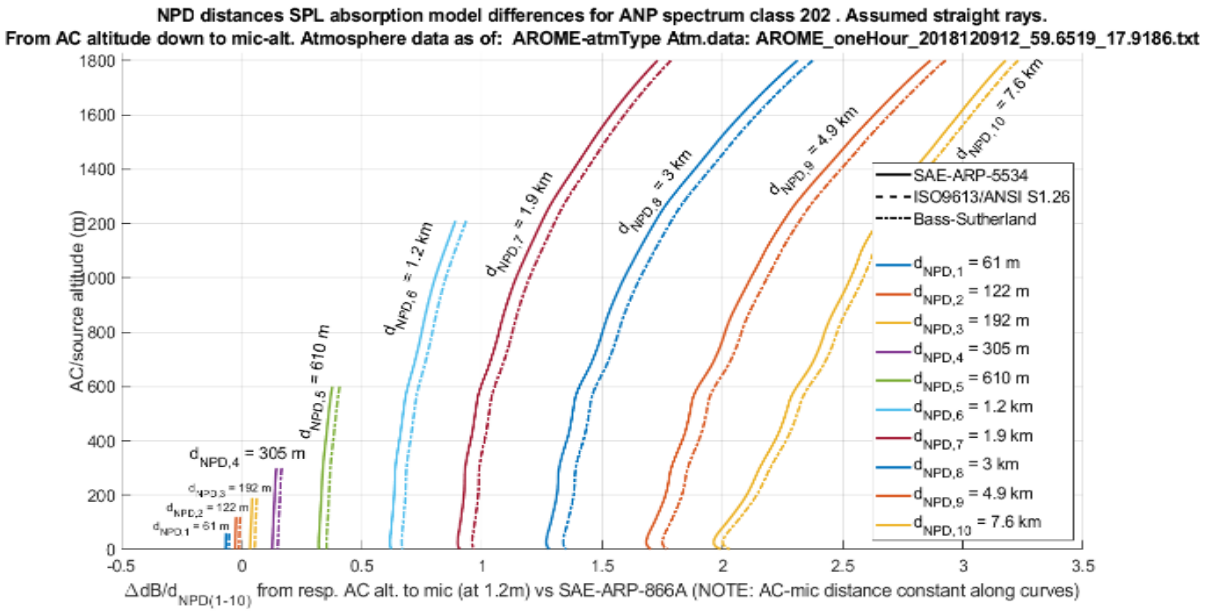

Figure 44. ΔTL from different absorption models vs ARP-866A. Meteo data: 2018-12-05 UTC12

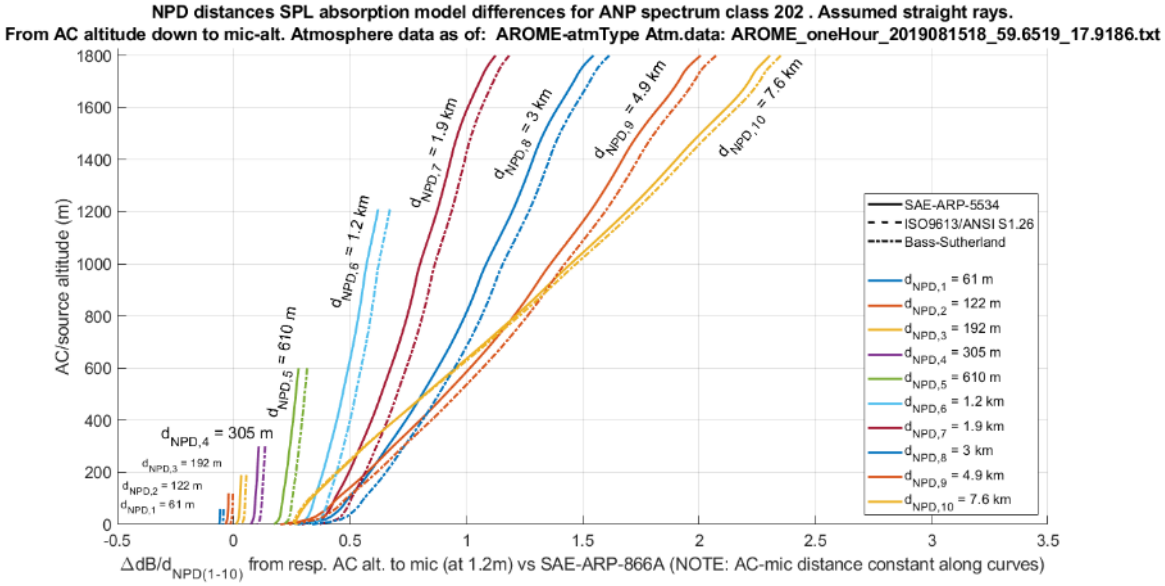

Figure 45. ΔTL from different absorption models vs ARP-866A. Meteo data: 2019-08-15 UTC18

Again we can see cleat differences between ARP-866A and the newer absorption models. The tendency is that the older ARP-866A estimates a relatively higher TL, i.e. slightly underestimates noise levels on ground.[21] As already mentioned, the Bass-Sutherland absorption model give the same

[21] This might be of concern for airports where air traffic noise contours previously have been computed with ARP-866A, where decisions has been taken based on those, where a notable ground area increase with higher noise levels can be anticipated in noise mappings when changing to SAE ARP-5534.

result as ISO-9613/ANSI-S1.26, for the altitudes of concern in our examples (the two different dashed curves not possible to separate visually).

Remark: in Figure 44 and Figure 45the x-axis represents $\Delta dB/d_{NPD,i}$ absorption, i.e. the difference in absorption along a fixed NPD-distance i, $d_{NPD,i}$, between ARP-866A and a "new noise model", ARP-5534 or ISO-9613/ANSI-S1.26 which may be written as:

$\Delta dB/d_{NPD,i} = dB/d_{NPD,i}$ (ARP-866A) - $dB/d_{NPD,i}$("new abs.model")

i.e. a $\Delta dB/d_{NPD,i}$ value > 0 denotes stronger absorption(and TL) predicted by ARP-866A.

For the "fall/winter"-example atmosphere data and distance 1.9 km we see differences from 1 to 1.75 dB, increasing with the altitude of the sound source/aircraft and for the 3 km distance from 1.25 to 2.25 dB. The "summer" case show in general weaker differences compared with ARP-866A, but still higher noise levels. The difference between SAE ARP-5534 (accounting for assumed 1/3-octave spectra) on one hand and the other "new" absorption models, i.e. ISO-9613 and the equivalent ANSI-S1.26, show a very small, ca 0.1 dB, stronger absorption/TL for SAE ARP-5534 which may indicate that the narrowband approximations could be acceptable in most situations.

NOTE: currently in SAFT we apply a 2D atmosphere data model, i.e. assuming that horizontal variations of atmospheric data are neglectable.

An initial study was carried out within the SAFT project for quantification of atmospheric impact over time on TL between fixed positions, the results is found in [48]. An attempt comparing a full 3D atmospheric and ground model with the SAFT 2D atmospheric data is made here but since different ground reflection/attenuation approaches (narrow band coherent [span: cancelation to +6 dB] vs. wideband uncorrelated [span: ±3dB] in SAFT) the largest differences could probably be attributed to this situation – in which differences due to other mechanisms would be hidden. NOTE: Here a more detail study separating different TL-mechanisms and assuring that the same model approaches should be used in both the 3D and 2D case, would be of interest.

4.9 The Transmission Loss (TL) and the SAFT TL-interpolant matrix

4.9.1 Over all Transmission Loss

The already mentioned concept of transmission Loss (TL) is very useful within the field of sound propagation. This is partly since it is closely related to the physics of sound propagation and thereby contribute to a good understanding of the processes behind sound propagation. But also, at least when applying a ray-tracing method [46], [49] + [50], as in SAFT, it makes it possible to separate the sound intensity loss contributions from the individual physical processes between source and receiver. The total TL[22] may be written as a sum of its constituents as:

$$TL = TL_{Sphere} + TL_{Refr} + TL_{GrRefl} + TL_{AirAtt} + TL_{\rho c} \quad (11)$$

where the individual mechanisms/contributions are:

[22] note that a negative TL, i.e. TL < 0, denotes an increase in sound level along the propagation path

TL_{Sphere} Transmission Loss due to spherical propagation between the assumed point source to the receiver [no refraction as in a homogenous medium, giving a 6 dB reduction in sound pressure and intensity levels per doubling of distance, *20log(p(2r)/p(r)) = 20log((1/2r)/(1/r)) = 20log(1/2) ≈20 -0.3 =-6 dB.*]

TL_{Refr} TL due to refraction, i.e. a curved, instead of a non-straight spherical-, propagation between source and receiver due to a change of effective sound velocity, eq.(6), with altitude

TL_{GrRefl} TL due to ground reflection (not an effect along the complete transmission path but a local effect caused by ground reflection, here called "TL" anyhow)

TL_{AirAtt} TL due to attenuation in the free air along propagation path between source and receiver

$TL_{\rho c}$ TL of sound pressure levels[23] due to a change in air acoustic impedance, ρc, ρ = density of air, c = sound velocity

All the TL terms are outlined in more detail in the following.

4.9.2 The TL refraction term, TL_{Refr}

The definition and the features of the TL_{Refr}-term implementation in SAFT are outlined in the following:

If a set of sound rays are emitted with a certain (small) space angle in between each other, from an assumed directional spherical point source, they will stay straight in an isotropic (uniform) medium. And, assuming no losses, the sound energy between the rays will stay constant along the (radial) propagation path. For a spherical propagation this means that the sound intensity, I, will depend only on the radial distance, r, from the point source, or: $I(r,\varphi,\theta) = I_0(\varphi, \theta)/4\pi r^2$, or 6 dB per doubling of distance, where $I_0(\varphi, \theta)$ = the sound intensity at a distance of one meter in the (φ, θ)-direction. In the case where we have a non-uniform atmosphere instead, i.e. a (vertical) gradient in the effective sound velocity, the sound rays will not be straight/radial any longer but refract (bend). Then the area between neighbouring rays will not follow the $1/4\pi r^2$ pattern anymore. Either the rays get closer to each other, resulting in a relatively higher sound intensity with regard to the spherical propagation case or vice versa. TL_{Refr} is a measure of this difference and becomes < 0 in zones of compressed ray packages and > 0 if the expansion is wider than the spherical. This refraction term has in the so called caustic zones, where rays are crossing each other and the related ray-cross area gets zero, resulting in an infinite value of the sound intensity. This un-physical behaviour may be handled in different ways, in SAFT simply by a curve smoothing approach in which a weighted moving window mean is applied for $TL_{Refr}(z_{AC}, r, \varphi)$ along the radial coordinate r and for all aircraft altitudes z_{AC} and propagation planes, φ. An example of atmospheric wind + effective sound velocity profiles and the resulting ray pattern and TL_{Refr} for two opposite φ-directions, headwind and

[23] this $TL_{\rho c}$ term is = 0 for sound intensity levels, Li, but when changing altitude, and thereby specific acoustic impedance, ρc, ≠ 0 for sound pressure levels, Lp. All other TL terms are identical for pressure and intensity.

downwind, are given for a sample AROME "spring morning" atmosphere data (20170420 UTC 6) in Figure 46 to Figure 49 below:

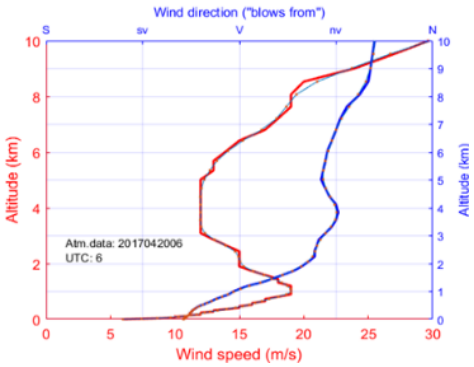

Figure 46. Meteorological data - Wind profiles met.no/SMHI [38], [39]

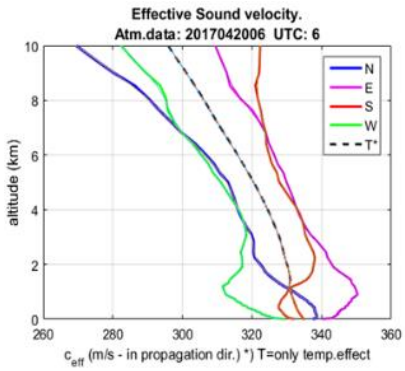

Figure 47. Effective sound velocity profiles

As seen above a strong wind speed increase up to 1 km, possibly showing an example of a low level jet (fast decrease of wind speed above 1 km). The wind speed gradient below 1 km is > 0 in the easterly sound propagation direction (tailwind sound propagation direction giving down-bending sound rays, Figure 49) and < 0 in the westerly direction, i.e. headwind propagation direction giving up-bending sound rays as shown in Figure 48. Note that in Figure 48 and Figure 49 below both 1. sample sound rays (bunch of curves, left y-axis) and 2. the TL_{Refr} (yellow curve, right y-axis), is plotted for: r = 0 to 10 km, z_{AC} = 500 m and φ = 270° and 90° respectively.

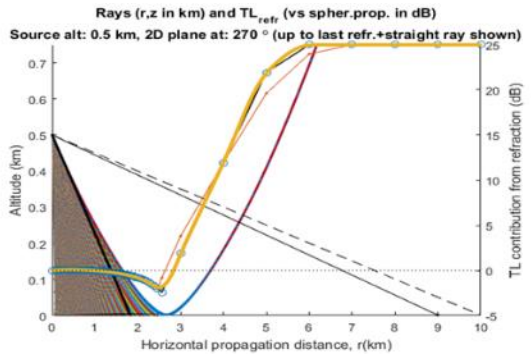

Figure 48. Headwind sound rays + TL_{Refr} (yellow curve)

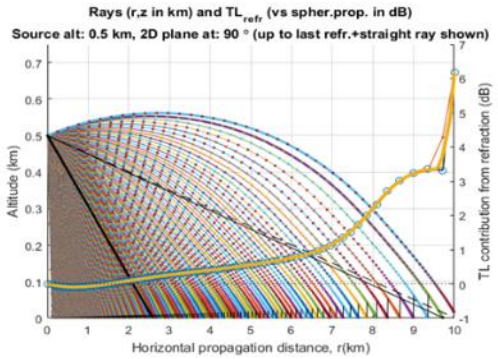

Figure 49. Tailwind sound rays + TL_{Refr} (yellow curve)

The SAFT implementation of ray-tracing is limited to a first and single ray-bounce and to a maximum horizontal distance of 10 km. The max altitude is 10 km but can be limited to a lower level if wanted by the user (could be that trajectories to study are at lower altitudes).

In the headwind case, Figure 48, we see a last ray "touching" ground and then bending upwards. To the right of the touchdown of this limiting ray, $r \gtrsim 2.7$ km, we have no rays penetrating and according to the approximate ray-theory neither any sound energy. A situation usually called "sound shadow" for $r \gtrsim 2.7$ km. Such zones, completely free from sound energy, would not be the situation in reality though. Instead we would have some but comparably much weaker sound intensity in the sound-shadow zones, typically several 10th's of dB lower than within in the neighbouring sonified regions at the same distance. Even more detailed solution techniques for the wave equation, e.g.

numerical field models, which do result in a finite sound intensity within shadow zones, usually strongly underestimate these levels if one do not account for the atmospheric turbulence and its effect of scattering and refraction into the shadow zones. Typically just inside a shadow zone, close to but beyond the "last bounding ray", the reduction of sound is typically of the order of 20-25 dB [51] depending on the atmospheric turbulence. Stochastic methods, which do exist for estimates of sound levels within the shadow zone, accounting for the strength in the random turbulence, but becomes soon very costly since most of them involve a high number of repetitions (say N > 10) since we need to get a statistically significant result. This holds whether we apply a field method or a ray method. Though, we are often more interested in the higher noise levels and where they occur and consequently a simplified approximation of how noise decay is often enough. Currently in SAFT a simple 10 dB/km decay within shadow zones (for all frequencies) is applied. This is believed to be a conservative estimate. Some analytical approaches tries to circumvent the need for the statistical, repeated computations by applying curve fit to parameter studies based on previous statistical algorithms applied on the physics of turbulent sound scattering. One such method is proposed in [52] and applied in [53]. This method involve only two variables, the radius of the limiting ray + the turbulent kinetic energy, TKE. The TKE is directly given in atmospheric profile data within weather forecasts such as from [38], [39], while the limiting ray radius is a result of ray-tracing based on wind, temperature and pressure (+ humidity) as a function of altitude. NOTE: This [52], or any other physics based shadow-zone noise prediction method, is not yet implemented in SAFT – though, if found needed basic matlab-functions for this task are prepared.

4.9.3 The ground reflection term, TL_{GrRefl}:

Ground reflections for outdoor sound are typically modelled by a locally reacting sound impedance models for porous materials [54], assuming a plane wave, a stationary harmonic source. For a moving broadband source the standard ground reflection models assuming stationary narrowband sources tend to exaggerate the effect of ground reflections on the final noise levels close to ground. The narrowband models, for perfectly correlated direct and reflected noise at a hard wall give up to 6 dB amplification and down to total cancelation while uncorrelated direct and reflected noise typically would result in a mean amplification of 3 dB. Currently a variant of a standard ground reflection model which accounts for a broadband source, has been implemented in SAFT. This model corresponds to equation 21 from ref. [55] (= equation 2.7 in ref. [49]).

Input data for the locally reacting ground reflection model implemented in SAFT is limited to one variable, the flow resistivity of ground. The flow resistivity for any part of Sweden may be estimated from the knowledge of ground type class as given in the European database CORINE with a resolution of 25x25 m (Swedish resources to be found in [56]). The ground type class can then be related to an approximate value of flow resistivity or acoustic impedance [57].

NOTE: currently in SAFT only a possibility to input a fixed ground type (flow resistivity, ground impedance) over a ground grid is implemented. An extension to "real" varying ground data is planned. This matter is related to 1. the planned inclusion of topography (incident angle also of concern for the resulting noise at receiver some height above ground) and 2. compatibility with the TL-interpolation matrix concept, where the TL-interpolation matrix might be possible to de-couple from the ground reflection effects.

Remark: The matter of snow cover, potentially changing the ground effects rather drastically, is in SAFT simply handled by a fixed (low) flow resistivity set by the user.

Examples of ground reflection impact on receiver noise levels are found in chapter 5.3.2.

In Table 2 below typical flow resistivity values for different ground types are given.

Ground surface	**Flow Resistivity (cgs rayls = kPa*s/m²)**
Dry, new fallen snow	15-30
Sugar snow	25-50
In forest, pine or spruce	20-80
Grass, rough pasture	150-300
Roadside dirt, ill-defined, small rocks up to 10 cm diameter	300-800
Sandy silt, hard packed	800-2500
Clean limestone chips, thick layer (12-25mm mesh)	1500-4000
Earth, exposed and rain-packed	4000-8000
Quarry dust, fine, very hard packed by vehicles	5000-20000
Asphalt, sealed by dust and use	>20000

Table 2. Example flow resistivity values *[51]*, *[58]*

NOTE: SAFT TL interpolation matrix approach in SAFT (4.9.4) involve currently the ground reflection effect. In coming studies this situation may be overlooked aiming for a separation of this TL-effect from the TL-interpolation matrix to the propagation "post-processing".

NOTEs: 1. During the coming implementations also of narrow band noise in SAFT the current ground reflection model has to be overlooked and supplemented with a narrowband model accounting for a moving source. 2. Upcoming deeper studies of aircraft noise measurement results from the CSA ULLA project [12] might support the selection of alternative ground reflection models.

4.9.4 The air attenuation term, TL_{AirAtt}

This term contain the reduction in sound intensity levels between source and receiver due to the absorption of sound energy along the propagation path. I.e. data of the kind shown in Figure 42 for a vertical propagation but for general propagation paths through the atmosphere. Strongly frequency dependent.

Remark: The effect of propagation model choice, straight or refracted rays, tend to have only a very small effect on the resulting TL_{AirAtt}– see Figure 50 and discussion below - whereas *the choice of absorption model is shown to have a rather strong impact* – as already seen in Figure 44 in chapter4.8.3 above.

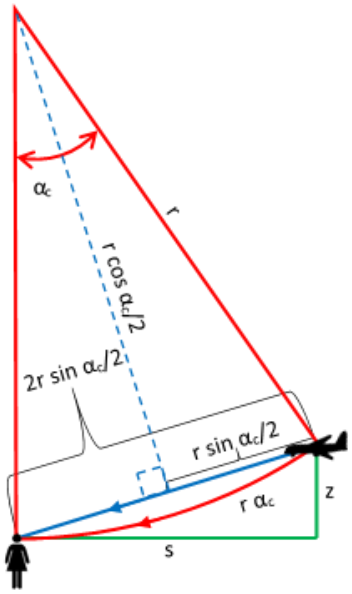

Figure 50. Comparison curved (red) vs straight (blue) sound ray with regard to absorption.

Figure 50 above is used to estimate typical impact on TL from solely absorption, depending on if a refractive or straight ray-model is applied. First we assume a constant radius of curvature for the curved ray, and for both the straight and curved ray a constant absorption in dB/m, while other factors, such as refraction, do not contribute to the TL. Then we study the elongation of the refractive propagation, or more precisely, the difference in distance, ΔR_{CuStr}, between the curved ray and the straight ray. This may be written as:

$\Delta R_{CuStr} = r\alpha_c - 2r\sin(\alpha_c/2) = r(\alpha_c - 2\sin(\alpha_c/2))$ where r is the ray bending radius and α_c is the angle it spans in radians. Further: $z = 2r \sin(\alpha_c/2)\sin(\alpha_c/2)$ and $s = 2r \sin(\alpha_c/2)\cos(\alpha_c/2)$

For some sample strongly conservative values on r, (5km, 10 km) and α_c (15°, 30°, 45°) we get:

Ray radius r(km)	α_c°	z(m)	s(km)	absorption in dB assuming straight ray 1kHz and 5dB/km	Elongation ΔR_{CuStr} (m)	**ΔdB absorption assuming 1kHz and 5dB/km**
5	15	170	1.3	6.5	4	**0.02**
5	30	670	2.5	12.9	30	**0.15**
5	45	(1465?)	3.5	19.1	100	**0.5**
10	15	340	2.6	13.1	7.5	**0.0375**
10	30	1340	5.0	25.9	60	**0.3**
10	45	(2930, non-realistic)	7.1	38.3	200	**1**

Table 3. Example cases of simplified ray-length elongations when going from straight to curved rays model together with estimated added absorption at 1kHz.
(Remark: 5 km and even 10 km bending radius considered unrealistically short/curved)

As seen in Table 3, even for such a probably unrealistic value as for a 10 km ray bending radius and a propagation over ca 5 km, the longer path, compared with a straight ray, would not add more absorption than ca 0.3 dB at 1 kHz. The situation is further emphasised within were a maximum ray elongation, versus straight rays, for a specific but "typical" atmosphere situation is shown. Such ray elongation maxima are by default identified when computing SAFT TL-interpolation matrices.

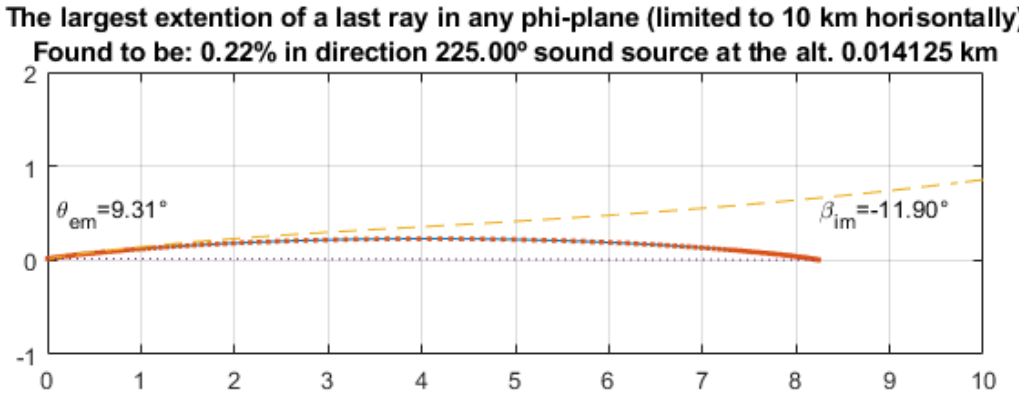

Figure 51. Example of max sound ray extension when going from straight to refractive rays.
Red large dotted = curved ray, (red small dotted = straight ray),
yellow dashed = straight ray emitted at same angle, θ_{em}, as the curved ray.
(β_{im}= incident ray angle)

We may from this conclude that the refraction impact on final noise levels typically depend on other factors than the effect of added absorption, such as refraction and changed source emission- and receiver immission angles.

NOTE: SAFT TL interpolation matrix approach in SAFT (4.9.4) involve currently the absorption effect. In coming studies this situation may be overlooked aiming for a separation of this TL-effect from the TL-interpolation matrix to the propagation "post-processing". Together with the same way of handling with regard to the TL-ground reflection effects, the TL-interpolation matrix would represent the refraction mechanisms only.

4.9.5 Transmission Loss interpolation matrix

This is, as far as we know, a new concept not found previously in the literature, where a TL-interpolation matrix, TL_{ip_mat}, is established and applicable for estimation of the TL as a function of frequency between any relevant (aircraft) position in the 3D space to any receiving point close to ground[24], for a given arbitrary atmospheric profile condition[25]. These TL_{ip_mat}:s are established by 2D ray-tracing in vertical planes emanating from a vertical z-axis and stretching radially outwards. All planes represents a user selected specific atmosphere profile, including horizontal wind components[26], and one of the previously listed absorption models that have been selected.

A SAFT TL_{ip_mat} is a 4D matrix spanning the 3D aircraft–to-receiver space in discrete steps + frequency, as follows (given in Matlab format as "start:step:end"):

Z_{TLmat}, aircraft (sound source) altitudes	$10^{\,1:0.15:4}$ = *10 14 20 28 40 56 79 112 158 224 316 ... 447 631 891 1259 1778 2512 3548 ... 5012 7079 10000 m*
R_{TLmat}, horizontal propagation distances	*0 : 100 : 10000* m
φ_{TLmat}, angles of vertical propagation planes	*0 °:* [user input step, $\Delta\varphi_{TLmat}$] : *360 °*
$f_{1/3\text{-octave}}$, 1/3-octave frequencies	*24* frequency bands between *50Hz to 10kHz*

Also needed input are:

θ_{TLmat}, emission angles[27]	- *78 °*: [user input step, $\Delta\theta_{TLmat}$] : *45 °*, a fcn of R_{TLmat}

... and a last internal variable needed for the final TL_{ip_mat} generation and application:

β_{TLmat}, angles of incidence	a function of R_{TLmat} , value between 0 °and 90 °

As noted above both the emission angles, θ_{TLmat}, and the angles of incidence, β_{TLmat}, in respective φ_{TLmat}-plane are involved in the TL_{ip_mat}. This is in order to keep track of the sound source strength (via θ_{TLmat} and φ_{TLmat}) and getting the correct ground reflection (via angle of incidence, β_{TLmat}). In the final use of the TL_{ip_mat} the emission and incidence angles are functions of all three independent TL_{ip_mat} variables Z_{TLmat}, R_{TLmat} and φ_{TLmat}.

As indicated above the user inputs with regard to TL_{ip_mat} definition is, beside the atmospheric data and choice of absorption model, limited to the vertical propagation planes step, $\Delta\varphi_{TLmat}$, and the emission angles step, $\Delta\theta_{TLmat}$. $\Delta\theta_{TLmat}$ is kept the same within each φ_{TLmat}-plane and typically given a value around 1° (a max of 3° may be used, could be a good choice for faster test runs) and a typical $\Delta\varphi_{TLmat}$ value could be 15°.

---

[24] limits: source height 0-10 km, receiver height 0-10 m, horizontal distance 0-10 km

[25] Atmospheric profile data from the ground surface up to slightly above the flight trajectory

[26] The 2D simplification involves a limitation in that lateral bending of rays due to wind- (or temperature-) gradients cannot be covered.

[27] horizontal emission angle = 0, vertically downward = -90. Max = +45 but this is usually reduced to a lower value, either due to a situation with an up-bending ground touching limiting ray occurs at a smaller angle or because the ground-hit takes place outside the limiting 10 km radius

It can be mentioned that TL_{ip_mat} levels are smoothed (see Figure 48 and Figure 49) and then interpolated to the final *r*-values = R_{TLmat} (current ray-tracing method create a random ground hit distribution).

Sound source altitude values, Z_{TLmat}, are as seen given in a logarithmic sequence. There are two reasons behind this approach, 1. The atmospheric wind profiles tend to have the largest gradients in the atmospheric surface layer, "Law of the wall", 2. We get a simpler and faster interpolation by introducing a constant step in the interpolation variable which are taken as the equidistant step of the exponent series of Z_{TLmat} , currently 0.15, i.e. using the exponent $log(Z_{TLmat})$ as interpolation variable instead of a varying step size in the Z_{TLmat} values.

NOTEs: Future improvement here could be 1. an adaptive emission angle algorithm, i.e. adaptive to an even distribution of *r*-values and 2. sound intensity in the current ray tracing implementation rely on the perpendicular distance between rays – by adding an equation it would be possible to trace the sound intensity along a single ray.

The established TL_{ip_mat} matrices are then applied in SAFT sound propagation studies by interpolation of sound intensity loss in dB between the aircraft (noise source) along the flight trajectory to a grid of receiving points on a fix height above ground. This method, i.e. applying an TL-interpolation matrix, linking any source point in the air with any ground point, is, since the ray-tracing is accomplished only once for each TL_{ip_mat} altitude Z_{TLmat} and for the limited set of vertical planes, φ_{TLmat}, instead of within a vertical plane for each trajectory- grid point combination, resulting in a significant reduction in computational time when computing noise contours for an aircraft passing.

A set of example data related to a TL_{ip_mat} matrix are shown in Figure 52 and Figure 53 below. Both sets are results of a SAFT ray-tracing run based on the previous atmosphere AROME data example for 20181205 UTC12 at Arlanda given in Figure 32 a) above. In Figure 52, we can see a representation of the TL_{Refr} part of the TL_{ip_mat} for this atmosphere data for some of the fixed sound source altitudes, namely for ~ 55, 110, 220, 450 and 900 m in the set of sub-figures a to f. Here, the strong TL_{Refr}-gradient, from dark blue to yellow in the north-east direction, indicate a sound shadow zone – seen to agree with ray bending radii in northern and easterly direction as shown in Figure 35 a). Note here that thicker dark contour line represent a zero TL_{Refr} and the area surrounded by this ticker curve relate to "amplified areas" where $TL_{Refr} < 0$, i.e. (slightly) higher noise levels than for a non-refractive model would be predicted. An corresponingly, outside such thicker dark contour "islands" we have predicted a reduction of noise levels compared with a non-refractive/straight rays approach. We may also note the rather smooth transition of the TL_{Refr} contours pattern when going towards higher altitudes – this is even more striking when considering that every second (logarithmically "stepped") altitude is left out in the sub-figure series of Figure 52.

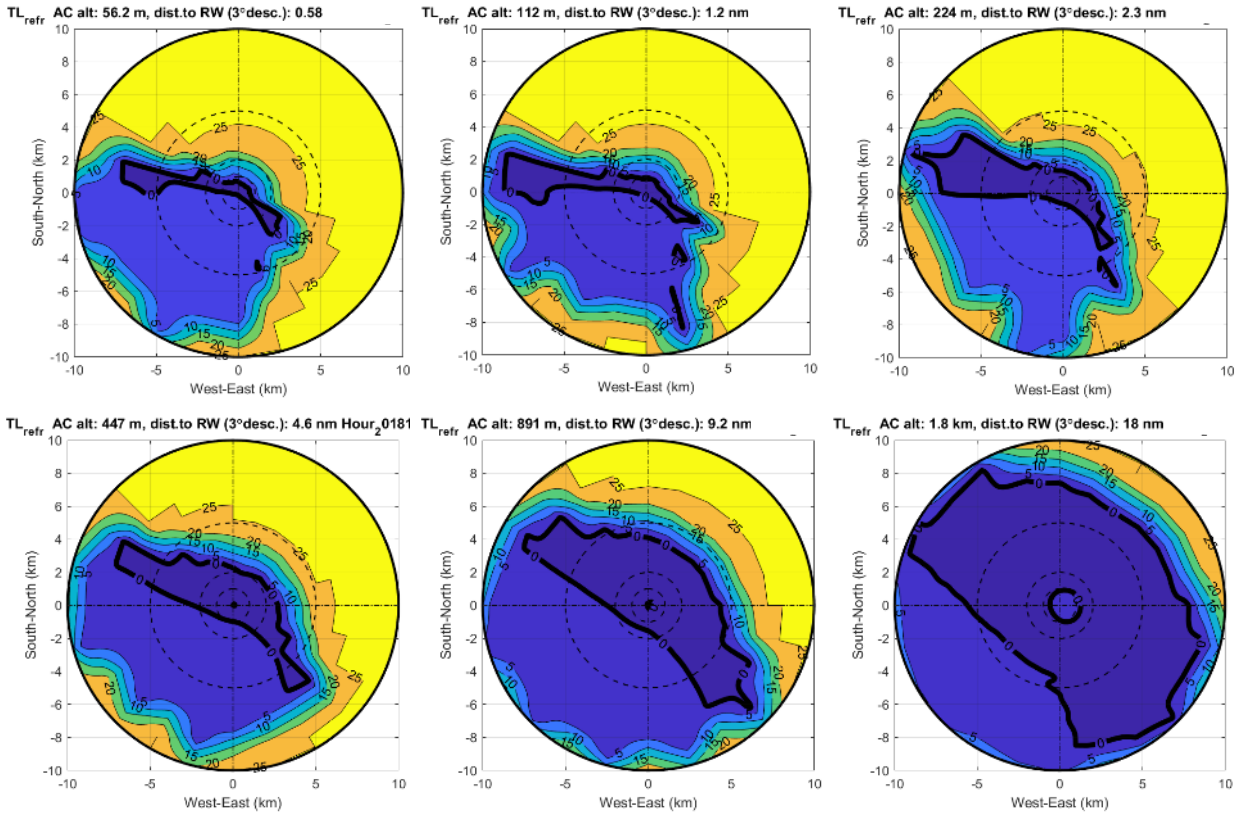

Figure 52 a-f. TL_{Refr} example in a TL_{ip_mat} matrix for aircraft altitudes ca:
55, 110, 220, 450 and 900 m given for the atmosphere as of Figure 29 a

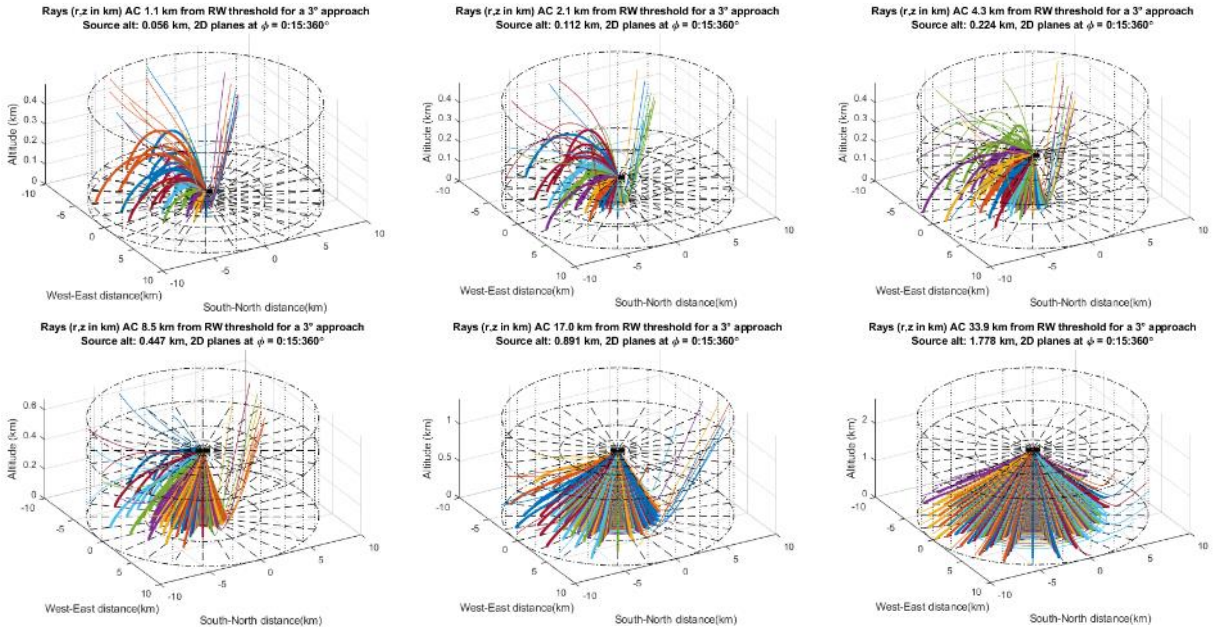

Figure 53 a-f. Ray patterns example behind the TL_{ip_mat} data in Figure 52 for aircraft altitudes ca: 55, 110, 220, 450 and 900 m given for the atmosphere as of Figure 29 a

In Figure 53 above the ray-patterns behind the TL_{Refr} contours shown in Figure 52 is shown. Here a limited set of rays for the same selected Z_{TLmat} sub-cases as Figure 52 are shown. Thicker lines

represent sound-rays hitting ground within the 10 km limiting radius while the thinner ones are limiting rays that bend upwards without reaching (an assumed flat) ground, i.e. a first ray within a shadow zone. Note that horizontal planes are plotted with a dashed-dotted circle at *r=10* km at *z=0* and *z*=source altitude with φ-vertical planes intersections plotted with dashed lines.

The same data as in Figure 53 is presented again in Figure 54, but this time in a 2D projection from above.

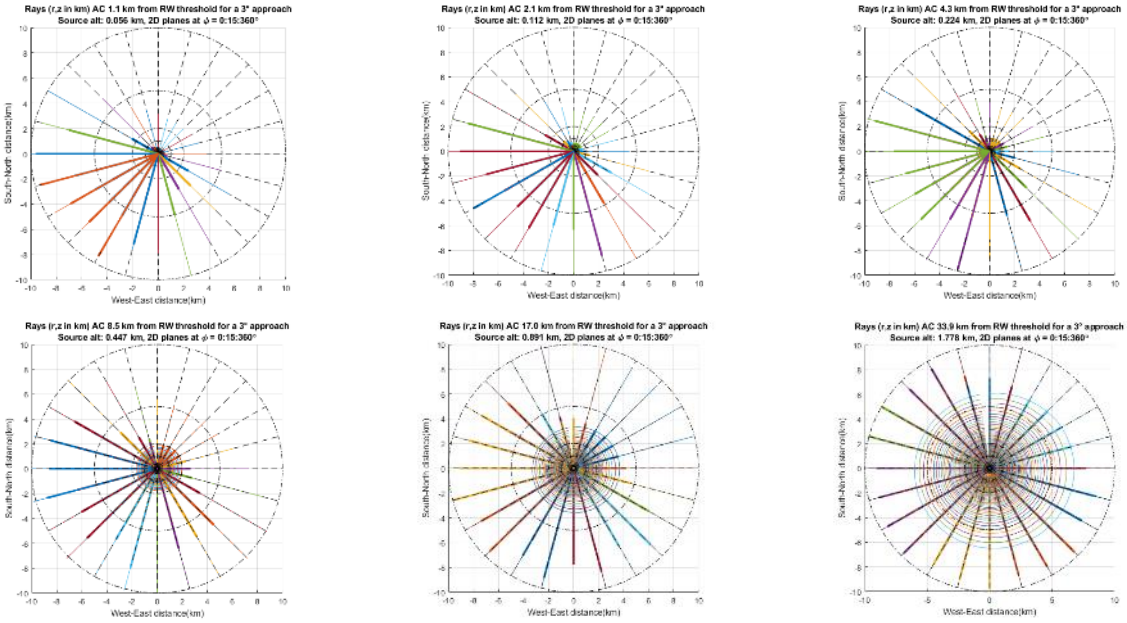

Figure 54 a-f. 2D ray patterns from same data as in in Figure 53 i.e. aircraft altitudes ca: 55, 110, 220, 450 and 900 m given for the atmosphere as of Figure 29 a

In Figure 54 we clearly see the $\Delta\varphi_{\text{TLmat}}$ = 15° increment between computational planes, and – if zooming in – the thicker rays related to ground hits within 10 km + the thinner representing rays not reaching ground. If zooming in one may also see coloured solid thin lines, depicting slightly distorted circles which are not closed between 345° and 360°. These show the distance to the closest shadow zone and follows the corresponding last ground hitting ray (identified by its emission angle) around all φ-planes. Looking carefully we see that the distortion from perfect circles tend to shift ground hits further from origo in the head wind direction and vice versa. Another noticeable pattern is that we get a significant TL>0 also in the tailwind direction (propagation towards south west) close to the 10 km limit (see e.g. sub-figures b in Figure 53 to Figure 54 above). This is sometimes a result of a kind of bifurcation where ray bundles below a certain emission angle are compressed and reach ground but a small increase of emission angle make the "next" ray take another higher path due to the atmospheric profile.

In An already mentioned limitation with the current implementation is that the ground topography is not allowed to vary much – though, also addressed above, the method is deemed to work very well in flat landscape types such as around Arlanda, example in Figure 55.

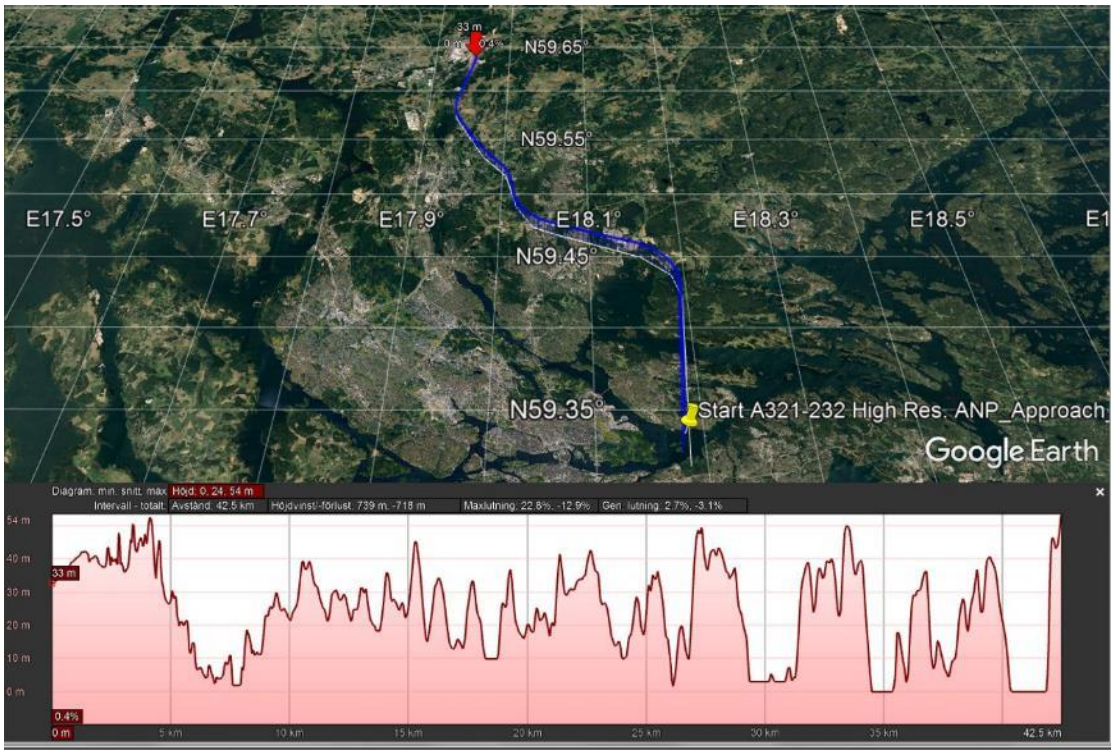

Figure 55. Example ground topography profile along approach route TMA entry from south (NILUG) to RW01L

To sum up: The TL-interpolation matrix is established with ray-tracing and given as a function of: 1/3-octave *frequency*, *aircraft altitude*, *horizontal distance* and *azimuth propagation angle*. To these data are also the *aircraft sound emission-* and *ground incident* angles related. The TL_{ip_mat} contains all significant physical mechanisms that affects the sound intensity along a propagation path.

4.10 Time stepping trajectory to ground grid

The time-stepping from aircraft trajectory positions down to ground grid points involves in the general case computation of noise levels in all grid points from all discrete aircraft positions covered with the selected time increment, typically one or a few seconds. In SAFT, as for a standard SEL computation or measurement, a reduction of time period, and thereby discrete source-receiver combinations, are based on a noise level decay of 10 dB compared with the max along the time interval of concern. This reduction of source point to grid points is in SAFT based on the distances between source to receiving points along grid lateral borders (see chapter 4.6 above and Figure 56 below). More precisely the distance from the aircraft in each trajectory point to receiving points along the longitudinal grid borders are compared with the closest among these distances for each trajectory position. Based on the mentioned distance relation factor of 10 dB the related matrix operations for ground grid noise histories and SEL are limited. The same distance based restriction is applied both for straight rays and refracted sound rays computations. A reason for this Euclidian distance based approximation of noise level decay to work as a good approximation also for (most) refracted rays modelling cases is that the refracted propagation tend more seldom to give strong

amplifications over larger areas[28], but more frequently large reductions ("sound shadows") in noise levels compared with the non-refractive sound propagation modelling.

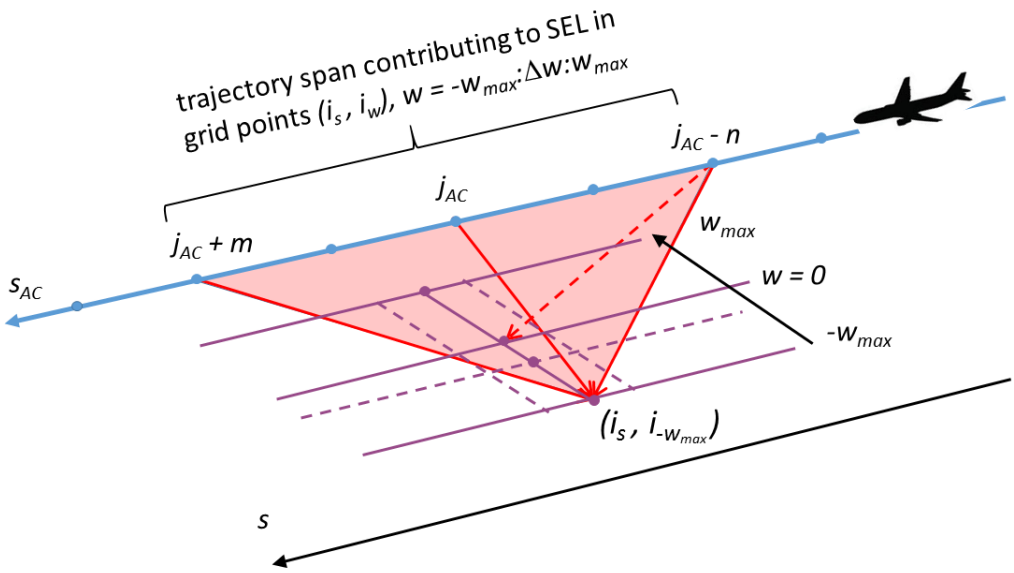

Figure 56. Schematic view of trajectory section contributing to $L_p(t)$ and SEL in grid column points at longitudinal grid coordinate s (same trajectory part assumed for all lateral *w*-values at *s*) Only trajectory points j_{AC-n} to j_{AC+m} contribute to SEL and sound pressure level history in points (i_s, i_w) $w = -w_{max}:\Delta w:w_{max}$

A corresponding relation as for "trajectory span to single ground point" exist also for "grid sections sonified above the criteria L_{pmax}-10dB from single trajectory points". In the figure above the straight sound ray borders of the red zone, e.g. from trajectory point j_{AC-n} to point $(i_s, i_{w_{max}})$ constitute borders also for such ground sectors where these trajectory points contribute significantly with regard to the 10 dB SEL-criteria.

In this time-stepping procedure the orientation of the aircraft is essential in order to get the correct sound source strength directivity in the propagation direction. Several coordinate systems, and transformation of coordinates between them, are involved in a standard SAFT-run. The most important ones are the *aircraft body system*, in which the noise source strength is defined, x-axis pointing in length direction, y-axis along the right wing and z- axis down. Then *ENU (East-North-Up)* systems, origo could be put at a RW threshold (altitude could here either be set as of curved earth – for coordinate transformation purposes - or flat, for initial noise computation), *lat long*, i.e. for final noise mapping. Beside these some intermediate coordinate systems are needed for transformation between *body, ENU* and *lat, long*. We also have the previously mentioned s, w coordinates for the ground grid.

[28] Typical atmospheric situations such as (temperature) inversions which are known to create strong increases of noise levels, e.g. "cylindrical propagation", $p^2 \sim 1/R$ instead of $p^2 \sim 1/R^2$ as for spherical propagation, is more sensitive to sound sources (and receiver) close to ground rather than at typical aircraft approach altitudes. The topic of elevated inversions has not yet been studied in enough detail but is not expected to drastically change this conclusion about refractive increases of noise levels except at very local sound propagation concentration zones (so called caustic points where ray cross section area =0 when applying ray tracing methods)

5. Examples of output from SAFT-runs

In this chapter some sample results from SAFT runs are gathered. The idea is not to present any conclusions from a directed study but primarily aimed to verify that SAFT works in the way it's designed for and also to show some features in SAFT that can find their application in future studies.

5.1 Noise mapping in contour plots

General input to example run 1 and 2

The example is taken for an Airbus A321-232 approaching Arlanda airport from the south and is landing on RW01R. The atmospheric conditions are taken from the previously shown AROME atmospheric data for Arlanda dated 20181205 UTC12 and presented in Figure 29 a. SAFT is run as a type 3. noise computation, i.e. *"3. Reversed engineering combined sound source from NPD-SEL and given spectral and directivity data"* with variation of the longitudinal directivity 1-default "forward heavy" or 2 – flat/zero longitudinal directivity. Since we deal with a sound source established with "back-propagation" and fitting to NPD-data, as briefly discussed in chapter 4.3, the source strength is coupled with the assumed directivity. With this follows that we get different source strengths in example run 1, see Figure 11 and Figure 12, compared with example run 2, with an assumed zero directivity. Example run 2 is shown to give to ca 3 dB higher source strength at $\theta = 90°$ (ca 5 dB lower at $\theta = 0°$ and ca 3 dB higher at $\theta = 180°$) as seen when comparing the levels between Figure 11 and Figure 57. The ground type is modelled as "grass" and given a fixed flow resistivity of 200 cgs rayls (kPa*s/m^2).

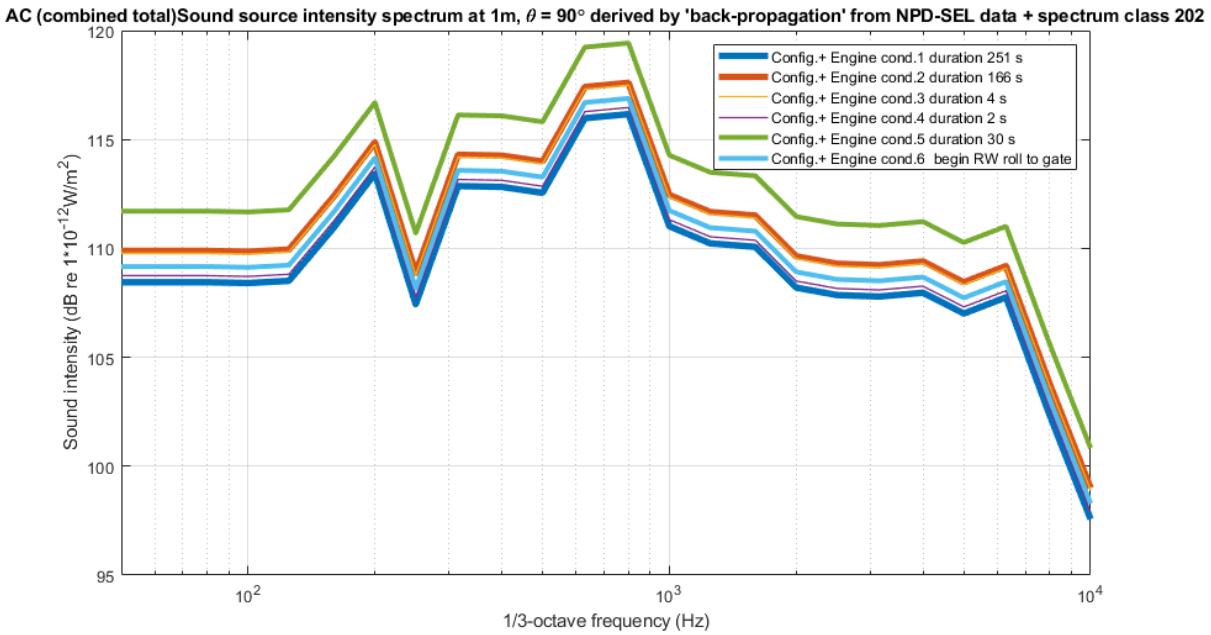

Figure 57. Sound source spectrum given for A321-232 if default ANP-state trajectory and a zero longitudinal directivity is assumed together with the default ANP-spectra 202.

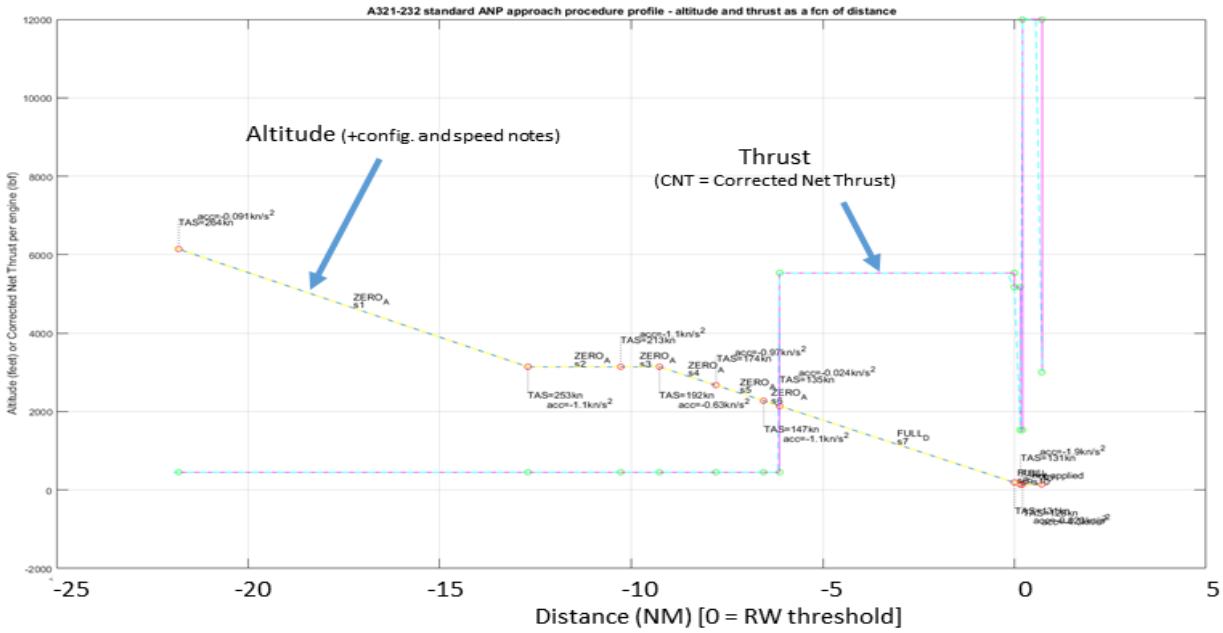

Figure 58. Assumed standard ANP-data altitude and CNT for an Airbus 320-211 as a fcn of distance
Text: TAS =True Air Speed, acc = acceleration, ZERO_A, FULL_D = configurations denoting "clean" and full slat+flap + L(anding)G(ear) down respectively

Results presentation – run 1"forward heavy" longitudinal directivity

The results shown in Figure 60 to Figure 62 relate to a longitudinal directivity as of Figure 12, i.e. a constructed directivity with strongly "forward-heavy" character representative for modern high by-pass turbo fans (but not necessarily for A321-232 with an older type of engines) in parts of the frequency regime where fan-noise tend to dominate during approach. The directivity is simplified to So, the results presented here are not intended for conclusions about A321-232 absolute levels but to give an example for ideas of the use of SAFT capabilities – which include not only comparative and trend analyses, but with validated source models, also absolute sound level measures.

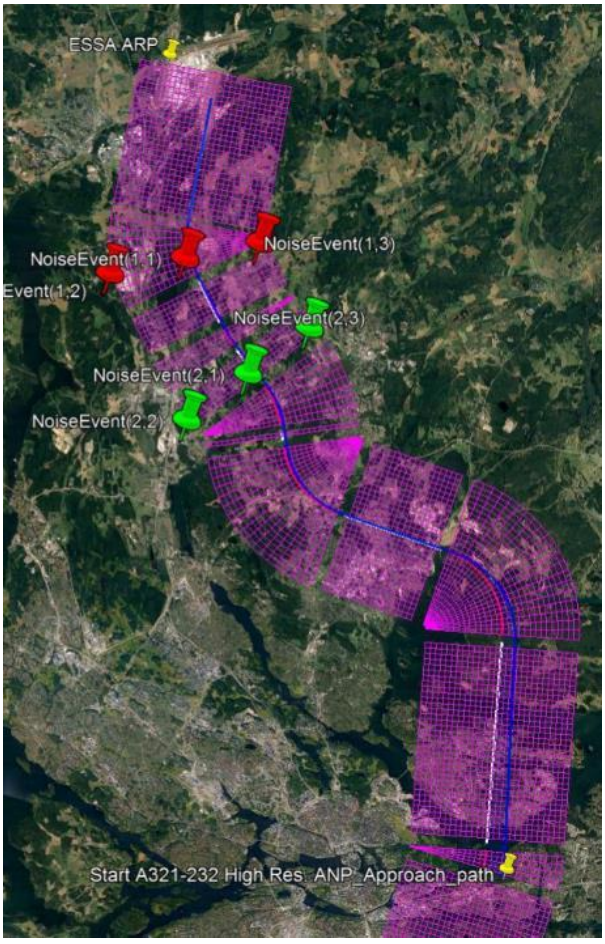

Figure 59. Grid, trajectory and "microphone" positions run examples 1 and 2

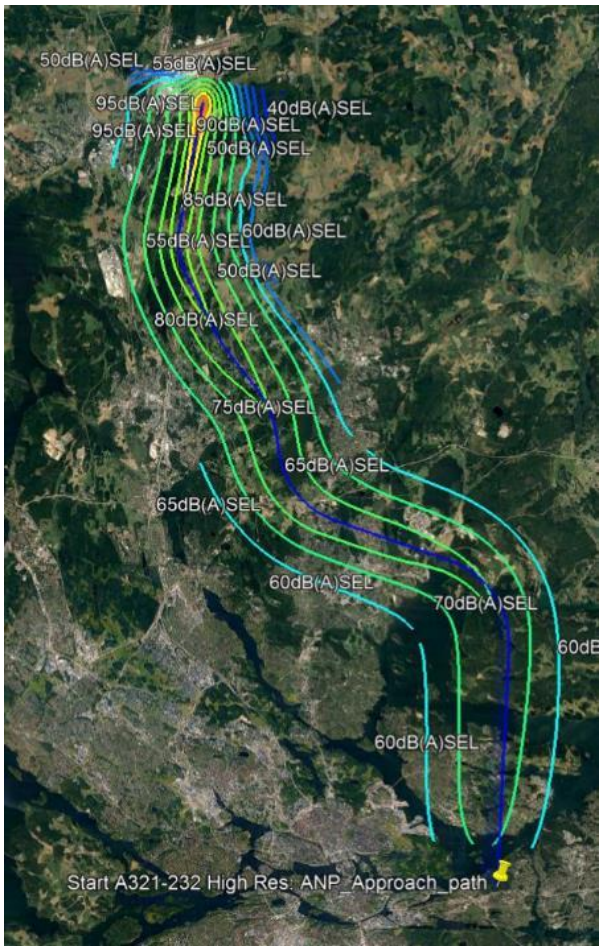

Figure 60. SEL refracted rays model contours run example 1

In Figure 59 above we see the example trajectory (blue), which stretches approximately 35 km in the South-North direction and 15 km in the West-East direction. Here, at some parts underneath the trajectory, the groundtrack can be discerned (white = straight and red = curved parts). The red ("Noise Event" 1.2, 1.1 and 1.3 from west to east) and green placemarks indicate positions where detail noise event data is collected, and presented in a large number of figures below. The receiving point 1.1 is placed almost straight below the trajectory, close to the groundtrack, while points 1.2 and 1.3 are positioned ca 3.5 km sideways, perpendicular, to the groundtrack. Note the curved groundtrack following closely after passing the receiver position line, this situation will quite naturally cause the noise levels in position 1.2 to decay faster than in 1.3, i.e. giving slightly lower SEL levels in 1.3 (for simulation methods with or without refraction included).

Figure 60 above shows noise contours for a refractive modelled atmosphere. Below in Figure 61 and Figure 62 differences between a straight ray model versus a refracted/curved rays model is presented. This is made for max levels and time history integrated SEL-levels respectively, in both cases A-weighted.

Figure 61. ΔdB L_{Amax} straight - refracted rays
contours (ΔdB>0 ⇒ straight>refr.)
white curve: ΔdB=0
contour line step = 1 dB

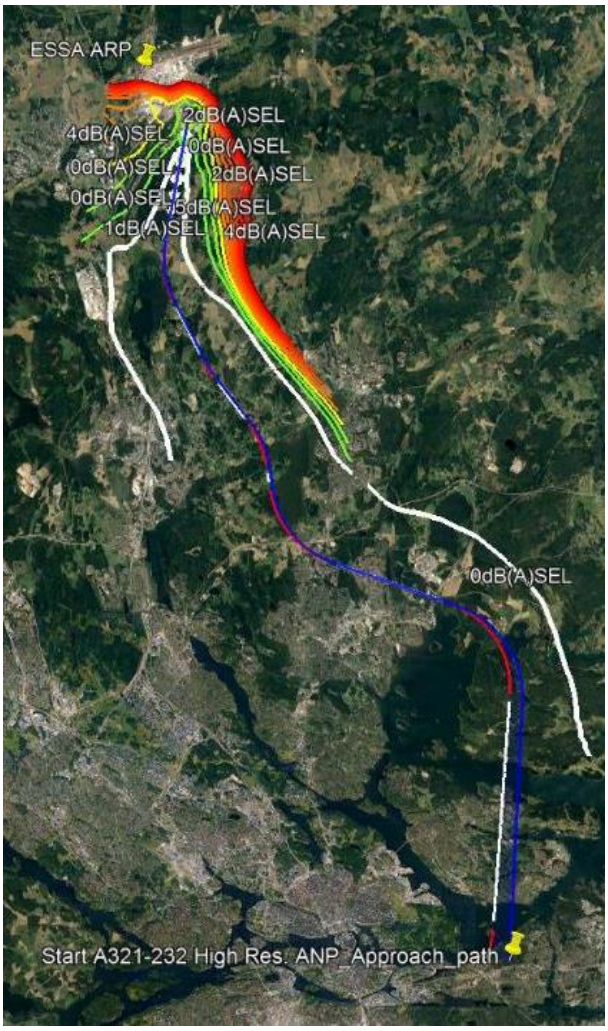

Figure 62. ΔdB SEL straight - refracted rays
contours (ΔdB>0 ⇒ straight>refr.)
white curve: ΔdB=0
contour line step = 1 dB

In Figure 61 and Figure 62 above we see a strong impact from the north-easterly wind, with its gradient and impact on effective sound velocity (see Figure 29 a and the following ”a”-figures for atmospheric wind-data and its impact on sound propagation). I.e. a reduction of levels in the north-easterly direction along the last half of the flight path, with a stronger impact on SEL-levels than on max levels.

Results presentation – run 2 "zero" longitudinal directivity

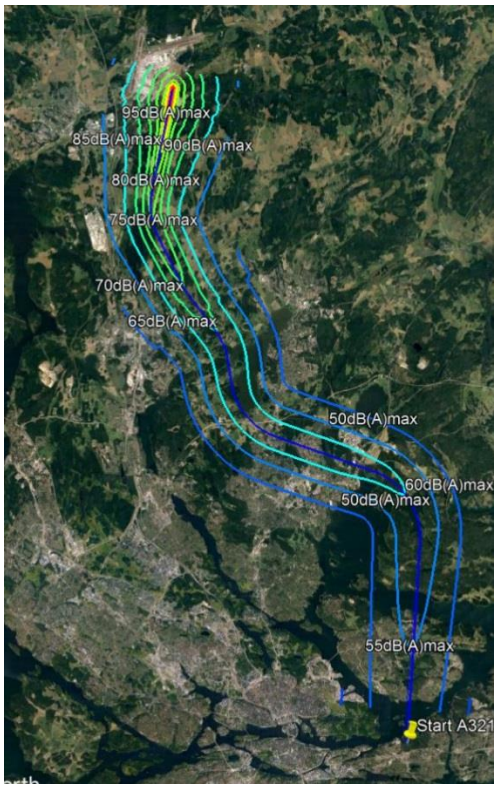

Figure 63. ECAC Doc.29 L_{Amax} contours run example 2

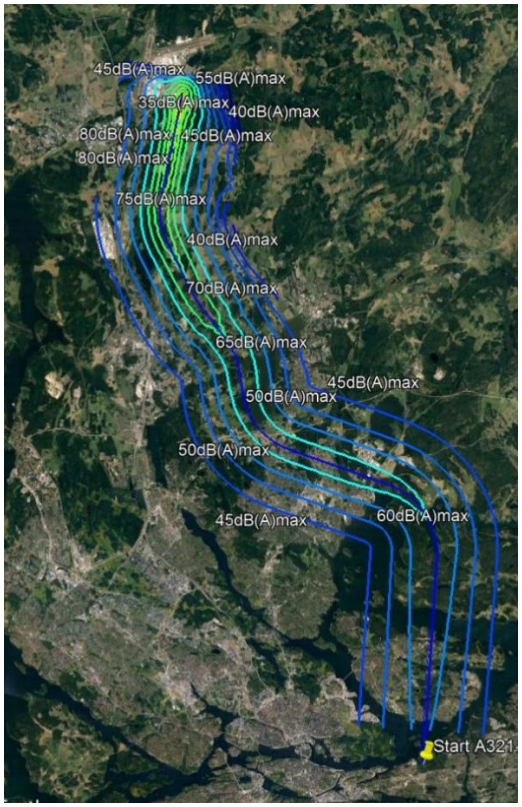

Figure 64. Refracted rays L_{Amax} contours run example 2

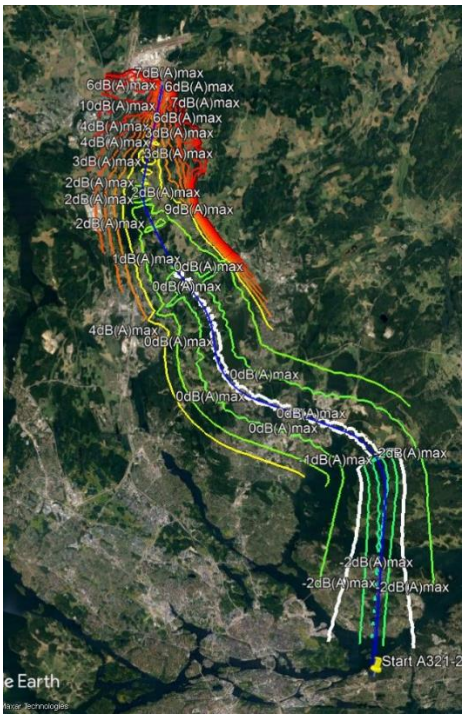

Figure 65. ΔdB L_{Amax} ECAC Doc.29 - refracted rays contours. White curve: ΔdB=0, contour line step = 1 dB.

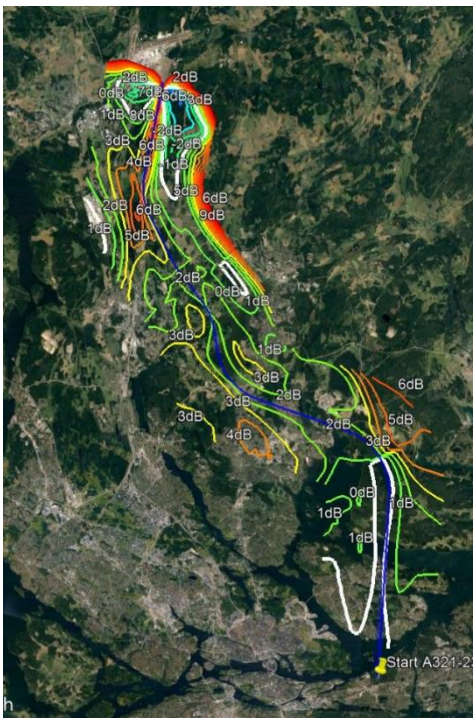

Figure 66. ΔdB SEL ECAC Doc.29 - refracted rays contours. White curve: ΔdB=0, contour line step = 1 dB.

Figure 63 and Figure 64 above show L_{Amax} contours for the example 2 input for an ECAC Doc.29 computation and a refractive "reversed-engineering", SAFT run type 3. In a first glimpse at these two contour plots one find two rather similar patterns, with e.g. turquoise contour denoting 60 dB spanning about the same region in the two cases. Looking outside this turquoise contour region, to the side of the flightpath, we see, as a general pattern, more contour lines in the "refractive" Figure 64 case than in the Figure 63 ECAC-case, implying a stronger lateral decline of noise levels in the refractive" case. This situation with slightly lower L_{Amax} levels predicted with SAFT-"refractive" simulation method is more explicitly shown in Figure 65 where contours for difference in dB, ΔdB, taken as: L_{Amax} of ECAC Doc.29 – L_{Amax} of SAFT "refractive" is plotted.

Note here that for ΔdB-plots contours colour holds:

- *white contour lines = 0 dB*
- *green = -2 to 2 dB (except for 0!)*
- *yellow/orange/red = +3 dB and higher*
- *turquoise/blue = -3 and lower*

In Figure 65 we see a rather small difference between ECAC Doc.29 and SAFT "refractive" L_{Amax} values close to the groundtrack (white contour line). The difference tend to increase with lower source/aircraft altitude and is except for the initial ca 10 km > 0, i.e. ECAC Doc.29 is predicting a higher level along the remaining part most clearly where the headwind sound propagation towards north east experience a sound shadow for lower aircraft altitudes – darker read contour lines.

Looking at ΔdB SEL-levels instead, in Figure 66, a more complex pattern is shown compared with the Figure 65 ΔdB L_{Amax}. Though, also here ECAC Doc.29 tend to estimate higher levels in general with a biggest difference in north-easterly direction.

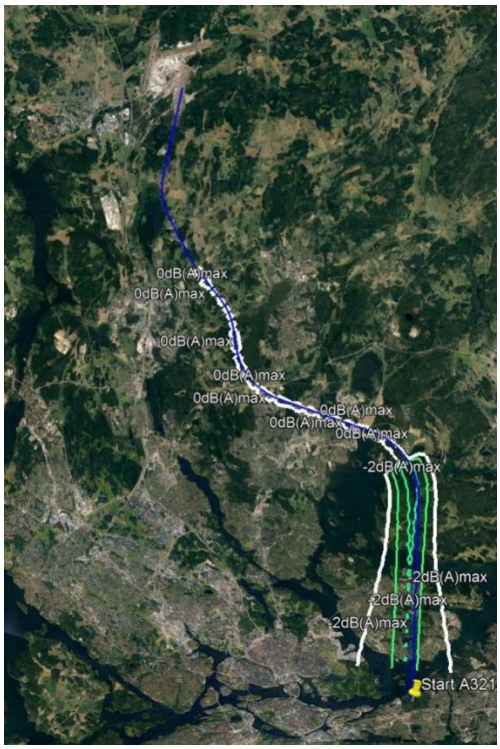

Figure 67. ΔdB L_{Amax} ECAC Doc.29 - refracted rays contours. Only ≤ 0 shown!

Figure 68. ΔdB SEL ECAC Doc.29 - refracted rays contours. Only ≤ 0 shown!

Data in Figure 67 and Figure 68 above contain the same data as Figure 65 and Figure 66 but with all "ECAC Doc.29 > "SAFT-refractive" contours removed, i.e. solely the small zones where "refractive" gives a higher level shown simply in order to clarify the presence of such zones.

NOTE: an error in the SAFT code was noticed when choosing the alternative to run the ECAC Doc.29 computation in the same run as a path 3 "reversed engineering simulation"- a gap on runway of noise contours was experienced. Until corrected it's recommended as a work-around to run ECAC Doc.29 cases for comparison in separate SAFT path 2 runs.

Results presentation – comparing run 1"forward heavy"- and run 2 "zero" longitudinal directivity

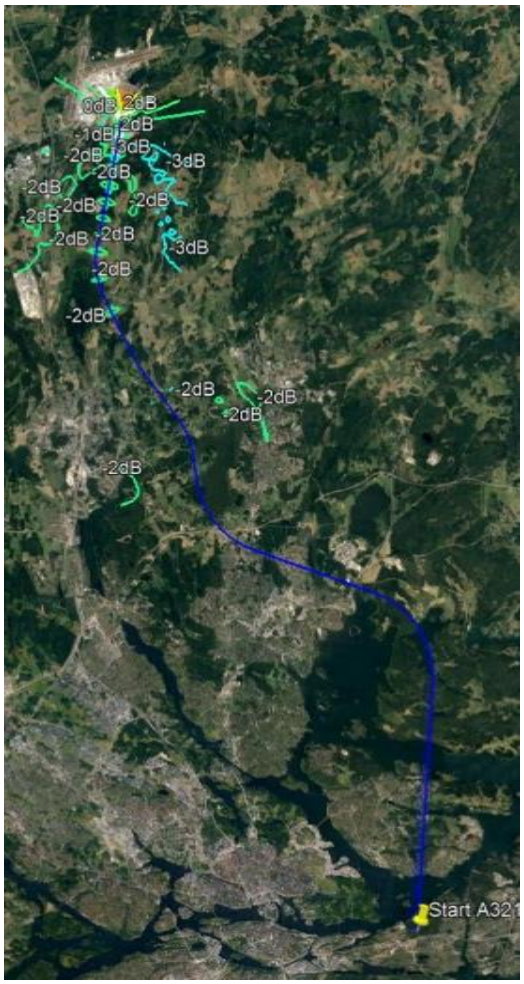

Figure 69. ΔdB L_{Amax} "forward heavy - zero dir"

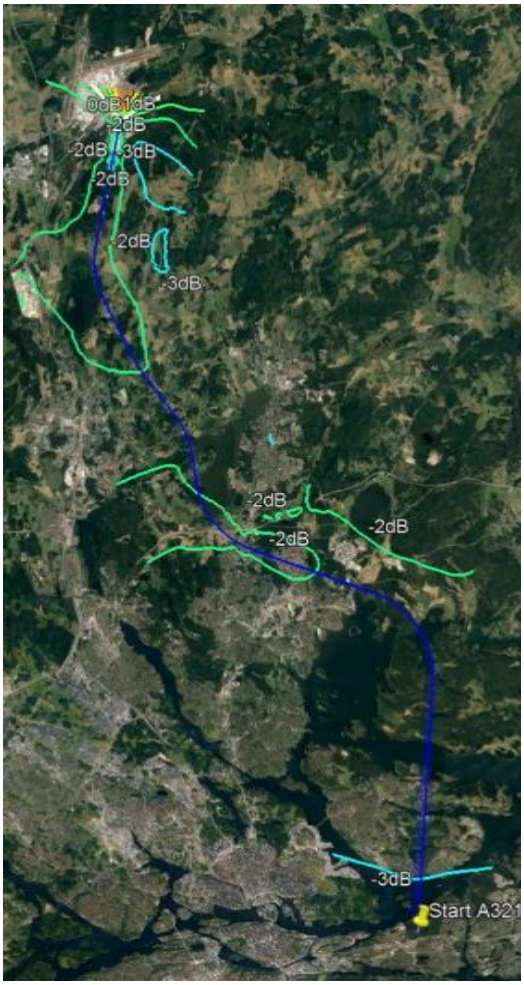

Figure 70. ΔdB SEL "forward heavy - zero dir"

In Figure 69 and Figure 70 we take a look at the impact from the longitudinal directivity of the aircraft. The "forward heavy" directivity as of example 1 data gives in general lower sound levels, in the L_{Amax} case between -2 and -1 dB. The exceptions are, quite naturally, a very small region in the airport area in front of aircraft last studied position. In the SEL-case the difference tend to be slightly higher, from -3 dB in the beginning of the studied groundtrack to around -2 at half the distance to the runway and on. Why this difference of about 2 dB between the different directivities occur is not yet clarified. At least for NPD-data generation conditions, 160 kt level flight and 1000 ft distance and for a SAE AIR-1845 atmospheric absorption, the NPD SEL level would be regained within the accuracy of inherent curve fitting in the SAFT path 3 "reversed engineering simulation". The deviations could be coupled to the spectra and changes of absorption from SAE AIR-1845 fix data to SAE ARP-5534

model, given the example atmosphere. Though, intuitively result such in Figure 70 would be expected to go in the opposite direction, this since SAE AIR-1845 is known to underestimate levels (i.e. overestimate absorption damping) and consequently the stronger impact from longer distances would turn out in higher SEL values when going to the SAE ARP-5534 model for a "forward heavy" longitudinal directivity.

Comment: No more investigations of the above SAFT path 3 variations with regard to directivity are planned. This is motivated by the anticipated implementation of measured sound sources in SAFT, see chapters 0 and 5.3.1. The focus will then turn to these "real data"-based sources, with expected much higher potential in general noise propagation simulations and with a better basis for validation than of the path 3 run types studied here. The path 3 would probably be used more for testing and educational purposes in the near future .

Run Example 3 – atmospheric AROME data examples run with ECAC Doc.29

In this run example we look at solely ECAC Doc.29 runs, but with different atmospheric data and absorption models. The samples atmospheric profile data is taken from a) 20 April 2017 UTC14 and b) August 2018 UTC14 (atmospheric data not shown.)

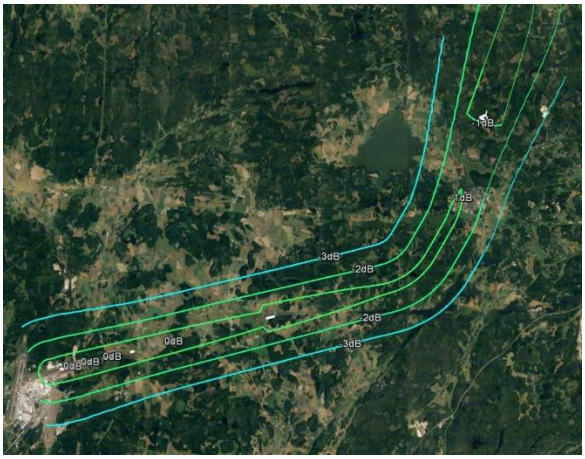

Figure 71. ΔL_{Amax} AIR1845 vs ARP866A atm. a)

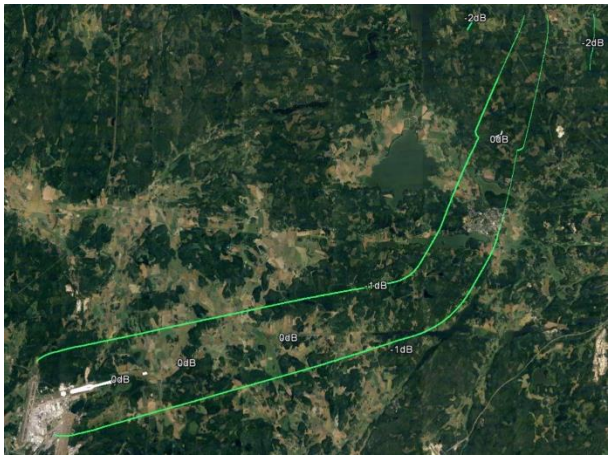

Figure 72. ΔL_{Amax} ARP866A vs ARP5534 atm. a)

Figure 73. ΔL_{Amax} ISA vs atm. a). with ARP5534

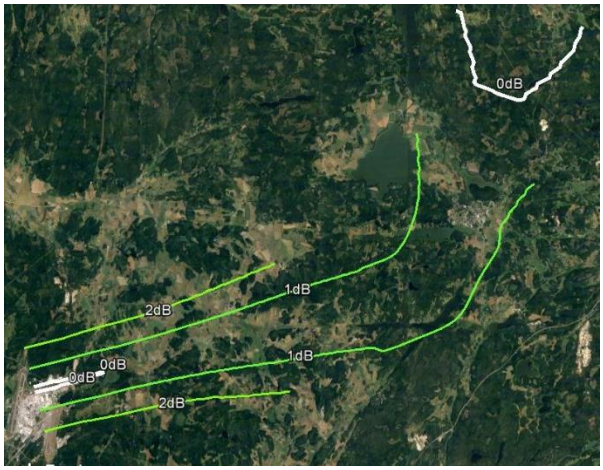

Figure 74. ΔL_{Amax} AROME atm. a) vs atm b)

5.2 Noise events in ground positions

In the examples 1 and 2 SAFT runs as defined above also noise time histories were computed in selected positions. The two examples differs, as already mentioned, only in regard to their source directivity (and thereby also slightly in $\theta = 90°$ source strength as discussed above) are gone through with regard to total noise level time histories and the different mechanisms behind these results.

See Figure 59 for the selected "microphone" positions. Green placemarks correspond to a groundtrack distance of 12 km from the runway threshold and red to ca 6 km distance. The same colours (about) corresponds to curve colours in Figure 75 and Figure 76 below. Herein the thickness of curves is linked to the lateral distance to the groundtrack such as, thickest curves: on (or close to) the groundtrack, medium thick: -3.5 km = 3.5 km laterally to the left in in the flight direction, and the thinnest: (+)3.5 km to the right in flight direction. And: solid lines = refracted rays simulation, dashed = straight rays simulation.

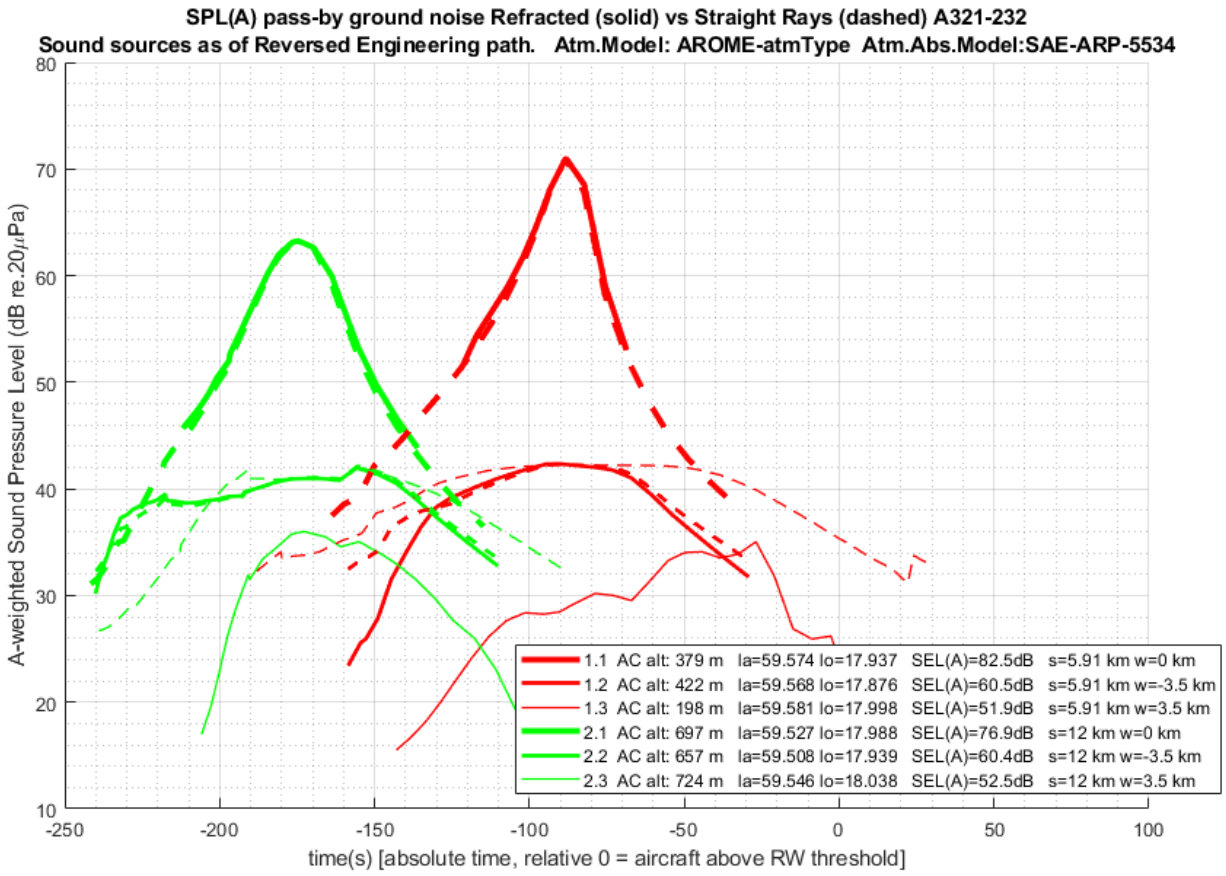

Figure 75. Total L_{pA} time histories in the 6 mic. points for example 1 "forward heavy" directivity

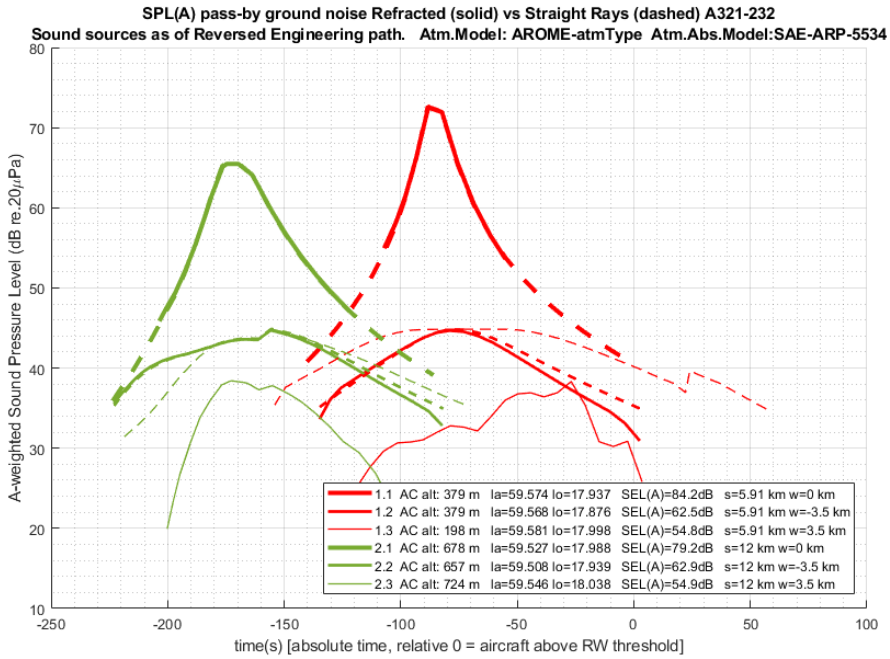

Figure 76. Total L_{pA} time histories in the 6 mic. points for example 2 zero longitudinal directivity

The results in in Figure 75 and Figure 76 above show slightly higher peak as well as SEL-levels for the flat/zero-directivity case. Comparing the results we get:

Property	**Directivity**	**Model↓\Point→**	**1.1**	**1.2**	**1.3**	**2.1**	**2.2**	**2.3**
s (km)		-	6	6	6	12	12	12
w(km)		-	0	-3.5	+3.5	0	-3.5	+3.5
SEL(dBA)	"forward"	refractive	82.5	60.5	(51.9)	76.9	60.4	(52.5)
SEL(dBA)	zero	"	84.2	62.5	(54.8)	79.2	62.9	(54.9)
SEL(dBA)	"forward"	straight rays	≈82.5	≈60.5	≈60.5	≈76.9	≈60.4	≈60.4
SEL(dBA)	zero	"	≈84.2	≈62.5	≈62.5	≈79.2	≈62.9	≈62.9
L_{pmax}(dBA)	"forward"	refractive	71	42	(35)	63	42	(36)
L_{pmax}(dBA)	zero	"	73	45	(38)	65.5	45	(38)
L_{pmax}(dBA)	"forward"	straight rays	71	42	42	63	42	42
L_{pmax}(dBA)	zero	"	73	45	45	65.5	45	45
Sound shadow			no	no	YES	no	no	YES

Table 4. Summary of noise time history models and levels as of SAFT run example cases 1 and 2.

In Table 4 we get a summary of what is already shown in Figure 75 and Figure 76 + indicated in Figure 69 and Figure 70 for the final part of the example trajectory. I.e. slightly higher levels, 2-3 dB, for the zero-directivity example 2 than in the "forward heavy" example 1 case. This seems quite natural looking at max levels when accounting the zero-directivity higher source strength in $\theta = 90°$, closest distance, -direction. Other things one may note here are:

- the laterally symmetric (with regard to the groundtrack) receiving point pairs, 1.2-1.3 and 2.2-2.3, respectively, showing a significant noise level difference due to that the 1.3. and 2.3 is found within the sound shadow.

- comparing the time histories within Figure 69 and Figure 70 shows a relative time delay (later rice towards peak levels) in the second figure, which can be attributed to the difference in directivity – i.e. a qualitative check that SAFT tend to work well in this sense.

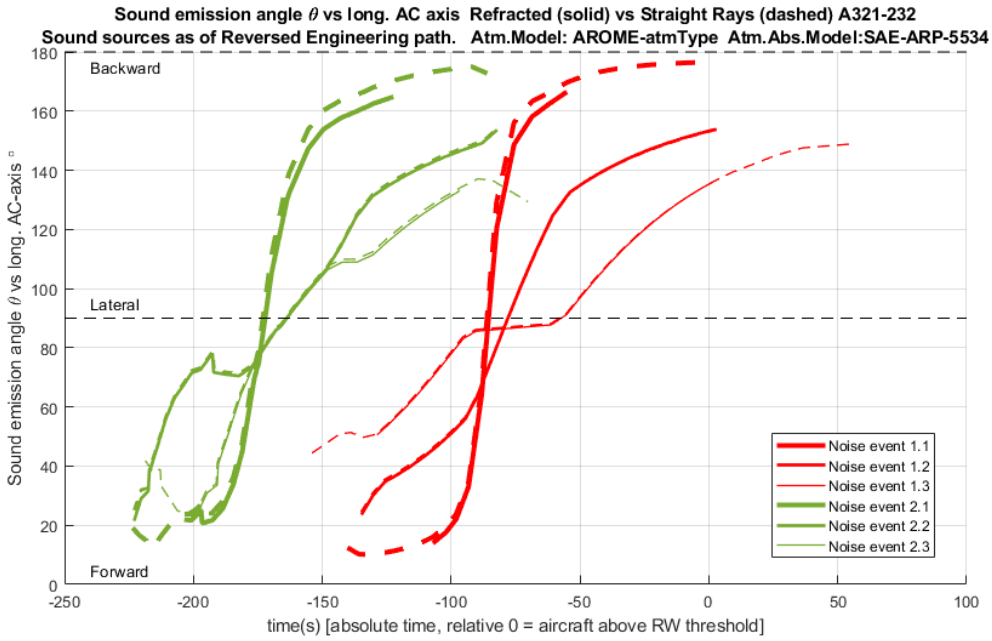

Figure 77. The longitudinal sound emission angle related to noise impinging at resp. pos. at time t

Results in *Figure 77* (from the example 2 case) show only a small difference between refracted and straight rays computation for the emission angle θ over time.

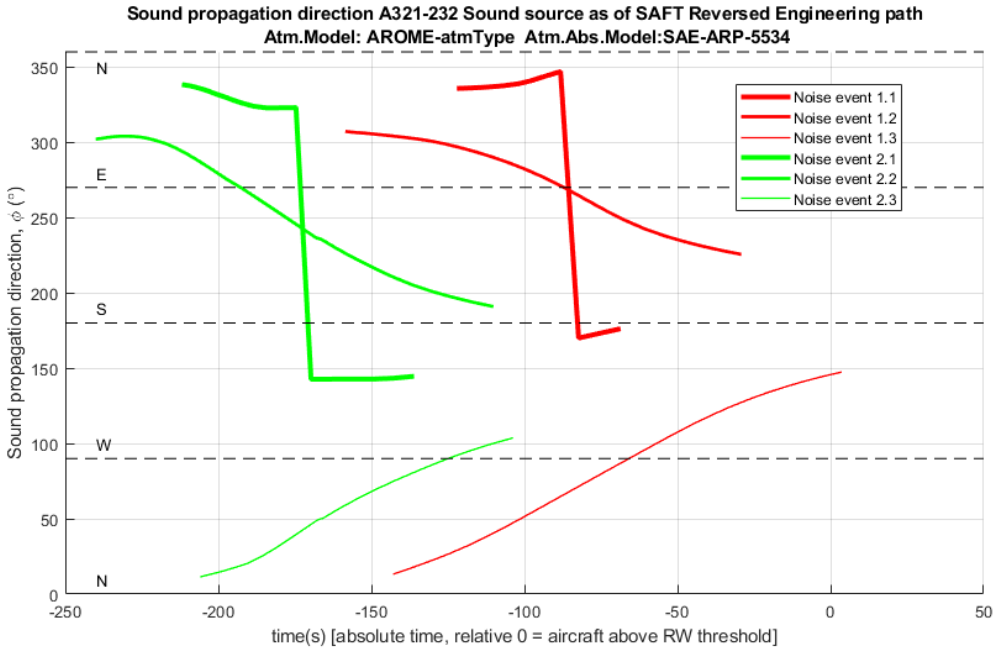

Figure 78. Sound propagation direction as a function of time for the 6 receiving points

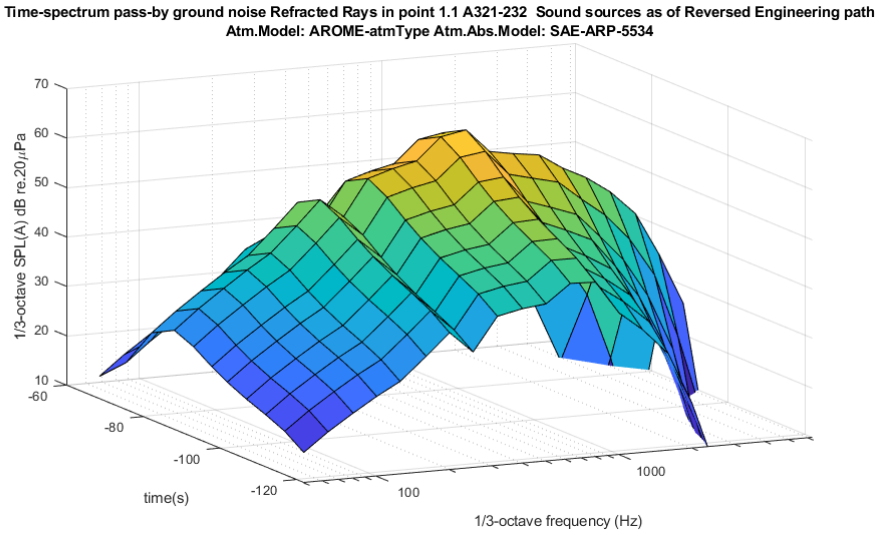

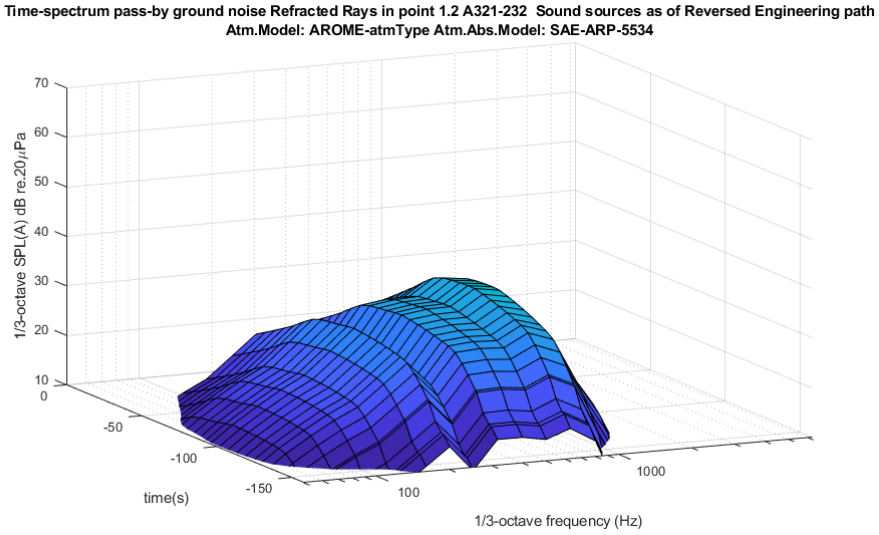

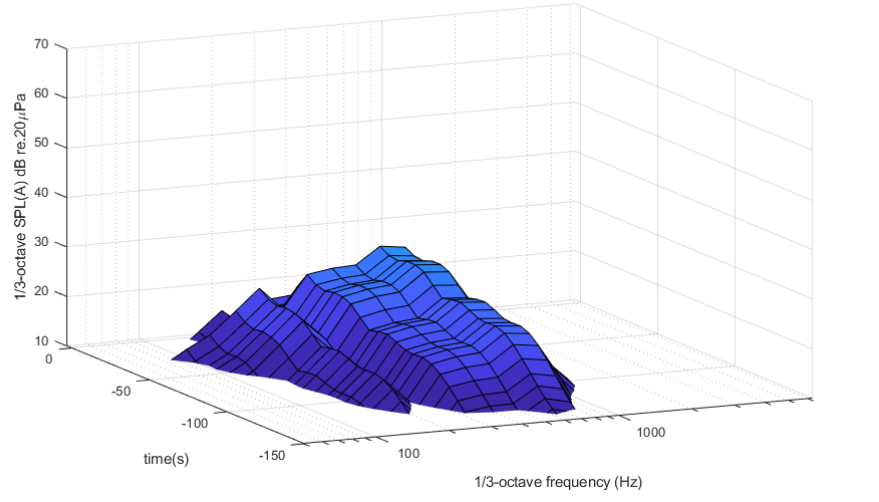

Figure 79.a-c Noise event time-spectra in points 1.1, 1.2 and 1.3

5.3 Partial TL-mechanisms in noise events - example plots

In the following a sample of plots are presented where we look into some of the physical mechanisms behind the previously presented noise levels, $L_p(t,f)$, experiensed as a function of time. The studied results are again taken from SAFT-simulations example 1("forward heavy directivity) in the three receiving points 1.1,1.2 and 1.3 as of Figure 59. In each plot we compare straight rays with refracted rays resulting levels, dashed = straight, solid = refracted. The

5.3.1 TL from absorption

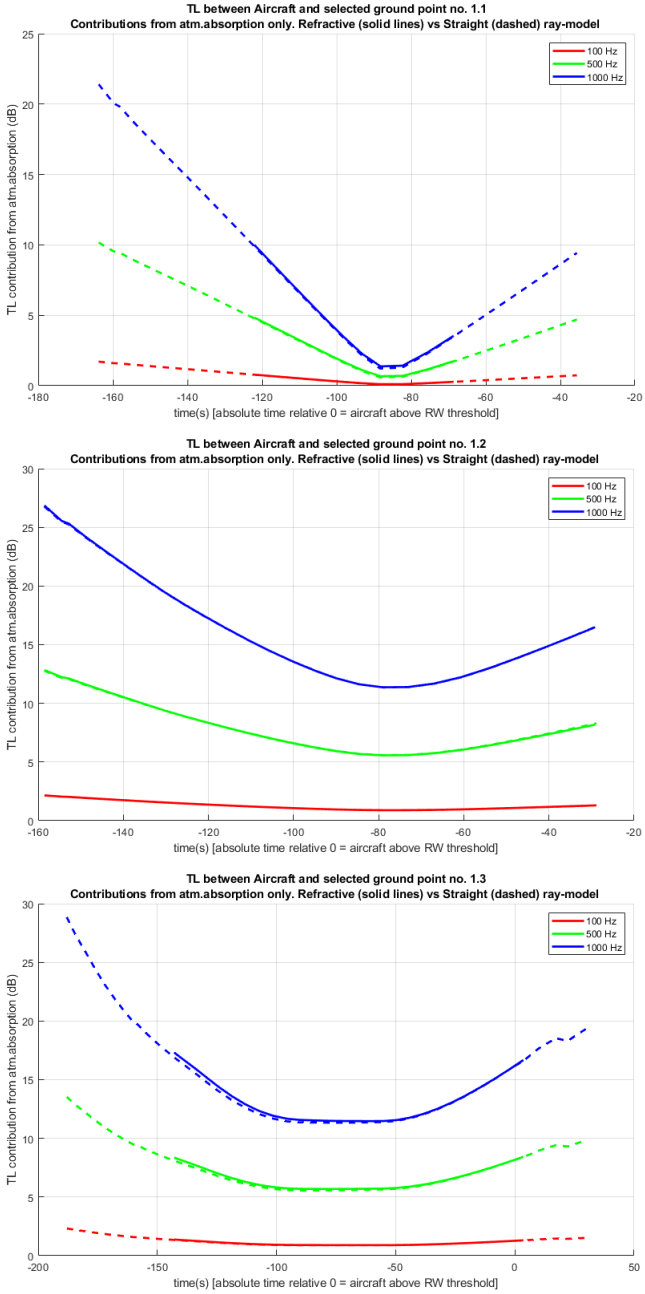

Figure 80 a-c. TL from absorption in points 1.1, 1.2 and 1.3
(solid = refractive, dashed = straight rays)

As seen above, Figure 80, the TL computed with or without refraction have not a signifficant impact, which is in line with previous reasoning about this matter.

5.3.2 Refraction and ground reflection impact

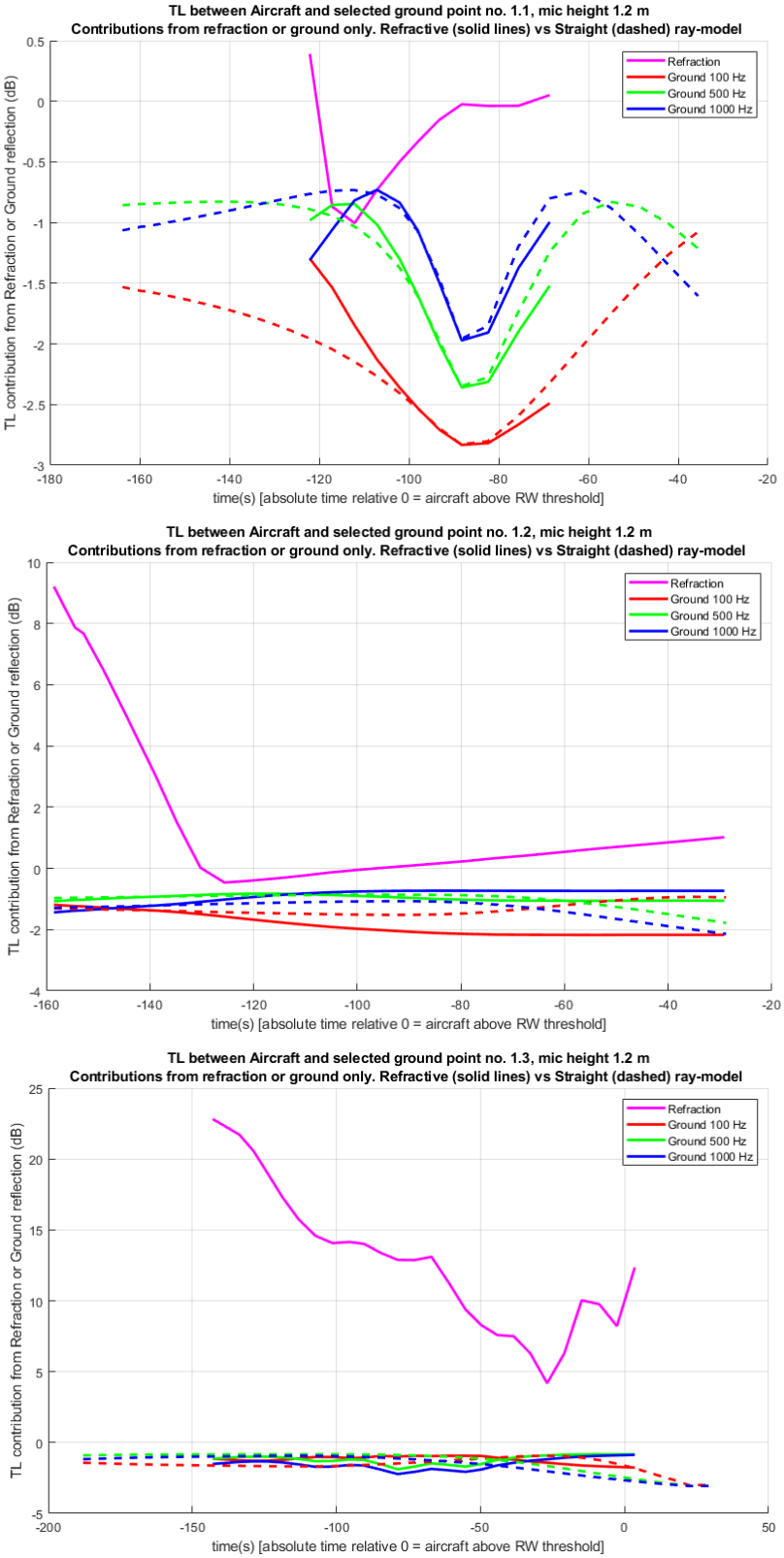

Figure 81 a-c. Ground effect and TL from refraction and in points 1.1, 1.2 and 1.3
(solid = refractive, dashed = straight rays)
NOTE: ground effect defined as a loss, i.e. < 0 with the applied model.

As already discussed, refraction impact can change drastically when the source-receiver system is close enough to a sound shadow region (and is hard to estimate in absolute numbers partly due to impact from stocastic turbulence and a lack of detailed enough models of the local atmosphere). But, on the other hand, in many cases a simple empiric model is enough since we know that levels inside the sound shadow becomes > 10 dB less than outside, making these zones of less concern.

5.3.3 Sound source directivity impact

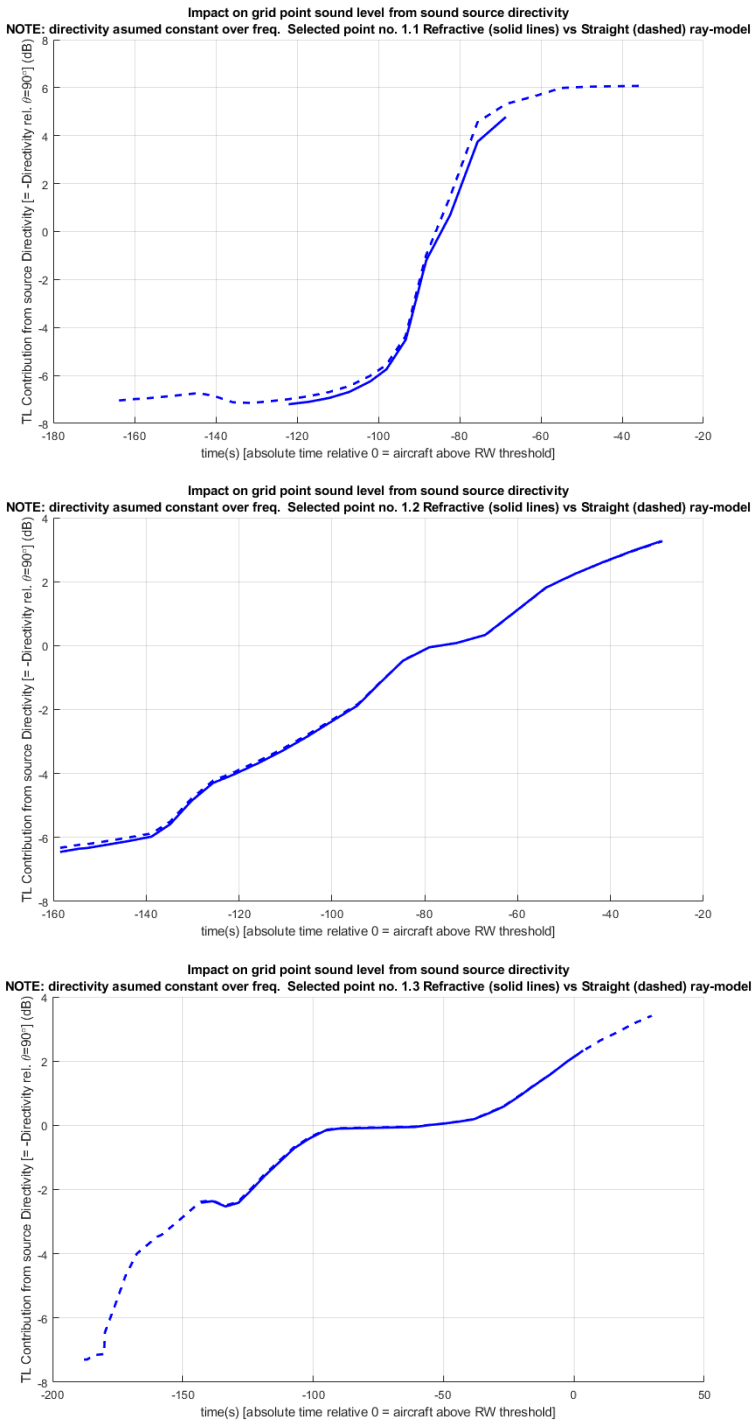

Figure 82 a-c. Impact from θ-dir. in points 1.1, 1.2 and 1.3 (solid = refractive, dashed = straight rays)

As of Figure 80 and Figure 82, and previously stated, the refractive ray-bending effect, compared with straight rays, tend to have only a small impact on the resulting absorption and directivity influence on the final noise levels on ground for typical aircraft noise applications.

NOTE: among the checked separate contributing mechanisms, giving the final noise level at the receiver, also the angle of incidence, β (used to compute ground effect as shown in Figure 81), would be interesting to plot. The same holds for the circumferential emission angle – which is applied in the code but not yet plotted together with the background mechanisms above.

The *impact from ground effects* (red, green and blue curves in Figure 81) are, for a specific ground type, with the applied model determined solely by the change in incident angle. Given the simplified flat ground, the used reflection model for wide band noise and impedance (flow resistivity as of "grass"), these effects tend to be rather small, 0.5 dB between straight and refracted rays in our example case . The direct *refraction* (purple curve) effects are of course larger, especially when looking at "low enough" flight. Though, for noise mapping of air traffic over longer time scales it is believed that these refractive effects in most cases would not change the over all picture significantly – this since the dominating sonified cases will dominate the integrated noise exposure levels. But, it is clear that the full understanding of the sound propagation mechanisms, and even more: the possibility to quantify them, including refraction, is of strong concern. This becomes especially clear when performing and judging aircraft noise measurements. This can involve such delicate matters as in the planned ULLA/CIDER/SAFT aircraft noise source strength estimations, where one have to judge the quality of each candidate noise measurement record. I.e. questions like: "- Why do we experience these low or strongly variating noise levels this period of time?", "- Could a sound shadow situation be the case?", "-Was it measured during a gusty turbulent weather situation?", ... , and similar are expected to occure, and buy support by SAFT simulations in combination with weather data at the time of measurement, to be validated and possible to answer.

6. SAFT status and future

6.1 General

During the project of SAFT a code with the same name has been established. The code is simple to understand and use. This is partly due to a code architecture and input flow that follows the computational path and its logics. The originally planned tool goals[29] are fulfilled, though during the work a need for other development routes has been identified, among them the possibilities for measurement-based noise sources.

The SAFT program has been applied in a follow-up work to the CSA project Brantare [59] where different approach procedure strategies involving a steeper than 3 degreee descent where studied with regard to noise (article under review).

6.2 Validation

The SAFT code has been verified in a number of test runs. Validation is harder to accomplish due to a lack of aircraft noise measurements open data to find in the literature, at least given in enough detail. Though, high quality noise measurements are expected in the coming CSA project cooperation between ULLA and CIDER. Together with this, ULLA/CIDER will actively search for cooperation with other actors in the field of aircraft noise source and propagation, both with regard to modelling and measurements – were we are willing to share experiences as well as data.

Moreover, results given by the SAFT NPD-based reversed engineering computational path has been compared with ECAC Doc.29 computations[30], and indicate, as shown in chapter 5, a good agreement along the ground track, where a difference of less than 1 dB is shown. Our refractive simulations show expected trends by giving unsymmetrical lateral noise contours with regard to straight groundtracks (where straight rays SAFT computations result in symmetric d:o) when strong enough side-wind and wind speed gradients occur.

Here it might be noted that performed tests of noise levels sideways separated from the groundtrack, SAFT tend to estimate slightly lower noise levels than ECAC Doc.29 (given the same atmospheric profile data and absorption model). If this is in line with reality has to be further investigated in coming work.

[29] From SAFT application 2016: "to establish a computational platform which allows for the simulation of noise exposure on ground from air traffic, taking into account the complete chain: type of aircraft/engine, trajectory, aircraft-/engine condition, noise generation and sound propagation in the given weather condition."

[30] ECAC Doc.29 runs with our SAFT implementation of the method

6.3 Dissemination

SAFT work has been presented at a number of national and international conferences and workshops, among them:

- Euronoise Crete June 2018 [60]
- CAES– Aeroacoustics Specialists Committee, Workshop NLR Amsterdam 2018 [61]
- Internoise Madrid June 2019 [62]

Future activities include internal (KTH, Chalmers, CSA) as well as external SAFT courses.

6.4 Future

The SAFT computational platform is planned to be extended with new functionalities to be developed within upcoming CSA-projects recently decided, June 2019. The development and implementation of these models and functionalities will mainly be carried out as sub-parts in projects CIDER and ODESTA (preliminary namee), outline to be presented on the CSA website.

These future developments of SAFT involve three anticipated major features:

- File input + batch run capabilities
- Noise measurement based noise sources for a representative number of aircraft types
- A multi-level gridding technique covering complete TMAs and able to cover air traffic over longer timespans, e.g. years

Other activities involve writing a manual, code verification and validation, eximine possibilities for CPU-time reductions.

7. References

[1] WHO, “Environmental Noise Guidelines for the European Region,” 2019. [Online]. Available: http://www.euro.who.int/__data/assets/pdf_file/0008/383921/noise-guidelines-eng.pdf?ua=1. [Accessed 7 July 2019].

[2] Transportstyrelsen - Sektionen för analys, “TRAFIKPROGNOS FÖR SVENSK LUFTFART, PROGNOS 2019–2025,” Transportstyrelsen , 2019.

[3] C. Zellmann, L. Bertsch, O. Schwab, F. Wolters and J. Delfs, “Aircraft noise assessment of next-generation narrow-body aircraft,” in *InterNoise 2019*, Madrid, 2019.

[4] LFV AROweb, “LFV AROWeb - AIS MET and Flight Planning IAIP – ESSA STOCKHOLM/Arlanda,” [Online]. Available: https://www.aro.lfv.se/Editorial/View/5695/ES_AD_2_ESSA_4-1_en. [Accessed 07 06 2019].

[5] LFV AROweb, “LFV AROWeb - AIS MET and Flight Planning IAIP – ESSA STOCKHOLM/Arlanda,” [Online]. Available: https://www.aro.lfv.se/Editorial/View/5439/ES_AD_2_ESSA_2-1_en. [Accessed 07 06 2019].

[6] ECAC, “ECAC Doc29 4th Edition: Report on Standard Method of Computing Noise Contours around Civil Airports. Vol.2 Technical Guide,” ECAC, 2016.

[7] Eurocontrol Experimental Centre , “The Aircraft Noise and Performance (ANP) Database,” [Online]. Available: https://www.aircraftnoisemodel.org/. [Accessed 7 6 2019].

[8] FAA, “Aviation Environmental Design Tool (AEDT),” [Online]. Available: https://aedt.faa.gov/. [Accessed 7 6 2019].

[9] P. Houtave and J.-P. Clairbois , ““Single aircraft pass-by: Modelling relevant noise at ground”,” in *Euronoise 2018*, Crete, 2018.

[10] C. Zellman, “Dr.Thesis: Development of an Aircraft Noise Emission Model Accounting for Flight Parameters,” Technischen Universität Berlin, Berlin, 2017.

[11] D. Mavris and C. Perullo, “Noise Power Distance Re-Evaluation, FAA Project 043,” 2018.

[12] A. Johansson, “Acoustic Measurements around Arlanda (presentation at CSA workshop 5 October 2018),” 2018. [Online]. Available: https://www.kth.se/polopoly_fs/1.874098.1550154409!/CSA%20workshop%202018%20ULLA%20A%20johansson.pptm.

[13] Center for Sustainable Aviation , “Centrum för Hållbar Luftfart,” 10 07 2019. [Online]. Available: https://www.kth.se/en/sci/centra/hallbarluftfart.

[14] Eurocontrol Experimental Centre, “The aiircraft Noise and Performance (ANP) Database: An intenational data resource for aircraft noise modellers,” [Online]. Available: https://www.aircraftnoisemodel.org.

[15] M. Schäfer, M. Strohmeier, V. Lenders, M. and M. Wilhelm, “Bringing up OpenSky: A large-scale ADS-B sensor network for research,” in *ACM/IEEE International Conference on Information Processing in Sensor Networks*, 2014.

[16] T. Grönstedt, ""Development of Methods for Analysis and Optimization of Complex Jet Engine Systems", PhD Thesis," Department of Thermo and Fluid Dynamics, Chalmers University of Technology, Gothenburg, 2000.

[17] SAKNAS, "CHOICE".

[18] Eurocontrol Laurent Cavadini, "ANP Data Verification and Validation," in *DG ENV-DG JRC Workshop on AIRCRAFT NOISE*, Brussels, 2010.

[19] Airbus, *PEP - Performance Engineer's Programs for Windows Version 5.6.1.*

[20] Eurocontrol, "BADA: aircraft performance model," [Online]. Available: https://simulations.eurocontrol.int/solutions/bada-aircraft-performance-model/. [Accessed 30 06 2019].

[21] SkyBrary, "Flight Data Recorder (FDR)," [Online]. Available: https://www.skybrary.aero/index.php/Flight_Data_Recorder_(FDR). [Accessed 30 06 2019].

[22] C. Struempfel and O. Lehmann, "Challenges and potentials of aircraft noise modeling using enhanced aircraft performance parameters and flight deck procedures," in *Internoise*, Hong-Kong, 2017.

[23] J. Suni, Henk Blom, J. Ellerbroek and J. Hoekstra, "Aircraft Mass and Thrust Estimation Using Recursive Bayesian Method," in *International Conference on Research in Air Transportation*, Barcelona, 2018.

[24] J. Sun, Joost Ellerbroek and J. Hoekstra, "Modeling Aircraft Performance Parameters with Open ADS-B Data," in *12th USA/Europe Air Traffic Management Research and Development*, 2017.

[25] Society of Automotive Engineers, "SAE AIR-1845 Procedure for the Calculation of Aircraft Noise in the Vicinity of Airports," SAE, 1986.

[26] EMPA ,R. Bütikofer, "Default aircraft source description and methods to assess source data," IMAGINE project 6th Framwork Programme IMA4DR-061204-EMPA-10, 2006.

[27] John A. Volpe National Transportation Systems Center, "Spectral Classes for FAA's Intgrated Noise Model vers.6," Federal Aviation Administration, Cambridge, MA, 1999.

[28] H. Ishii, T. Yokota, K. Makino, N. Shinohara and M. Sugawara, "Measurement of noise exposure planar distribution in aircraft approach path vicinity," in *Internoise* , Sydney, 2014.

[29] M. F. Heidmann, "Interim prediction method for fan and compressor source noise," NASA, 1975.

[30] P. Gliebe, R. Mani, H. Shin, B. Mitchell, G. Ashford, S. Salamah, S. Connell and D. Huff, "Aeroacoustic prediction codes," NASA, 2000.

[31] U. Vonglahn and E. Krejsa, "Correlation of core noise obtained by three signal coherence techniques," NASA, 1982.

[32] D. G. Dunn and N. Peart, "Aircraft noise source and contour estimation," NASA, 1973.

[33] J. W. Russell, "An empirical method for predicting the mixing noise levels of subsonic circular and coaxial jets," NASA, 1984.

[34] R. A. Golub, R. Sen, B. Hardy, K. Yamamoto, Y.-P. G. and G. Miller, "Airframe noise sub-component definition and model," 2004.

[35] R. A. Golub and Y.-P. Guo, "Empirical prediction of aircraft landing gear noise," 2005.

[36] F. d. Roo, E. Salomons, D. Heimann and P. Hullah, “IMAGINE - Reference and Engineering Models for Aircraft Noise Sources, IMAGINE project Deliverable 9,” 2006.

[37] Meteorologisk institut Norway, “MetCoOp,” 2019. [Online]. Available: https://www.met.no/en/projects/metcoop.

[38] Norwegian Meteorological Institute, “Free meteorological data,” [Online]. Available: https://www.met.no/en/free-meteorological-data. [Accessed 12 July 2019].

[39] SMHI - Swedish Meteorological Institute, “Meteorologiska modeller (in swedish),” [Online]. Available: http://www.smhi.se/kunskapsbanken/meteorologi/meteorologiska-modeller-1.5932. [Accessed 12 July 2019].

[40] Wikipedia, “Roughness length,” [Online]. Available: https://en.wikipedia.org/wiki/Roughness_length. [Accessed 22 06 2018].

[41] Society of Automotive Engineers, Standard values of atmospheric absorption as a function of temperature and humidity, SAE ARP 866A, SAE, 1975.

[42] Society of Automotive Engineers, Aerospace Recommended Practice, Application of pure-tone atmospheric absorption losses to one-third octave-band level, SAE-ARP-5534, SAE, 2013.

[43] American National Standards Institute, Methods for Calculation of the Absorption of Sound by the Atmosphere, ANSI/ASA S1.26-2014, 2014.

[44] International Organization for Standardization, Attenuation of sound during propagation outdoors -- Part 1: Calculation of the absorption of sound by the atmosphere, ISO 9613-1:1993, ISO, 1993.

[45] L. C. Sutherland and H. E. Bass, “Atmospheric absorption in the atmosphere up to 160 km,” *Journal of Acoustic Society of America,* vol. 115(3), p. 1012–1032, 2004.

[46] A. Pierce, Acoustics: an introduction to its physical principles 2nd ed., New York: McGraw-Hill, 1989.

[47] Wikipedia, “Convective planetary boundary layer,” [Online]. Available: https://en.wikipedia.org/wiki/Convective_planetary_boundary_layer. [Accessed 22 06 2019].

[48] I. Karasalo, “"Assessment Of A Simplified Environmental Model For Aircraft Noise Prediction"," in *Internoise 2019*, Madrid, 2019.

[49] K. Poulain, “Numerical Propagation of Aircraft En-Route Noise, A Thesis in Acoustics,” The Pennsylvania State University, 2011.

[50] J. Lamancusa and P. Daroux, “Ray tracing in a moving medium with two-dimensional sound-speed variation and application to sound propagation over terrain discontinuities,” *Journal of the Acoustical Society of America,* vol. 93, p. 1716–1726, 1993.

[51] K. Attenborough and (. T. D.Rossing), “4. Sound Propagation in the Atmosphere,” in *Springer Handbook of Acoustics*, New York, Springer, 2007, pp. 113-143.

[52] Y. W. Lam, “An analytical model for turbulence scattered rays in the shadow zone for outdoor sound propagation calculation,” *Journal of the Acoustical Society of America,* vol. 125(3), p. 1340–1350, 2009.

[53] U. Tengzelius and I. Karasalo, “Sound in shadow zones due to atmospheric turbulence - comparison of ray-based predictions with experimental data,” Sevilla, 2013.

[54] E. M. Delaney, “Acoustical Properties of fibrous absorbent materials,” *Applied Acoustics,* vol. 3, p. 105–116, 1970.

[55] C. Chessell, “Propagation of noise along a finite impedance boundary,” *Journal of the Acoustical Society of America,* vol. 62, no. (4), p. 825–834, 1977.

[56] Lantmäteriet, “CORINE Land Cover,” [Online]. Available: https://www.lantmateriet.se/en/about-lantmateriet/Samverkan-med-andra/internationell-samverkan/corine-land-cover/. [Accessed 22 06 2019].

[57] M. Sohlman and H. Jonasson, “Using Satellite data for the determination of the acoustic impedance of ground, Report to the Swedish National Space Board,” Metria, 2004.

[58] J. S. Lamancusa, “10. OUTDOOR SOUND PROPAGATION,” [Online]. Available: https://www.mne.psu.edu/lamancusa/me458/10_osp.pdf. [Accessed 22 June 2019].

[59] B. M. Johan Rignér, “Slutrapport projekt Brantare,” CSA, Stockholm, 2019.

[60] U. Tengzelius, T. Grönstedt, F. Bahmani and I. Karasalo, “SAFT – Simulation of atmosphere and Air traffic For a quieter environmenT,” in *Euronoise 2018*, Krete, 2018.

[61] U. Tengzelius, “Simulation of atmosphere and Air traffic For a quieter environmenT (SAFT),” in *22nd Workshop of the Aeroacoustics Specialists Committee of the CEAS Future Aircraft Design and Noise Impact*, Amsterdam, 2018.

[62] U. Tengzelius and M. Åbom, “Aircraft pass-by noise on ground modelled with the SAFT-program,” in *Internoise 2019*, Madrid, 2019.

[63] BBN Laboratories Inc., “Revision of the civil aircraft noise data for the Integrated noise Model (INM),” Dep.of Transportation U.S., Cambridge MA, 1986.

[64] ICAO, Manual of the ICAO Standard Atmosphere 3rd edition Doc 7488/3, 1993.

Appendix 1: In Swedish ONLY

Kommentarer från Swedavia med svar (i rött) från inblandade forskare

Bakgrund: Slutrapport_SAFT_2019 har granskats översiktligt av Swedavias akustiker och här sammanfattas några synpunkter av Christer Heed.

Not: I den följande texten redovisas Christer Heeds (Swedavia), synpunkter i svart text medan kommentarer till dessa från projektgruppen-SAFT/CSA ges i röd text.

Fokus vid denna granskning har varit myndigheters krav på och flygplatsers behov av en ny och nationellt utvecklad beräkningsmetod som, i samband med miljöprövningar och Riksintressepreciseringar, bättre skulle bidra till att beskriva flygbullerexponering enligt de av regeringen uppsatta riktvärden, än den metod som används idag.

Allmänt:

Syftet med det arbete som gjorts inom projekt SAFT har varit att ta fram ett verktyg som medger beräkning av buller nära marken vid flygplanspassager.

Mot bakgrund av att den metod, ECAC Doc.29, som idag används rutinmässigt för flygbullerkartering över längre tidsperioder, typiskt ett år, endast kan ge en grov uppskattning av ljudnivåer för enstaka bullerhändelser[31] ansågs det vid starten av SAFT-projektet föreligga ett behov av förbättrade beräkningsmetoder – med bättre ljudkälls- och utbredningsmodeller som möjliggör analys av effekten av nya start/landningsprocedurer, flygplanstyper med syfte att på sikt förbättra bullersituationen kring flygplatser.

Bakom detta bedömda behov ligger, vid sidan om brister avseende frekvens- och tidsinformation, bland annat det faktum att Doc.29, tillsammans med den kopplade bullerdatabanken, NPD-data, saknar möjligheten att inkludera effekter av flygplanens procedurer (fart och konfiguration). Detta är speciellt känsligt för ”approach” beräkningar där det finns stora variationer i sättet att föra fram flygplanet och därmed påverka resulterande buller vid marken. En av konsekvenserna av detta är alltså att man inte kan utnyttja Doc.29 för optimering av inflygningar med avseende på fart och konfiguration. Kopplat till detta anser vi också att det finns ett intresse att studera flygbullrets egenskaper ur fler aspekter än att reducera det till en konturlinje/siffervärde på en karta representerande säg ett års flygtrafik – d.v.s till vad som är betingat av de krav som miljölagstiftningen ställer på verksamhetsutövaren.

Syftet med SAFT har alltså inte varit att på kort sikt verka för att få ECAC Doc.29 ersatt som nationell kod i rättsligt relaterade flygbullerfrågor – utan att möjliggöra studier – och i förlängningen förbättringar av bullersituationen för boende kring flygplatser genom förslag till flygoperativa förändringar . Med SAFT kan dessa frågor studeras mer generellt än med Doc.29.

[31] Doc.29 och motsvarande s.k. ”integrerade metoder ”saknar t.ex. möjlighet att ge information av frekvensinnehåll (bortsett från grovt skattade s.k. typ-spektra för äldre flygplanstyper) eller ljudtryck som funktion av tiden.

Vi vill här passa på att påpeka att det redan för c:a 10 år sedan även i ECAC Doc.29 uttrycktes att integrerade metoder, av typ Doc.29, har begränsade möjligheter jämfört med s.k. simuleringsmetoder (t.ex.SAFT):

> "... integrated models represent current best practice. This situation may change at some point in the future: 'simulation' models have greater potential and *it is only (1) a shortage of the comprehensive data they require*, and *(2) their higher demands on computing capacity, that presently restrict them* to special applications (including research)"

För de nämnda, "enda", hindren (1) och (2) ovan kan man konstatera att:
(2) "datorkapacitet" utgör knappast något hinder med dagens datorkapacitet medan (1) "brist på data" (läs: fram till idag, data = NPD-data) kräver en längre diskussion. Vi, kopplade till projeket SAFT, bedömer det som fullt möjligt att, även för mindre organisationer, etablera databaser som är vida överlägsna NPD-databasen vad gäller täckning av olika existerande flygplanstyper och dess egenskaper som frekvensberoende ljudkällor relaterat till fysikaliska parametrar såsom hastighet, konfiguration och mottorvarvtal. Det handlar som vi ser det mer om en bedömning av behovet för en förbättrad simuleringsmetod och "buller"-databas samt om viljan att driva frågan på nationell och internationell nivå. Det kan i sammanhanget tilläggas att tillgången på överkomlig avancerad mätteknik och öppna data idag, gör att flygindustrins marknadsmässigt motiverade ovilja att dela med sig av bullerrelaterad information för sina produkter, som kan erfaras sen säg tidigt 90-tal, inte längre behöver utgöra ett hinder av typ (1).

Även om vårt ursprungliga syfte med SAFT var att möjliggöra studier av enstaka bullerhändelser/överflygningar, har vi under arbetets gång övertygats om att det som inte ansågs möjligt för säg 10 år sedan, d.v.s. ersätta ECAC Doc.29/integrerade metoder med simuleringsmetoder även för flygtrafik över tid, vore fullt möjligt idag rent metodmässigt och ekonomiskt. Bland annat genom etablering av ovan nämnda data för ljudkällor som erbjuder möjlighet till ersättning av NPD-data tack vare: (i) ljudmätningar i fält, (ii) goda möjligheter till etablering av trajektoriedata från verklig flygtrafik, (iii) dataöverföring och (iv) högkvalitativa meteorologi-data samt tillgång (v) tidsstegande simuleringskoder. Intressant i sammanhanget är det motstånd som flygindustrin har uppvisat mot att släppa information kring buller gällande sina produkter, åtminstone sen början av 90-talet. Fullt förståeligt ur ett företagsperspektiv men olyckligt sett från brukare/boendes sida. Vi gör dock bedömningen att detta skyddande av kunskap kring flygbuller genereering i viss mening har kortslutits i och med de möjligheter till ljudmätning och positionsbestämning av flygplan i fält som föreligger idag. Detta kan exemplifieras av projekt ULLA som bedrivs på KTH sedan 2 år och är finansierat av TRV.

Ett exempel i omvärlden som understryker dessa möjligheter och visar på sätt att använda simuleringsmetoder även för större flygtrafikscenarior ges t.ex. i referensen (Zellman 2018):

https://www.dora.lib4ri.ch/empa/islandora/object/empa%3A16574/datastream/PDF/Zellmann-2018-Development_of_an_aircraft_noise-%28published_version%29.pdf

Ett citat ur denna rapport är: "... Doc.29 are designed to calculate yearly air traffic. Effects of spatial modifications such as changes in track dispersion or the introduction of preferred routes can be reliably calculated. *However, effects of changes in the vertical flight profile are limited to a simplified acoustical description of the source. The main drawback of the noise-power-distance (NPD) data is the lack of airframe noise parameters like airspeed or aeroplane configuration to account for source effects at approach. Therefore, the best practice programs*

are currently of limited use for the assessment of vertical noise abatement procedures for approach."

Sammanfattningsvis, det har inte varit SAFT-projektets syfte att ta fram en ny "nationell kod för flygbuller" med avsikten att ersätta Doc.29 däremot att ta fram metoder och ett komplement för fall som integrerade metoder inte klarar av. I slutrapporten vill vi dock lyfta fram möjligheterna med dagens tidsstegade simuleringskoder och belysa detta för både akustiker och beslutsfattare inom området flygbuller.

Kommentarer:

Sammanfattningsvis är det främst två principer som kommenteras och det gäller: 1. mål med projektet samt 2. validering av resultat:

1. Mål med projektet.

    a. Det skrivna målet med SAFT (Kap 2 Background) tolkas som att det föreligger ett behov av en bättre beräkningsmetod. Det saknas dock en tydlig diskussion om varför det skulle finnas ett behov av en lokal/nationell egenutveckling av beräkningsmetodik för flygbuller.

    SAFT-rapporten utgår från och jämförs med nu gällande beräkningsmetod för flygbullerberäkningar i Sverige som finns beskriven i det internationella metoddokumentet ECAC Doc 29[1] och det Kvalitetssäkringsdokument[2] som tagits fram av Transportstyrelsen, Naturvårdsverket och Försvarsmakten och som numera underhålls av Trafikverket. SAFT har dock fokus på andra tillämpningar än vad som är syftet med ECAC Doc 29.

    Först kan nämnas som diskuterats ovan att det finns en stark konsensus inom forskarvärlden rörande behovet och idag möjligheterna att faktiskt utveckla bättre metoder.

    Sedan är det värt att påpeka att projekt SAFT startades baserat på en ansökan som KTH lämnade in till TRV, som efter granskning av oberoende experter tillstyrktes av Trafikverkets portfölj för luftfart. Detta dels baserat på expertutlåtandena men förstås även på stödet från flygportföljens ledamöter. TRV ser uppenbarligen att det finns ett behov att utveckla nya verktyg för att bättre hantera bullerfrågor och är villiga att satsa på detta. Man har ju nyligen även godkänt en fortsättning på projekt SAFT benämnt CIDER som leds av Chalmers.

    b. Den anledning som nämns är att det behövs en bättre metod för att kunna reducera bullerexponering på boende runt flygplatser genom att optimera de flygoperativa procedurerna, rutter, luftrumsdesign och fördelning av trafik över tid. Redan med befintliga beräkningsmetoder kan man idag göra detta, vilket också görs, men det är oklart vad SAFT i detalj menar hur detta ska genomföras.

    Vi har flera tankar och ideer kring detta bla inspirerade av vad vi sett att Dr. Zellmann på EMPA har gjort (se länk ovan). Vidare är det helt klart att Swedavias

erfarenheter och kunnande är viktiga för oss och vi behöver en fortsatt dialog för att förstå hur vi bäst kan utveckla verktyg som blir till nytta.

c. SAFT-rapportens uttalade strävan är att skapa en beräkningsmetodik som är noggrannare än Doc. 29, med syftet är att skapa ett verktyg för att beräkna enskilda flygningars bullerexponering mer exakt, bland annat med hjälp av information om momentana väderförhållanden. SAFT nämner också ett behov av att förstå komplexiteten med flygbuller runt en flygplats. Man diskuterar dock inte vilket behov som föreligger i samband med miljöprövningar och arbeten med Riksintressen. Riktvärden för flygbuller gäller för årsmedelvärden och dessa har tagits fram baserat på beräkningar från den typen av metod som beskrivs i Doc 29. Resultat från utfalls- och prognosberäkningar som jämförs med riktvärden eller andra referenser bör räknas med samma typ av metod.

Vi håller i stort sett med om detta. Men inför de utmaningar som står framför oss inom flyg och miljöområdet behöver vi fundera och arbeta kring nya metoder och lösningar. T.ex. hur vi kan nyttja bättre kunskap och bättre modeller kopplat till mer exakt styrning av flygplan/procedur/profil och rutt för att försöka minimera emissioner och buller. Detta är det vi försöker arbeta med i samtliga de projekt som vi driver inom Centrum för hållbar luftfart tillsammans med TRV.

d. Syftet med ECAC Doc 29 är inte att skapa de mest noggranna bullerkurvorna som kan åstadkommas, men rätt utfört kan det leverera bullerkurvor runt en flygplats för hela årstrafikfall med en noggrannhet tillräckligt bra för bland annat miljöprövningar och beräkning av influensområden i samband med Riksintressepreciseringar. Syftet med Doc 29 är att skapa en kostnadseffektiv och enhetlig tillämpning i Europa och globalt för olika typer av användare. Utveckling av Doc 29 utförs av ECAC i samarbete med bland annat ICAO som utvecklar den internationella motsvarigheten ICAO Doc 9911. Swedavias uppfattning är att utveckling av metod för flygbullerberäkning fortsatt ska ligga på internationell nivå. Dels för kostnadseffektiviteten, men dels också för att tillämpa en enhetlig metodik.

Se våra svar ovan samt under rubriken ”Allmänt”.

2. Validering av resultat

a. Det bör förtydligas i inledningen av rapporten att SAFT inte är en färdigutvecklad och komplett metod eller ett färdigt beräkningsprogram. Ingen komplett beräkning har redovisats. Endast vissa delberäkningar (bidrag) visas och enskilda delar räknas fristående, varpå man dragit slutsatser.

Vi håller inte med om detta i Sammanfattningen står det ” Since the SAFT-program is intended to be further developed in upcoming projects, current limitations and future updates and implementations are noted in the text. Typically these notes are given in in red text like: [NOTE: ...] and mostly intended for SAFT developers and users. Vi förstår inte heller kommentaren om komplett beräkning flera exempel ges på ”single events” dock inget trafikscenario fall (1 års medelvärde eller dylikt).

b. En implementation av ECAC Doc 29 har redovisats för Approach (det vill säga endast för inflygningar) och inte utflygningar

I samtal med Swedavia och andra verksamma inom området har vi fått uppfattningen att Approach har visat på störst avvikelser mot beräkningar och varit svårare att uppskatta. Därav vårt fokus på dessa. Det är också så att normalt är inflygning t.ex. på Arlanda ett större problem bullermässigt än start. Det finns dock inget principiellt problem att modellera utflygningar i SAFT.

c. Ingen validering av resultat till Doc 29 vol 3 eller Doc 29-ekvivalenta verktyg så som AEDT har redovisats.

Lite oklart vad kommentaren avser? Efterfrågas en jämförelse med SAFT Doc.29 beräkning med motsvatrande oberoende Doc.29 baserad beräkning. T.ex. i ett samarbete med Swedavia?

Det vi har gjort är att ha kört ECAC Doc.29/NPD fall och jämfört dessa inkluderande olika vädertyper samt "reversed engineering"-baserade fall inkluderande olika longitudinella riktingskarakteristiker och sett en stor känslighet. Men ja, vi saknar ännu egna mätdata, något som kommer att åtgärdas i projekt ULLA och det nya projektet CIDER där mätningar och validering+upprättande av källmodeller är planerat.

d. Som källdata till SAFT används nu den flygbuller- och prestandadatabas, ANP, som är anpassad till ECAC Doc 29. För att mäta in flygplan till en ny databas som är anpassad till SAFT skulle krävas stora resurser i förhållande till vad man skulle vinna. Det kommer också vara långa ledtider från det att flygplanstillverkare mäter in och beräknar detta till det att data finns validerat och tillgängligt i ANP.

Bra kommentar och förvisso krångligt som påpekas – men som vi, och andra organisationer, bedömer det har teknikutvecklingen gjort det fullt möjligt att till en överkomlig kostnad genomföra "egna" mätningar för estimering av ljudkällor (se diskussion ovan och länk till ref. Dr. Zellmann ovan där detta testats).

Det bygger på 4 delar:

1. autonom ljudmätning i fält under flygpassager, mikrofoner/dator/trådlös kommunikation ca 5000kr/mätplats

2. ADS-B trajektoriedata fritt tillgängligt via tex OpenSky

3. Atmosfärsdata AROME prognoser – kvalitetstestade (10 m) mot mätstationer

4. Tidsstegande simuleringskod typ SAFT

Till detta kommer bl.a. datahantering och statistiska metoder för etablering av statistiskt säkerställda tids-, frekvens-, mass-, hastighets-, pådrag/N1-, väder-, flyplanstyp- och konfigurationsberoende ljudkällor. Och i samband med detta tillgång till FDR-data.

e. Skillnaden i resultat mellan SAFTs ECAC Doc 29-implementation och SAFTs tillägg med hänsyn tagen till atmosfärisk refraktion ger en skillnad på ca 1 dB under flygvägen och en asymmetrisk skillnad på sidan om flygvägen. Detta är av förväntan då den typen av effekt varierar från tid till annan. Över längre perioder kommer den effekten troligen att reduceras och det blir ett slags medel. Menar SAFT att 1 dB är den förbättring i metod man kan förvänta sig?

Eftersom vi inte gjort några omfattande studier kan vi inte uttala oss om "förväntningar" med någon större säkerhet. Det vi ser hittills är dock exempel på skillnader på en eller ett par dB beroende på t.ex. väder, atmosfärsdata, använd absorptionsmodell, ... Naturligtvis kan redan några enstaka dB vara känsligt då det kan handla om stora skillnader i kostnad om en konturlinje för ett riktvärde flyttas utåt eller inåt c:a 1 km eller så (jämför t.ex. val av atmosfärsdämpnings modell inom ECAC och dess konsekvenser). SAFT skulle kunna simulera och bringa klarhet i t.ex. sådana fall som återges i Swedavias rapport "Flygbullermätning kurvade inflygningar över Fresta Upplands Väsby, 2019 " (Dok.nr D2019-004726). Här redovisas skillnader på upp emot 7dB mellan mätningar (högre ljudnivåer) och Doc.29 beräkningar (lägre nivåer) vars bakgrund lämnas oförklarade.

f. SAFT drar slutsatsen att SAFT-verktyget skulle ge något mindre bullerutbredning än motsvarande ECAC Doc 29 för en inflygning. Detta bör vara väntat då ECAC i första hand är konstruerat för att beräkna medelvärden och med tanke på de standardantaganden i flygprofiler och ljudutbredning i luft som specificeras i Kvalitetssäkringsdokumentet.

Vi uttrycker en tendens från ett fåtal fallstudier, inte en så generell slutsats som antyds i:"SAFT drar slutsatsen att SAFT-verktyget skulle ge något mindre bullerutbredning än motsvarande ECAC Doc 29 för en inflygning" men i det studerade fallet med given input+valda modeller, Ja.

g. Sammanfattningsvis kan man inte av rapporten förstå hur mycket det möjligen skulle kunna skilja i resultat om man räknar ett helt års trafik på en flygplats med ett färdigt SAFT-system eller om man räknar med Doc 29. En sådan diskussionsdel vore intressant med tanke på strävan att skapa en ny metod som är mer noggrann än den befintliga ECAC Doc 29.

SAFT är en mer komplett model som möjliggör mer detaljerade bullerberäkningar med hänsyn till meteorologi, flygplans hastighet och konfiguration samt 3D direktivitet för planets ljudkällor. Men om SAFT modellen reduceras till samma antaganden som i Doc. 29 blir förstås resultaten, t.ex. årsmedelvärden, snarlika. Men frågan om hur SAFT bäst kan nyttjas praktiskt, t.ex. av Swedavia, är förstås viktig och vi hoppas på fortsatta diskussioner rörande detta.

3. SAFT verkar endast vara gjort för beräkning av utfall av enskilda flygplanshändelser och väderförhållanden och inte så som ECAC Doc 29 är tänkt att användas för hela trafikfall över ett helt år, både utfall och prognos.

Ja stämmer se ovan.

Slutord: Vi är tacksamma för fler synpunkter på SAFT, gärna om ni ser någon användningsmöjlighet för Swedavia eller möjlighet till att bidra med data som kan vara av intresse för vidare utveckling eller fallstudier.